LBL-25893

Center for Advanced Materials

CAM

Received by OSTI
APR 1 0 1989

The Preparation and Characterization of High Surface Area Transition Metal Nitrides

C.H. Jaggers
(Ph.D. Thesis)

DO NOT MICROFILM
COVER

August 1988

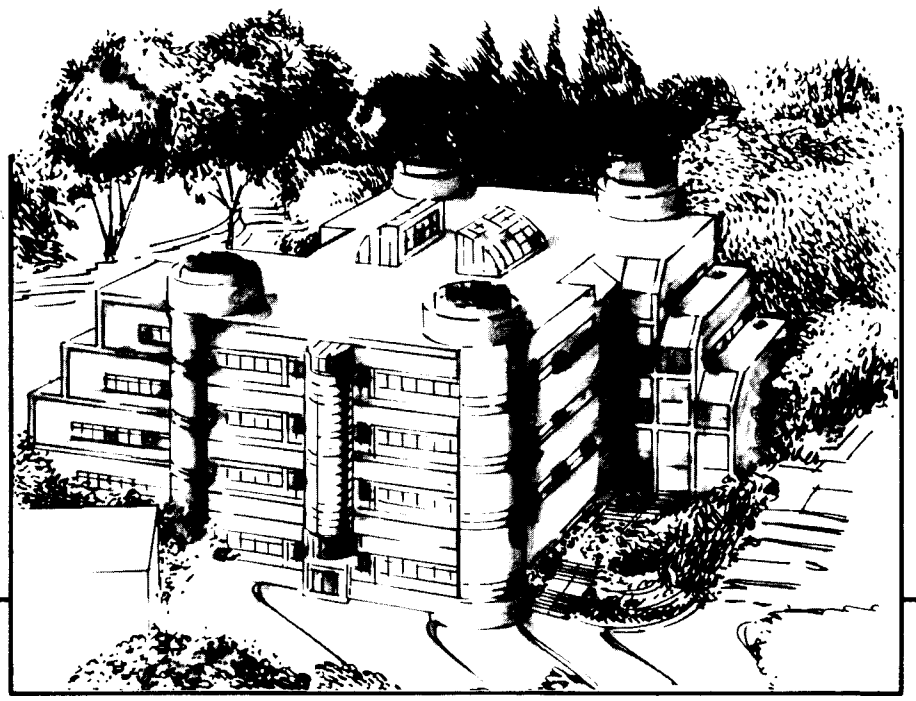

Materials and Chemical Sciences Division

Lawrence Berkeley Laboratory • University of California

ONE CYCLOTRON ROAD, BERKELEY, CA 94720 • (415) 486-4755

Prepared for the U.S. Department of Energy under Contract DE-AC03-76SF00098

DISTRIBUTION OF THIS DOCUMENT IS UNLIMITED

DISCLAIMER

This report was prepared as an account of work sponsored by an agency of the United States Government. Neither the United States Government nor any agency thereof, nor any of their employees, makes any warranty, express or implied, or assumes any legal liability or responsibility for the accuracy, completeness, or usefulness of any information, apparatus, product, or process disclosed, or represents that its use would not infringe privately owned rights. Reference herein to any specific commercial product, process, or service by trade name, trademark, manufacturer, or otherwise does not necessarily constitute or imply its endorsement, recommendation, or favoring by the United States Government or any agency thereof. The views and opinions of authors expressed herein do not necessarily state or reflect those of the United States Government or any agency thereof.

DISCLAIMER

Portions of this document may be illegible in electronic image products. Images are produced from the best available original document.

DISCLAIMER

This document was prepared as an account of work sponsored by the United States Government. Neither the United States Government nor any agency thereof, nor The Regents of the University of California, nor any of their employees, makes any warranty, express or implied, or assumes any legal liability or responsibility for the accuracy, completeness, or usefulness of any information, apparatus, product, or process disclosed, or represents that its use would not infringe privately owned rights. Reference herein to any specific commercial products process, or service by its trade name, trademark, manufacturer, or otherwise, does not necessarily constitute or imply its endorsement, recommendation, or favoring by the United States Government or any agency thereof, or The Regents of the University of California. The views and opinions of authors expressed herein do not necessarily state or reflect those of the United States Government or any agency thereof or The Regents of the University of California and shall not be used for advertising or product endorsement purposes.

Lawrence Berkeley Laboratory is an equal opportunity employer.

DO NOT MICROFILM
COVER

LBL--25893

DE89 009228

The Preparation and Characterization of High Surface Area Transition Metal Nitrides

Christopher Harold Jaggers
(PhD Thesis)

Center for Advanced Materials
Materials and Chemical Sciences Division
Lawrence Berkeley Laboratory
Berkeley, California 94720

and

Department of Chemical Engineering
University of California
Berkeley, California 94720

Contract No. DE-AC03-76SF00098

DISCLAIMER

This report was prepared as an account of work sponsored by an agency of the United States Government. Neither the United States Government nor any agency thereof, nor any of their employees, makes any warranty, express or implied, or assumes any legal liability or responsibility for the accuracy, completeness, or usefulness of any information, apparatus, product, or process disclosed, or represents that its use would not infringe privately owned rights. Reference herein to any specific commercial product, process, or service by trade name, trademark, manufacturer, or otherwise does not necessarily constitute or imply its endorsement, recommendation, or favoring by the United States Government or any agency thereof. The views and opinions of authors expressed herein do not necessarily state or reflect those of the United States Government or any agency thereof.

MASTER

DISTRIBUTION OF THIS DOCUMENT IS UNLIMITED

The Preparation and Characterization of High Surface Area Transition Metal Nitrides

by

Christopher H. Jaggers

Department of Chemical Engineering, University of California, and Center for Advanced Materials, Lawrence Berkeley Laboratory

Berkeley, CA 94720

ABSTRACT

In the preparation of new catalytic materials, maximizing the surface area is important to minimize the amount of catalyst needed. This study is concerned with the synthesis of high surface area molybdenum and vanadium nitrides by the reaction of oxide and ammonium oxide precursors with ammonia. The reactions have been followed using thermogravimetric analysis (TGA) and high temperature X-Ray diffraction (XRD) to determine reaction intermediates, while the development of surface area was investigated by interrupting the TGA experiments and measuring the surface area using the BET method.

Molybdenum trioxide and ammonium paramolybdate react to form high surface area Mo_2N and a mixture of MoN and Mo_2N, respectively. Both of these reactions are characterized by pseudomorphous particle morphologies of reactants and products. In contrast, diammonium molybdate reacts with ammonia to form low surface area MoN; it does not exhibit the same pseudomorphous behavior. Each compound reacts through a different

pathway to form a common MoO_xN_{1-x} oxynitride intermediate, which subsequently reacts to form the nitride product. The nitride phase formed is determined by the temperature at which the oxynitride reacts, while the structure of the oxynitride precursor influences the ultimate surface area.

The reactions of V_2O_5, VO_2, V_2O_3, and NH_4VO_3 with ammonia all produce low surface area vanadium oxynitrides at 750°C. Each reaction proceeds through a series of lower vanadium oxide intermediates. In all reactions, V_2O_3 is the precursor to the oxynitride.

The use of hydrogen bronzes of molybdenum trioxide and vanadium pentoxide as starting materials lowers the reaction temperatures, but does not alter the nitridification reaction networks. In the case of molybdenum trioxide, however, insertion of hydrogen eliminates the formation of molybdenum dioxide which is a by-product of the reaction of MoO_3 with ammonia.

This dissertation is dedicated to my parents
Edward and Wanda whose support and encouragement
have been greatly appreciated.

ACKNOWLEDGEMENTS

I would like to thank Dr. James N. Michaels and Dr. Angelica Stacy for their contributions to this thesis. The opportunity to work with both of them on a joint project between the Departments of Chemical Engineering and Chemistry has been the most rewarding of my experiences at Berkeley.

I would also like to thank my dissertation committee, Dr. Eugene Petersen and Dr. William Armstrong for their assistance.

I am also indebted to Rick Rosin for his assistance in preparing the V_2O_5/Pt compounds, and David Marr for his assistance in testing the hydrogen bronzes.

Finally, but certainly not least, I would like to thank all of the members of the Michaels/Reimer research groups, past and present, who have helped to retain some sanity to graduate school at Berkeley.

Funding for this work was provided in part by the Director, Office of Energy Research, Office of Basic Sciences, Materials Science Division of the U.S. Department of Energy under Contract DE-AC03-76SF00098.

TABLE OF CONTENTS

LIST OF FIGURES

LIST OF TABLES

Chapter 1. Introduction

Since the discovery that transition metal carbides and nitrides have catalytic activity for ammonia synthesis[1] and for reactions traditionally catalyzed by noble metals[2-6], these materials have attracted attention as alternatives to noble metal catalysts. In addition, recent research has focused on the nitrides such as Mo_2N as possible hydrodenitrogenation catalysts[7]. The use of these materials as catalysts necessitates their synthesis with high surface areas. Unfortunately, transition metal carbides and nitrides prepared by classical high temperature synthesis routes[8] have little utility as catalysts since the products of such reactions have very low surface areas, less than 1 m^2/g. To increase their usefulness as catalysts, new synthetic routes which yield high surface area nitrides must be developed.

Recently, Boudart[9] reported that the reaction of MoO_3 with NH_3 produces Mo_2N with a surface area in excess of 200 m^2/g. He described the reaction as a "topotactic transformation" with conservation of the two-dimensional layers of the oxide precursor in the nitride product. This description is not complete, as the reaction involves the breaking of all of the intralayer bonds to remove the oxygen and is therefore not topotactic. The reaction is more complex than first assumed, and its applicability to the synthesis of other transition metal nitrides with high surface areas is not obvious.

This study is concerned with the synthesis of high surface area molybdenum and vanadium nitrides by the reaction of oxide and ammonium

oxide precursors with ammonia. The primary interest is to compare and contrast the reaction pathways and to determine the relationship between structure and stoichiometry of the starting materials and the phase and morphology of the product.

The products of traditional routes for synthesizing nitrides have low surface areas because of sintering at the high reaction temperatures. It is therefore desirable to form the nitrides at low temperatures to avoid sintering. For this purpose, starting materials which intercalate and/or react with ammonia at low temperatures were chosen. Many layered oxides exhibit such behavior and several ammonium molybdenum oxides and ammonium vanadium oxides are known. Additionally, hydrogen bronzes of the oxides were used due to their similarity in structure but variation in oxidation state to the parent oxide.

The reactants, molybdenum trioxide, MoO_3, molybdenum dioxide, MoO_2, ammonium paramolybdate, $(NH_4)_6Mo_7O_{24}\cdot 4H_2O$, and diammonium molybdate, $(NH_4)_2MoO_4$ were chosen for several reasons. Boudart[9] has shown that the reaction of MoO_3 with ammonia can produce high surface area Mo_2N. The ammonium molybdates have similar structures to the molybdenum oxides, but they have ammonia, the reactant gas, inserted into the starting material. Indeed, several of these molybdenum oxide/ammonium molybdates have been shown to react with ammonia at room temperature[10-12]. These materials therefore have related but different structures with varying NH_3:H_2O:MoO_3 ratios.

The reactions of the vanadium oxide/ammonium vanadate system with ammonia to form vanadium nitrides were also studied to determine if the

behavior observed in the molybdenum oxide/ammonium molybdate system could be generalized to other transition metals. The vanadium oxide/ammonium vanadate system has several similarities to the molybdenum oxide/ammonium molybdate system; vanadium pentoxide, like molybdenum trioxide is a layered material which allows the insertion of guest molecules between the layers, including ammonia. Additionally, several ammonium vanadates exist, which are vanadium oxides with ammonia, the reactant gas, inserted into the material. This system is therefore ideal for comparison with the results for the molybdenum oxide/ammonium molybdate system. In this study, the reactants vandium pentoxide V_2O_5 and ammonium metavanadate NH_4VO_3 were used; additionally, the reduced oxides VO_2 and V_2O_3 were also used.

Chapter 2. Structures and Background

This study involves the reactions of several molybdenum oxides, ammonium molybdates, vanadium oxides, and ammonium vanadates with ammonia to form high and low surface area molybdenum and vanadium nitrides. The reactions of these compounds with NH_3, H_2, and H_2O have been studied widely. As a result, the structures of many of the intermediates and products of these reactions are known. These structures are important as many of these compounds are either reactants, intermediates, or products observed during the formation of molybdenum and vanadium nitrides.

MOLYBDENUM OXIDES

Phase Diagram of Mo-O System

There are several molybdenum oxides as illustrated by the Mo-O phase diagram in Figure 2.1[14]. All of these structures are built up of edge- and corner-sharing MoO_6 octahedra. As the phase diagram indicates, the highest oxide is molybdenum trioxide, MoO_3. In this study, molybdenum trioxide can be considered as the starting compound from which all other reactants can be derived.

Molybdenum trioxide, MoO_3, is a layered material which melts at 795°C[15]. The structure consists of 6.928 Å thick double layers of edge- and

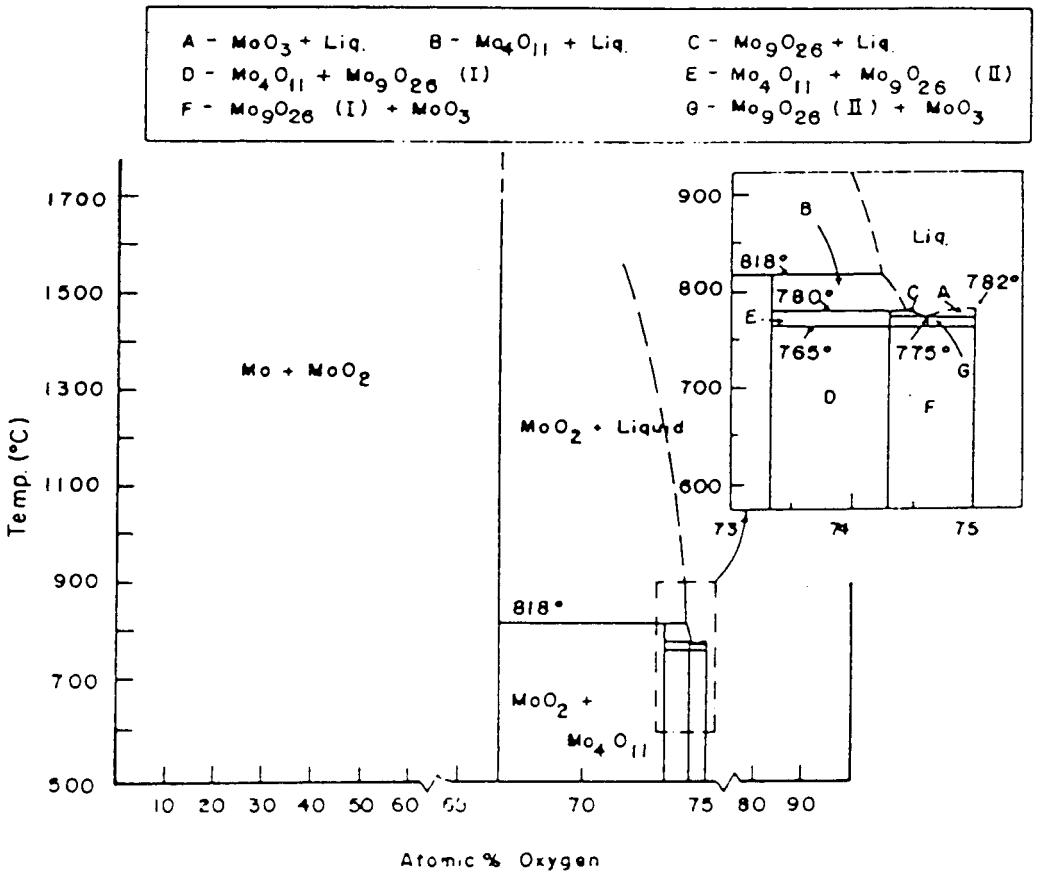

Figure 2.1. Molybdenum-Oxygen phase diagram[14].

corner-sharing MoO_6 octahedra as shown in Figures 2.2a and 2.2b[16]. These layers are held loosely together by Van der Waals interactions, resulting in a material with anisotropic bonding. The unit cell is orthorhombic, with lattice parameters of a=3.962 Å, b=13.858 Å, and c=3.697 Å.

Reduction of Molybdenum Trioxide

The reduction of molybdenum trioxide results in the formation of several reduced oxide species. Molybdenum trioxide will undergo a partial reduction to Mo_4O_{11}, Mo_8O_{23}, and Mo_9O_{26} under vacuum at temperatures between 550°C and 800°C[17]. In hydrogen, the reduction of molybdenum trioxide occurs in two distinct stages: (1) the reduction of MoO_3 to MoO_2 in the temperature range of 480°C to 600°C, and (2) the reduction of MoO_2 to Mo metal above 650°C[18]. In the presence of 0.01-0.1 wt% Pd at temperatures of 200-300°C, a rate of reduction in hydrogen comparable to the reduction without Pd in H_2 at 400-500°C can be attained[19]. The use of palladium, however, leads to the formation of hydrogen molybdenum bronzes H_xMoO_3 as an intermediate in the formation of MoO_2[20].

Molybdenum dioxide, MoO_2, has a structure which resembles the molybdenum trioxide structure. It is constructed of double layers of MoO_6 octahedra like MoO_3. However, these "layers" are covalently bonded to adjacent layers, resulting in a material with isotropic bonding and a distorted rutile structure as shown in Figures 2.2a and 2.2c. In the ideal rutile structure, the metal atoms are equidistant. In the MoO_2 structure, however, the metal atoms are not in the center of the octahedra but are attracted to adjacent

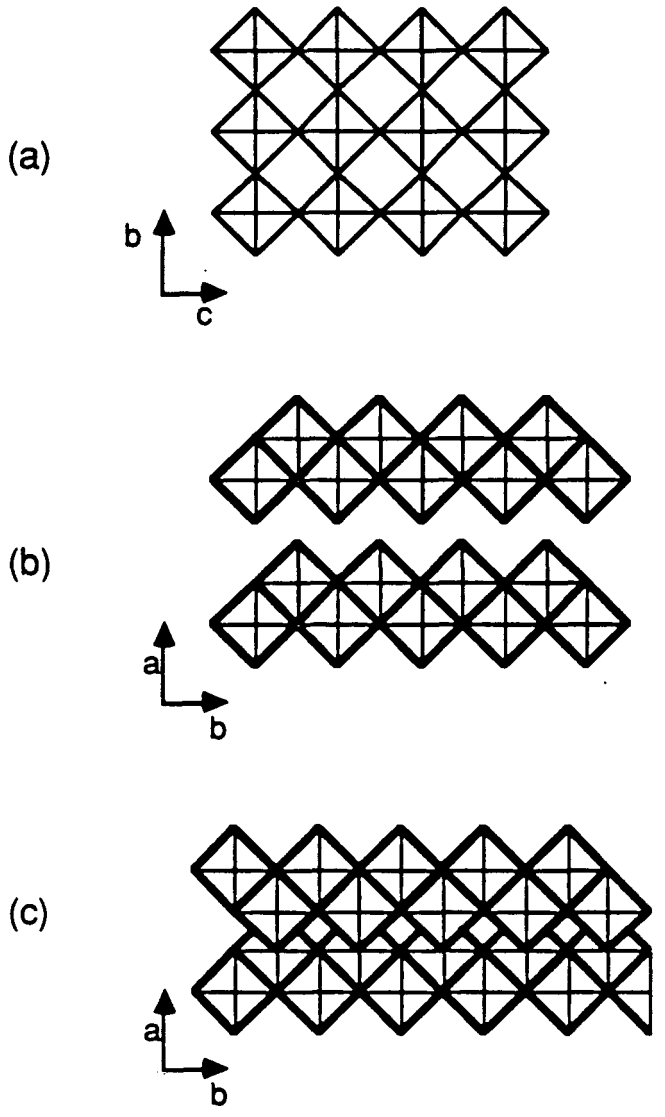

Figure 2.2. Structures of molybdenum trioxide and molybdenum dioxide: (a) layers of MoO_6 octahedra; (b) arrangement of Layers in MoO_3; and (c) arrangement of layers in MoO_2.

metal atoms, resulting in a pronounced formation of metal atom pairs and distortion of the MoO_6 octahedra[21]. The symmetry of the unit cell thereby is lowered from tetragonal to monoclinic , with unit cell dimensions of a=5.610 Å, b=4.843 Å, c=5.526 Å and β=119.62°[22].

Intercalation of Molybdenum Trioxide

The insertion of a guest molecule into a host lattice is a well-known reaction for layered materials at low temperatures[23], and molybdenum trioxide is no exception. These reactions are sometimes referred to as topotactic transformations, which are defined as processes in which the solid product is formed in one or several crystallographically equivalent orientations relative to the parent crystal. They are a consequence of a chemical reaction or a solid-state transformation proceeding throughout the entire volume of the parent crystal[24]. These reactions are usually accompanied by electron transfer between the guest species and the host lattice, while the host structure retains some dimensionality (either one, two, or three) of its original structure. The insertion of guest molecules between the layers of a layered material is an example of a two-dimensional topotactic transformation, in which the two-dimensional layers of the parent crystal are retained.

Water molecules can be inserted between the layers of molybdenum trioxide to form compounds with the formula $MoO_3 \cdot xH_2O$, where x=1,2. Molybdenum trioxide exists in three hydrated forms: (1) white $MoO_3 \cdot 2H_2O$, (2) yellow $MoO_3 \cdot H_2O$, and (3) white α-$MoO_3 \cdot H_2O$. Although these compounds have often been referred to as "molybdic acids", they are actually true oxide

hydrates. There also exists a class of compounds known as hydrogen molybdenum bronzes, H_xMoO_3 ($0<x\leq2.0$), in which hydrogen is inserted topotactically between the molybdenum trioxide layers. In addition, catalytic hydrogenation of $MoO_3 \cdot 2H_2O$ and yellow $MoO_3 \cdot H_2O$ yields hydrogen insertion compounds of the formula $H_{1.0}MoO_3 \cdot 2H_2O$ and $H_{1.0}MoO_3 \cdot H_2O$, respectively[25]. Also, pyridine and bipyridine have been inserted into molybdenum trioxide[26].

The dihydrate $MoO_3 \cdot 2H_2O$ exists in only one form, and is schematically represented by Figure 2.3c[27]. The compound retains the layered structure of molybdenum trioxide with two water molecules now coordinated between the layers. The unit cell is monoclinic, with a=10.476 Å, b=13.822 Å, c= 10.606 Å, and $\beta=91.62^{o}$. The crystal structure is built up from slightly deformed layers of strongly distorted octahedra [$MoO_5(H_2O)$] sharing corners, parallel to the (010) direction. These layers contain two kinds of H_2O groups. One-half of the H_2O molecules are coordinated to Mo within the $[MoO_3(OH_2)]_n$ layers, while the other half are found between the layers. The distorted octahedra are formed by five oxygen atoms and one coordinated water molecule. Each octahedron shares a corner with each of four neighboring octahedra within the layers. The octahedra form zigzag rows within the layers with alternating Mo-O bridge bonds. The layers are linked by a system of hydrogen bonds involving all hydrogen atoms from both types of water molecules[27]. Each coordinated water molecule acts as a hydrogen donor to two different interlayer water molecules. These interlayer water molecules are hydrogen bonded to two

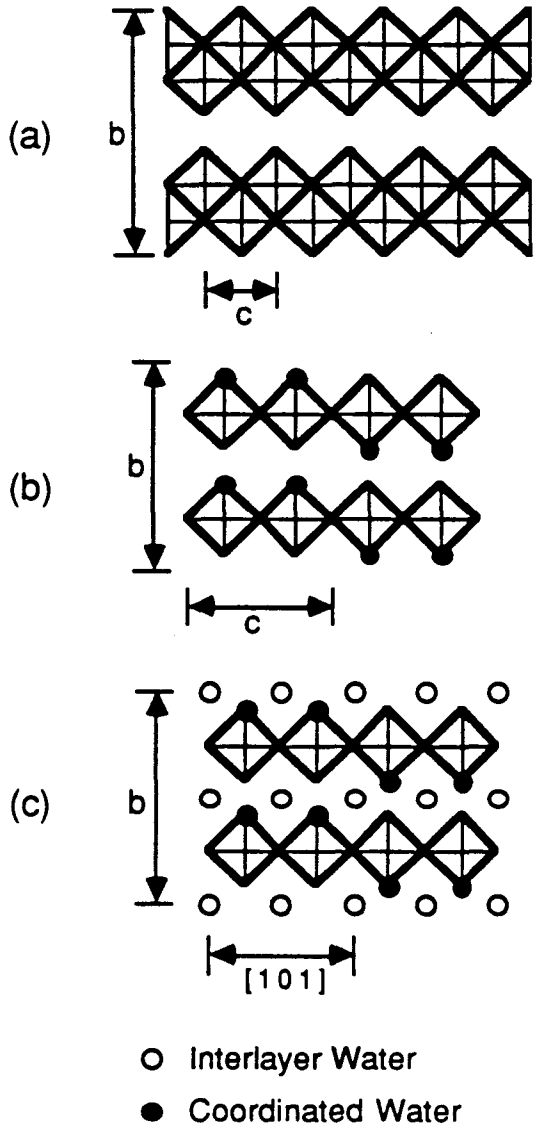

Figure 2.3. Structure of hydrated molybdenum trioxide. (a) MoO_3 structure; (b) $MoO_3 \cdot H_2O$ structure; and (c) $MoO_3 \cdot 2H_2O$ structure[27].

coordinated water molecules in one layer and acts as a hydrogen donor to a terminal oxygen atom in the next layer.

The yellow monohydrate $MoO_3 \cdot H_2O$ has been reported to be formed by the dehydration of the dihydrate. The dehydration results in the loss of the interlayer water molecules, while the coordinated water molecules are retained in the structure; this structure is shown in Figure 2.3b[28]. The layers are built up of distorted $[MoO_5(H_2O)]$ octahedra, with virtually no change from the dimensions of the dihydrate. The interlayer distance decreases from 6.91 Å to 5.35 Å. The unit cell is monoclinic, with a=7.55 Å, b=10.69 Å, c=7.28 Å, and $\beta=91^o$.

The white form of the monohydrate, α-$MoO_3 \cdot H_2O$, is not an intercalated molybdenum trioxide compound; rather, this structure consists of infinite double chains of edge-linked $[MoO_5(H_2O)]$-octahedra parallel to the [010] direction as shown in Figure 2.4. Each octahedron has two common edges with adjacent octahedra. In addition to the three bridging oxygen atoms, each molybdenum atom is coordinated by two terminal oxygen atoms and one terminal water molecule. The octahedral double chains are held together only weakly by hydrogen bonds[29]. The unit cell is triclinic with a=7.388 Å, b=3.700 Å, c=6.673 Å, and $\alpha=107.8^o$, $\beta=113.6^o$, and $\gamma=91.2^o$.

The hydrogen molybdenum bronzes, H_xMoO_3, were first synthesized by Glemser et al.[30-33] by the reduction of MoO_3 with (a) Zn and HCl, (b) Mo powder and water in sealed glass tubes at 110°C, (c) atomic hydrogen, and (d) $LiAlH_4$. The introduction of hydrogen into MoO_3 leads to the formation of four solid phases H_xMoO_3, or equivalently $MoO_{3-x}(OH)_x$, with $0<x\leq2.0$[30]. The

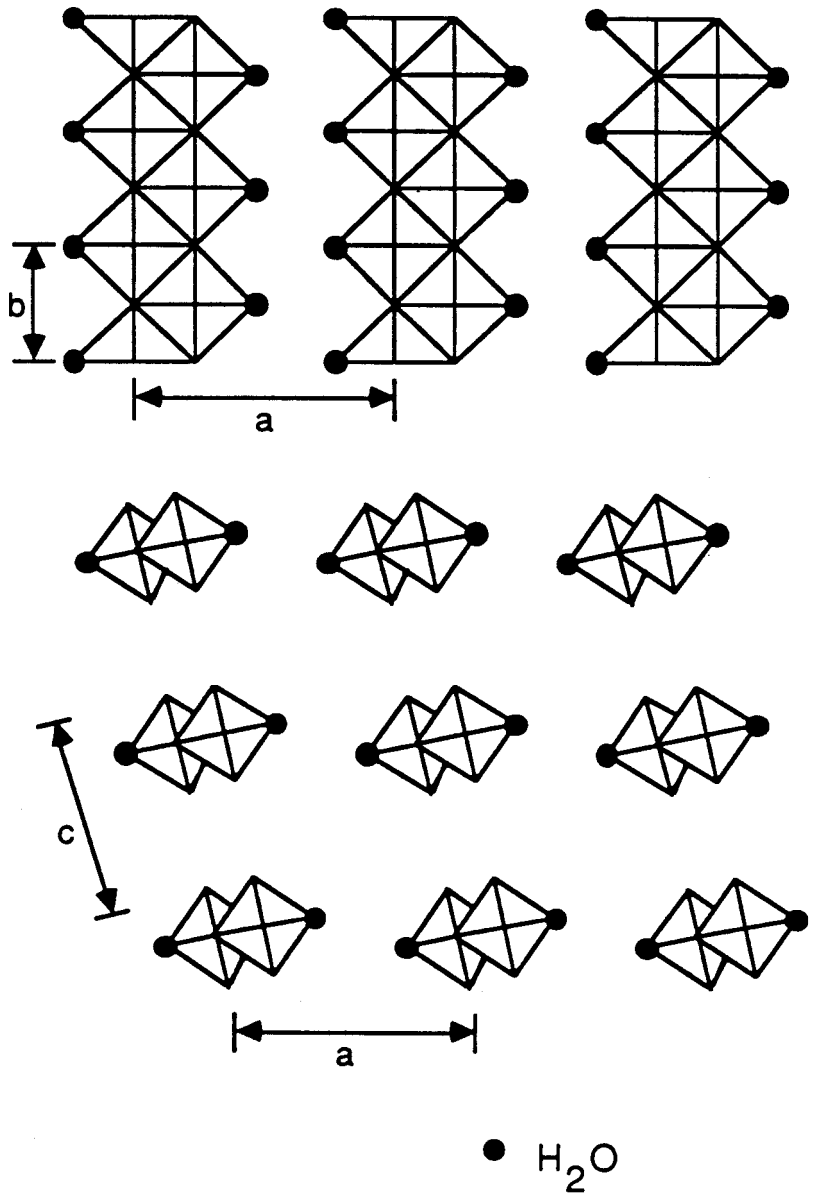

Figure 2.4. Structure of α-$MoO_3 \cdot H_2O$[28].

bronzes have X-ray diffraction patterns which are very similar to that of MoO_3, indicating that hydrogen is inserted topotactically between the layers with little crystallographic rearrangement[13]. These compounds are not line phases; they exhibit ranges of homogeneity as follows[34]:

blue orthorhombic	$0.23<x<0.4$
blue monoclinic	$0.85<x<1.04$
red monoclinic	$1.55<x<1.72$
green monoclinic	$x=2.0$

Based on neutron diffraction and neutron inelastic scattering studies, it was suggested that the hydrogen atoms in the blue orthorhombic phase are present in -OH groups, while in the other three phases with higher hydrogen content the hydrogen is present in $-OH_2$ groups[35]. A model for intralayer and interlayer proton positions for the green monoclinic bronze is shown in Figure 2.5[36].

Several additional intercalated compounds of MoO_3 have been formed. Both pyridine and bipyridine can be inserted topotactically into molybdenum trioxide at temperatures below 200°C[26]. The reaction of ammonia with molybdenum trioxide does not only produce an intercalated species but also forms ammonium paramolybdate and diammonium molybdate, as described in the next section[10]. However, the reaction of H_xMoO_3 with NH_3 does produce the intercalated compounds $(NH_4)_yH_{x-y}MoO_3$[37].

The hydrogen molybdenum bronze $H_{0.5}MoO_3$ forms several layered intercalation complexes $L_yH_xMoO_3$ with organic Lewis base (proton donor) molecules L, such as pyridine and ammonia[38]. The compounds are made by ion exchange with hydrated molybdenum bronzes, on cathodic reduction of

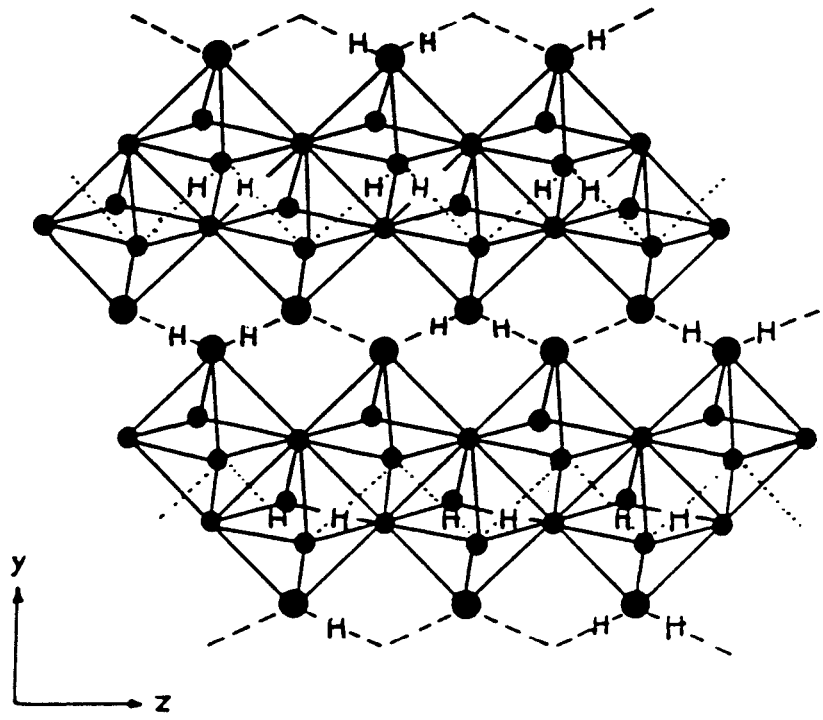

Figure 2.5. Model for proton positions in $H_{2.0}MoO_3$[36].

MoO_3 in aqueous LH^+ electrodes and by direct thermal reaction. Chemical or electrochemical reduction of MoO_3 in neutral aqueous electrolyte solutions can result in the reversible topotactic formation of a molybdenum bronze of the formula $A_x^+(H_2O)_y[MoO_3]^{x-}$. These compounds are built up by negatively charged $[MoO_3]^{x-}$ layers with exchangeable hydrated cations in the interlayer space; the interlayer distance is strongly dependent on the size of the cation A[38].

Reactions with Ammonia and Water

Molybdenum trioxide reacts readily with ammonia, even at room temperature. The reaction of MoO_3 with liquid NH_3 under anhydrous conditions was reported to yield an intercalated compound of the formula $MoO_3 \cdot 3NH_3$[11]. However, the XRD pattern of this compound led to the interpretation of this structure as the diammonium salt of an aquoammonomolybdic acid[12]. The presence of trace amounts of water, however, results in the formation of diammonium molybdate, $(NH_4)_2MoO_4$, in either liquid or gaseous ammonia[10]. When exposed to air, diammonium molybdate loses ammonia at room temperature to form ammonium paramolybdate, $(NH_4)_6Mo_7O_{24} \cdot 4H_2O$.

Diammonium molybdate, $(NH_4)_2MoO_4$, has an ammonia:water:trioxide ratio of 2:1:1. The compound contains loosely packed ammonium ions and almost regular tetrahedral MoO_4^{2-} groups. These tetrahedra are connected through hydrogen bonds with the ammonium ions in a monoclinic unit cell with

a=12.68 Å, b=6.51 Å, c=7.84 Å and β=117°; it has been shown to be isomorphous with K_2MoO_4 and K_2WO_4[39].

Ammonium paramolybdate, $(NH_4)_6Mo_7O_{24}\cdot 4H_2O$, differs from diammonium molybdate in that the structure is built up of MoO_6 octahedra. The structure consists of seven MoO_6 octahedra condensed by edge-sharing into a butterfly-shaped cluster as shown in Figure 2.6a. These heptamolybdate ions, $[Mo_7O_{24}]^{6-}$, are arranged in layers normal to the y-axis and are bound together through a complex system of ionic and hydrogen bonds with NH_4^+ cations and water molecules[40-41]. Ammonium paramolybdate $(NH_4)_6Mo_7O_{24}\cdot 4H_2O$ has a monoclinic unit cell with a=8.3934 Å, b=36.170 Å, c=10.4715 Å and β=115.958°.

The thermal decomposition of ammonium paramolybdate $(NH_4)_6Mo_7O_{24}\cdot 4H_2O$ in air to MoO_3 has been studied using TGA and XRD by a number of authors[42-52]. Most studies agree that the intermediates $(NH_4)_2O\cdot 2.5MoO_3$ and $(NH_4)_2O\cdot 4MoO_3$ are formed during the decomposition, although Funaki [45] reports the first intermediate to be ammonium paramolybdate without the waters of crystallization, $(NH_4)_6Mo_7O_{24}$, and does not observe the 2.5-molybdate. Louisy and Dunoyer[50] report the formation of the salt $(NH_4)_6Mo_7O_{24}\cdot 2H_2O$ based on TGA and XRD results. Hegadus and co-workers[51] distinquished two new compounds, $(NH_4)_2O\cdot 14MoO_3$ and $(NH_4)_2O\cdot 22MoO_3$, prior to the formation of MoO_3. Also, $(NH_4)_2O\cdot 3MoO_3$ and $(NH_4)_2O\cdot 12MoO_3$ have been reported by Schwing-Weill[53]. Onchi and Ma[49] studied the effluent gas stream during the decomposition using a mass

(a)

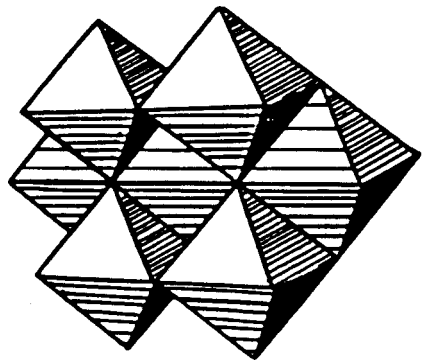

(b)

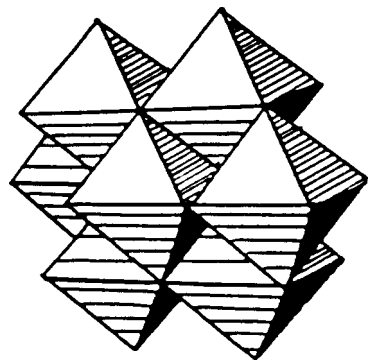

Figure 2.6. Structures of molybdate ions: (a) paramolybdate ion, $[Mo_7O_{24}]^{6-}$; (b) octamolybdate ion, $[Mo_8O_{26}]^{4-}$.

spectrometer and determined that the weight loss corresponded closely to the loss of $(NH_4)_2O$ groups.

The intermediate $(NH_4)_2O{\cdot}2.5MoO_3$ formed during the thermal decomposition of ammonium paramolybdate in air has been shown to be ammonium decamolybdate, $(NH_4)_8Mo_{10}O_{34}$[53]. The $[Mo_{10}O_{34}]^{8-}$ ions are built up of edge-sharing MoO_6 octahedra combined into a Mo_8O_{28} unit and connected at corners to two MoO_4 tetrahedra, as shown in Figure 2.7. The $[Mo_8O_{28}]^{8-}$ unit has the same arrangement of MoO_6 octahedra as described below for the $[Mo_8O_{26}]^{4-}$ ion in ammonium octamolybdate[54]. The decamolybdate ions are connected through a series of hydrogen bonds with ammonium ions, although the position of the ammonium ions has not been determined. The unit cell is tetragonal, with a=15.42 Å and c=29.32 Å[42].

The molybdate $(NH_4)_2O{\cdot}4MoO_3$ formed during the thermal decomposition of ammonium paramolybdate, $(NH_4)_6Mo_7O_{24}{\cdot}4H_2O$, is actually ammonium octamolybdate, $(NH_4)_4Mo_8O_{26}$. In addition, this molybdate is one of several molybdate intermediates observed in the reaction of ammonium paramolybdate with ammonia, as discussed in Chapter 4. The $[Mo_8O_{26}]^{4-}$ octamolybdate ion is built up of MoO_6 octahedra sharing edges, as shown in Figure 2.6b[54]. These ions are connected through a series of hydrogen bonds with ammonium ions, although the positions of these ions have not been determined. The unit cell is triclinic with a=7.76 Å, b=9.75 Å, c=9.78 Å and $\alpha=97^o2$, $\beta=100^o5$, and $\gamma=98^o$[54].

The ammonium "trimolybdate", $(NH_4)_2O{\cdot}MoO_3$, has been reported as a possible intermediate during the thermal decomposition of ammonium

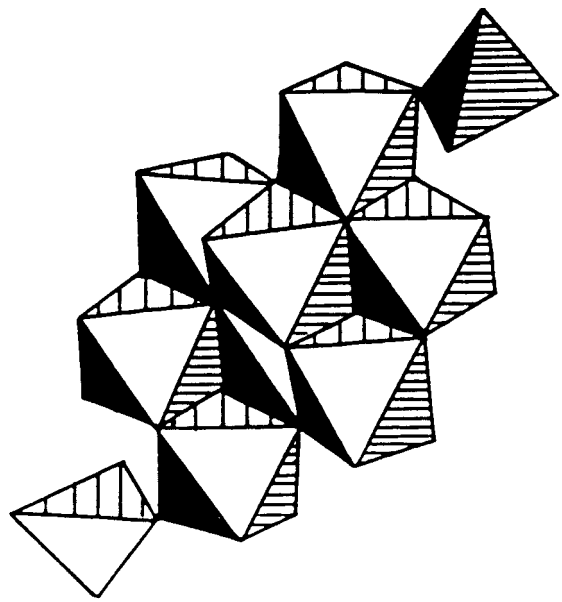

Figure 2.7. Structure of decamolybdate ion, $[Mo_{10}O_{34}]^{8-}$[54].

paramolybdate; an X-ray diffraction pattern was reported, but its structure is unresolved[43]. During the reaction of ammonium paramolybdate with ammonia, evidence for the formation of this compound based on TGA and XRD is presented. However, the literature fails to present a clear representation of its structure, and its existence as a unique phase is questioned. In an attempt to explain previous reports of its formation, Lindqvist discusses the improbability of a trimolybdate ion and postulates the existence of double salts of paramolybdates and octamolybdates[54].

The reaction of MoO_3 with NH_3 at elevated temperatures has been studied by several authors. Reduction of MoO_3 to MoO_2 occurs much faster and at lower temperatures with ammonia than the reduction with hydrogen[55]. However, at temperatures above 350-400°C, the formation of molybdenum nitrides competes with the reduction to MoO_2.

The molybdenum nitride phase diagram was first constructed by Hagg[56] and consists of three phases, as shown in Figure 2.8. The β-phase is stable above 600°C and has a stoichiometry range of $MoN_{0.38}$-$MoN_{0.43}$. The metal atoms form a face-centered tetragonal lattice. The γ-phase has a narrow homogeneity range in the vicinity of 33 atomic % N, corresponding to the formula Mo_2N. In this phase, the metal atoms form a face-centered cubic structure with the nitrogen atoms randomly occupying one-half of the octahedral voids, as shown in Figure 2.9(a). At 50 atomic % N, the δ-MoN phase exists in a simple hexagonal lattice with the WC type of structure in which nitrogen occupies trigonal prism sites, as shown in Figure 2.9(b)[58]. Hagg[56] noted several extra X-ray lines that do not belong to the WC lattice; Schonberg[57]

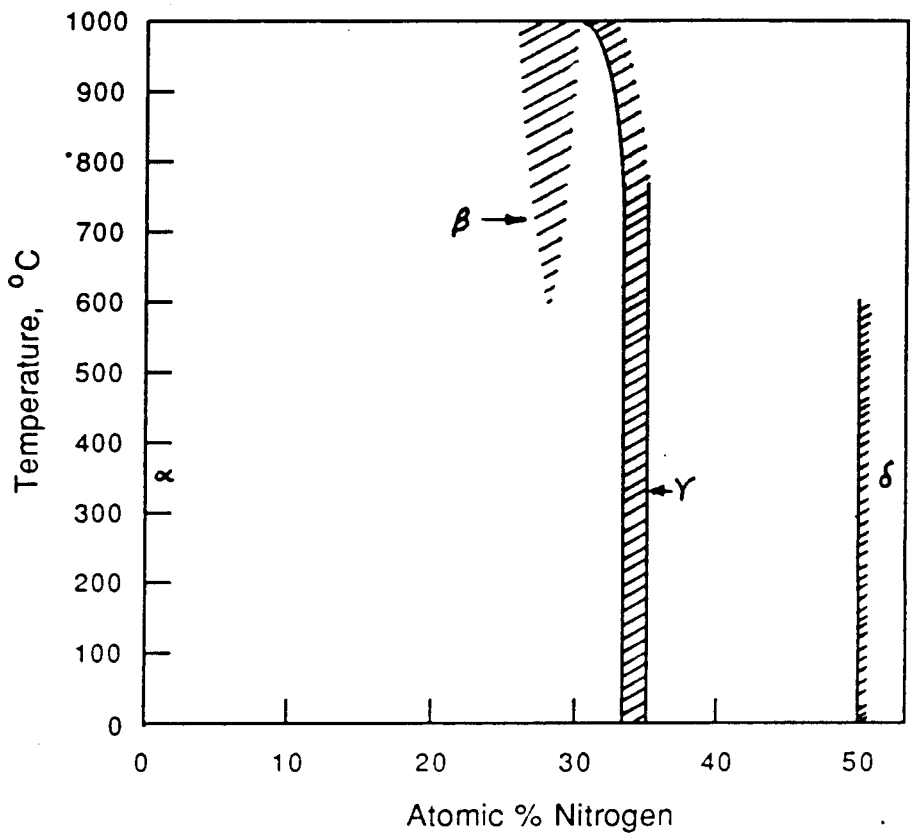

Figure 2.8. Molybdenum-Nitrogen phase diagram[58].

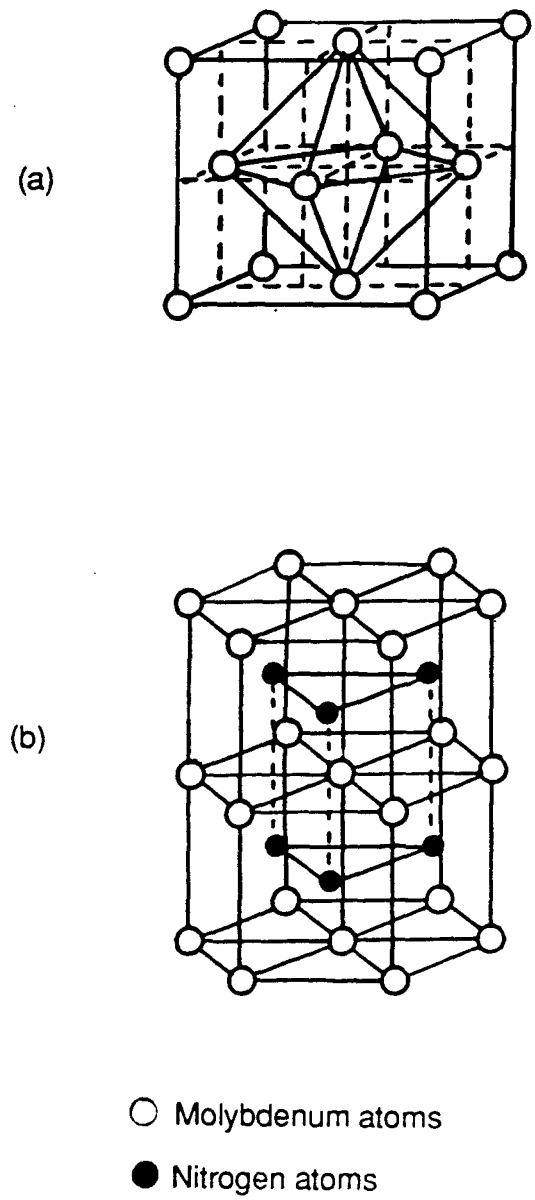

Figure 2.9. Structures of molybdenum nitrides: (a) fcc-Mo_2N, and (b) hexagonal MoN[58].

suggested that the WC structure is merely a subcell and that all lines could be identified with a hexagonal superstructure containing eight MoN units.

Hegedus et al.[59] reported the formation of molybdenum nitride phases from the reaction of molybdenum trioxide and ammonium paramolybdate with ammonia. Lyutaya reported that the nitridification of MoO_3 with NH_3 begins at temperatures under 400°C. He reported an fcc-oxynitride intermediate of composition $MoO_{1-x}N_x$ in route to forming an Mo_2N product. However, to obtain pure, oxygen-free molybdenum nitrides, a reduction-nitriding scheme was necessary. First, molybdenum trioxide was reacted in an ammonia stream at 900°C to remove the oxygen and convert the sample to activated molybdenum metal. This was followed by a lowerering of the temperature to form the nitride product. By nitriding at 700°C for 2 hours fcc-Mo_2N was obtained, while nitriding at 450°C for longer periods produced hexagonal MoN[60]. Bliznakov et al.[61] reported the formation of Mo_2N samples containing nitrogen in excess of the stoichiometric amount and two-phase samples of Mo_2N + MoN by nitriding MoO_3, $(NH_4)_6Mo_7O_{24}{\cdot}4H_2O$, and H_2MoO_4 with ammonia. The nitride phase and stoichiometry depended on the temperature, duration of nitriding, and gas flow rate. In addition, the possibility of the formation of a molybdenum nitride phase corresponding to $MoN_{0.68}$ was reported.

Boudart et al.[9] reported a temperature-programmed synthesis route for the reaction of MoO_3 and NH_3 to prepare Mo_2N powders with a surface area in excess of 220 m^2/g. The product consisted of highly porous nitride platelets, pseudomorphous with the original MoO_3.

VANADIUM OXIDES

In this study, the reactions of V_2O_5, VO_2, and V_2O_3 with ammonia to form vanadium nitrides were investigated. The results show that for each reaction, the starting oxide first reduces to lower oxides before forming the nitride product. The structures of these oxides and their relationship to each other are important in understanding these reactions and are described in the following section.

Phase Diagram of V-O System

There are several vanadium oxide compounds, as illustrated by Figure 2.10[62]. This phase diagram shows that the highest vanadium oxide is vanadium pentoxide, V_2O_5. In this study, vanadium pentoxide can be considered as the starting compound from which all other reactants can be derived.

Vanadium pentoxide, V_2O_5, has a layered structure similar to molybdenum trioxide. The structure is built up from distorted trigonal bipyramidal coordination polyhedra of oxygen atoms around vanadium atoms, in which four oxygens lie very nearly in a plane perpendicular to a considerably shorter V-O bond. The polyhedra share edges to form zigzag double chains along the [001] direction; this is shown in Figure 2.11. These chains are cross-linked along the [100] direction through shared corners to form sheets or layers in the xz plane[63]. Vanadium pentoxide crystallizes in an orthorhombic

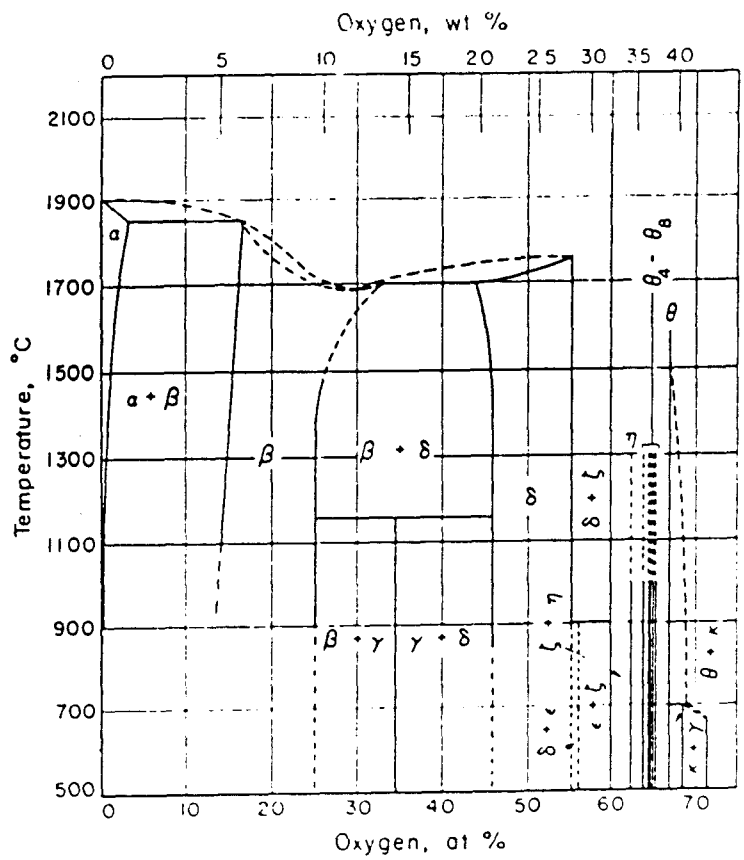

Legend:

α	$VO_{0.00}$-$VO_{0.01}$	ε	$VO_{1.27}$	θ_5	V_5O_9
β	$VO_{0.18}$-$VO_{0.33}$	ζ	V_2O_5	θ	VO_2
γ	$VO_{0.53}$	η	V_3O_5	κ	V_6O_{13}
δ	$VO_{0.85}$-$VO_{1.24}$	θ_n	V_nO_{2n-1}	λ	$VO_{2.47}$-$VO_{2.5}$

Figure 2.10. Vanadium-Oxygen phase diagram[62].

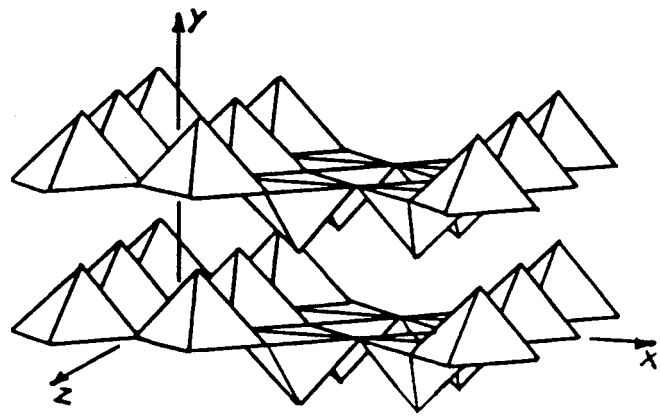

Figure 2.11. Structure of vanadium pentoxide, V_2O_5[63].

crystal structure with unit cell dimensions a=11.510 Å, b=3.559 Å, and c=4.371 Å [64].

Reduction of Vanadium Pentoxide

Vanadium pentoxide will reduce to form several lower vanadium oxides. Isothermal studies on the reduction of vanadium pentoxide V_2O_5 by hydrogen showed that V_2O_5 was directly reduced to V_2O_3 at temperatures above 500°C[65]. However, non-isothermal investigations showed that the reduction of V_2O_5 to V_2O_3 in H_2 occurs in several steps, as illustrated by temperature-programmed reduction (TPR)[66]:

$$V_2O_5 \text{ ===> } V_6O_{13} \text{ ===> } VO_2 \text{ ===> } V_2O_3$$

The actual temperatures at which these transitions occured depended upon flow rate, heating rate and sample weight. The apparent activation energy of 200 kJ mol^{-1} indicates that solid-state diffusion influences the reduction process of V_2O_5 in H_2.

Vanadium dioxide, VO_2, formed during the reduction of vanadium pentoxide, is isomorphous with molybdenum dioxide. The crystal structure of vanadium dioxide is monoclinic with a=5.743 Å, b=4.517 Å, c=5.375 Å and β=122.61°[67].

A second product of the reduction of vanadium pentoxide by hydrogen is vanadium sesquioxide, V_2O_3. Vanadium sesquioxide is isomorphous with corundum, α-Al_2O_3, in which the oxygen positions approximate hexagonal close packing, with trivalent cations occupying two thirds of the octahedral interstices[68]. Figure 2.12 shows this crystal structure. The structure

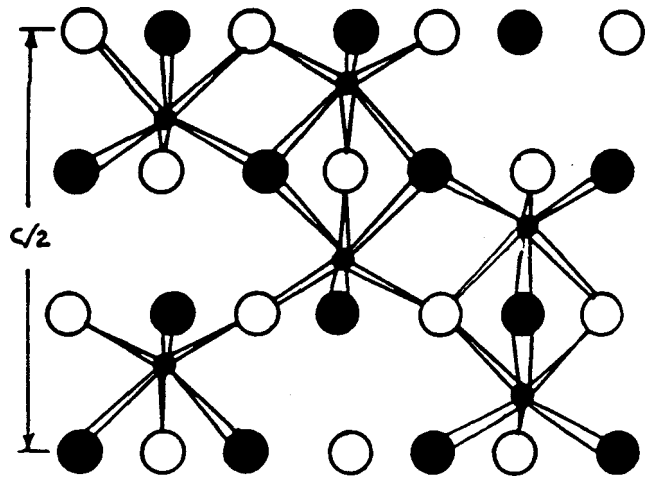

oxygen atoms in z=+1/2 plane

oxygen atoms in z=-1/2 plane

metal atoms

Figure 2.12. Structure of vanadium sesquioxide, V_2O_3[68].

contains VO_6 octahedra that share one face and three edges with other octahedra. The oxygen ions are coordinated by four cations. The cations across the shared octahedral face, however, are distorted[69], resulting in a hexagonal unit cell with a=4.952 Å and c=14.002 Å[68].

Intercalation of Vanadium Pentoxide

Like molybdenum trioxide, the layered structure of vanadium pentoxide can accomodate guest molecules between its layers. The compounds of most interest to this study are the hydrogen vanadium bronzes, which are analogous to the hydrogen molybdenum bronzes. Hydrogen vanadium bronze, $H_xV_2O_5$ where $0<x\leq3.77$, is an insertion compound of hydrogen within the vanadium pentoxide host lattice. The hydrogen is inserted topotactically over the range $0<x\leq0.55$ to form a dark-green phase with lattice parameters little changed from those of the parent V_2O_5[70-71]. The infrared absorption spectrum shows that the hydrogen is attached in -OH groups to the oxide matrix. For $x>0.55$, a number of black phases are formed. Two monophasic ranges have been proposed: $1.32<x<2.0$ and $x>3.0$[72]. For $x>1.0$, there is evidence for the formation of V-OH_2 groups from inelastic neutron scattering studies[73]. For $x>3.0$, amorphous products result, implying that considerable structural rearrangement of the V_2O_5 lattice has taken place[74].

Reactions with Ammonia

Vanadium pentoxide reacts with ammonia and water vapor at room temperature to form ammonium metavanadate, NH_4VO_3[75], which is stable in

air at room temperature. The structure of ammonium metavanadate is characterized by a VO_3^- chain extended along the c-axis, as depicted in Figure 2.13. The chain is formed by corner sharing of VO_4^{3-} tetrahedra, and these chains are linked by ammonium ions. The NH_4^+ coordination is 6-fold through hydrogen bonding with oxygen atoms of adjacent chains[76]. The unit cell is orthorhombic with a=4.96 Å, b=11.82 Å, and c=5.63 Å.

At elevated temperatures, ammonium metavanadate decomposes to form a product that depends upon the composition of the gas phase. In air or an inert atmosphere, the product is vanadium pentoxide, while lower oxides are formed in a reducing atmosphere[77-78]. Decomposition in ammonia leads to the formation of vanadium nitride[79-80].

The thermal decomposition of ammonium metavanadate, NH_4VO_3, to form vanadium pentoxide, V_2O_5, has been investigated by several authors[75,81-88], but there is no general agreement on the actual course of the reaction under a variety of atmospheres. During the decomposition in air, Taniguchi and Ingraham[85] obtained an intermediate product at 220°C with the empirical formula of ammonium hexavanadate, $(NH_4)_2V_6O_{16}$ (often represented as the "trivanadate", $NH_4V_3O_8$). Trau[81-82] determined from TGA that an intermediate corresponding to $(NH_4)_2V_4O_{11}$, ammonium "bivanadate", is formed at lower temperatures (<180°C); this decomposes (<210°C) to give the hexavanadate:

$$4\ NH_4VO_3 \text{ ===> } (NH_4)_2V_4O_{11} + 2\ NH_3 + H_2O$$

$$3\ (NH_4)_2V_4O_{11} \text{ ===> } 2\ (NH_4)_2V_6O_{16} + 2\ NH_3 + H_2O$$

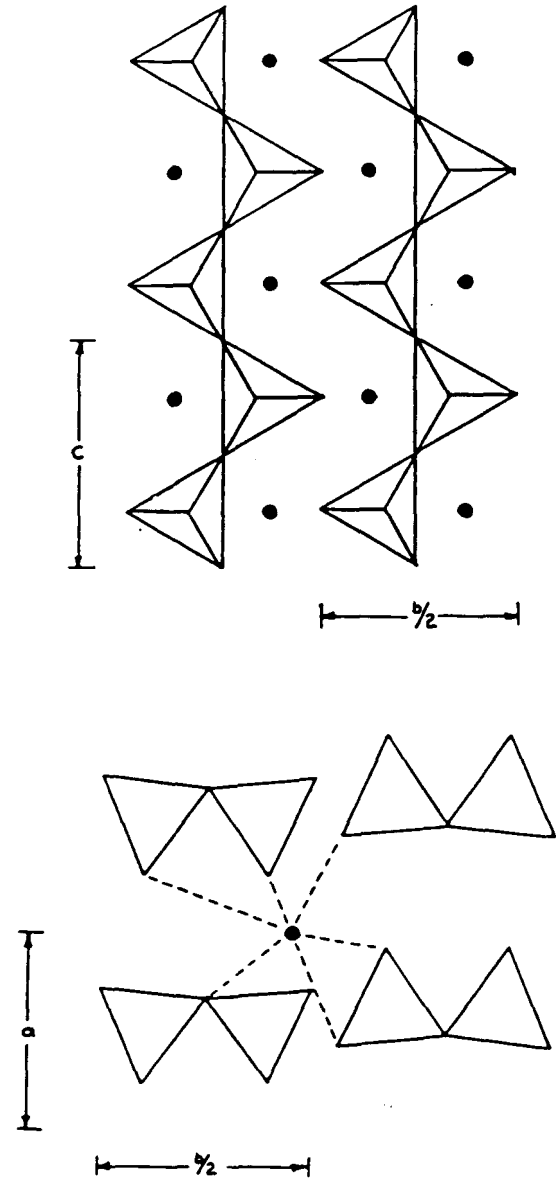

Figure 2.13. Structure of ammonium metavanadate, NH_4VO_3[76].

Finally, above 300°C

$$(NH_4)_2V_6O_{16} \text{ ===> } 3\ V_2O_5 + 2\ NH_3 + H_2O$$

Lamure and Colin[83] found that the bivanadate is only formed with small sample masses, slow heating rates and rapid removal of product gases. Selim et al[75] obtained an intermediate which was a hydrated form of vandium pentoxide, $3V_2O_5 \cdot H_2O$, formed from the decomposition of the trivanadate at 300°C. This hydrated vanadium pentoxide decomposed above 340°C to give V_2O_5.

Controversy over the nature of the final solid product of the decomposition of ammonium metavanadate has arisen largely from the differences in the reaction conditions, such as heating rate and surrounding atmosphere. Vanadium pentoxide is thought to be formed first, but if the gaseous products (NH_3, H_2O) are allowed to accumulate in large samples, or if the sample is heated in a reducing atmosphere such as NH_3 or H_2, lower oxides may be formed[77-78]. When ammonium metavanadate is heated in a stream of ammonia at temperatures form 500° to 1500°C, the products are very dependent on the temperature[79-80]. For example, at 500°C, the main product is V_2O_3, but above 600°C the nitride VN is formed. The proposed reaction pathway is

$$NH_4VO_3 \text{ ===> } V_2O_5 \text{ ===> } VO_2 \text{ ===> } V_2O_3 \text{ ===> } VO \text{ ===> } VN$$

After the formation of vanadium pentoxide, the reaction pathway is the same as the reduction of vandium pentoxide by ammonia, as previously described. The VN product contains some residual oxygen incorporated into the lattice, of which the amount decreases with increasing temperature[86]. At temperatures above 1000°C, pure VN is formed[79-80].

The intermediate compound ammonium hexavanadate, $(NH_4)_2V_6O_{16}$, has been reported by most authors to be the only stable ammonium polyvanadate[89]. It may be thought of as a structural derivative of vanadium pentoxide since the vanadium pentoxide structure is an essential part of its structure[90]. The structure is built up from highly distorted VO_6 octahedra linked together by sharing corners and edges into a layered structure, as shown in Figure 2.14[91]. The structure is monoclinic, with a=7.63 Å, b=8.43 Å, c=4.97 Å and β=96.75°, and has been shown to be isostructural with $K_2V_6O_{16}$, $Rb_2V_6O_{16}$, and $Cs_2V_6O_{16}$[92].

The presence of ammonium bivanadate $(NH_4)_2V_4O_{11}$ has been suggested as a second intermediate during the thermal decomposition of ammonium metavanadate NH_4VO_3 based on TGA results[81-83]. This compound has not been isolated and its structure has not been determined.

At temperatures above 300°C, the reaction of ammonia with vanadium pentoxide results in the formation of several reduced oxide species, followed by the formation of vanadium nitride, VN, above 600°C[79]. The reaction pathway is similar to the reduction of V_2O_5 to V_2O_3 in H_2, except the intermediate V_6O_{13} is not observed[95]. The vanadium nitride formed contains residual

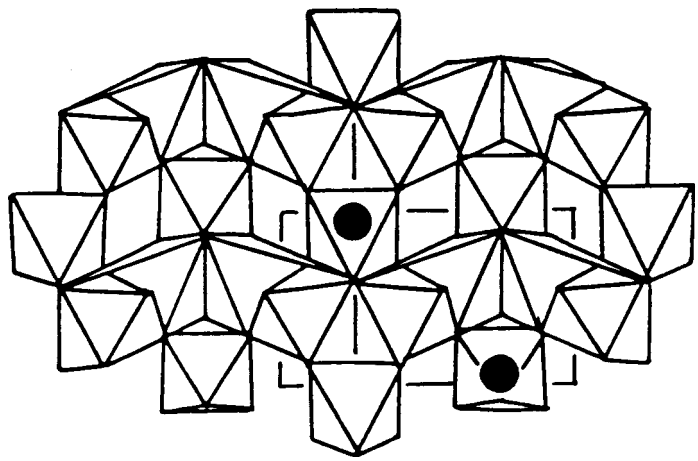

● NH_4^+ Ions

Figure 2.14. Structure of ammonium hexavanadate, $(NH_4)_2V_6O_{16}$[91].

oxygen; the amount of oxygen decreases with increasing temperature. Pure vanadium nitride is obtained at temperatures above 1000°C[78].

The vanadium nitride system contains two phases; the hexagonal β-phase at a composition of about V_2N, and the mononitride δ-phase with the NaCl (cubic close-packed) structure, as shown in Figure 2.15. The δ-phase has a stoichiometry range of $VN_{0.71-0.74}$ to $VN_{1.00}$[94-96], while the β-phase has homogeneity limits which are more uncertain ($VN_{0.35-0.40}$ to $VN_{0.43-0.49}$)[95-96].

The β-V_2N phase is hexagonal with the nitrogen atoms arranged in octahedral sites; the arrangement of the nitrogen atoms is of the ε-Fe_2N type, and is depicted in Figure 2.16[97]. The lattice parameters at the nitrogen-rich phase are a=4.910 Å and c=4.541 Å[95]. The lattice parameter varies linearly, from a=4.1398 Å to a=4.0662 Å for $VN_{1.00}$ to $VN_{0.72}$, respectively[94].

The contamination of VN with bulk oxygen, which results in a solid solution of VN-VO, has been shown to affect the lattice parameter of the cubic unit cell[98-99]. The crystal structure of VO, like VN, is cubic close-packed, with a=4.08 Å. In the VN lattice the oxygen atoms substitute for the nitrogen atoms; the slight difference in size between the nitrogen and oxygen atoms are reflected in the linear variation of the lattice parameter from 4.08 to 4.14 Å for the compounds VN_xO_{1-x} as x increases from 0 to 1.0[99].

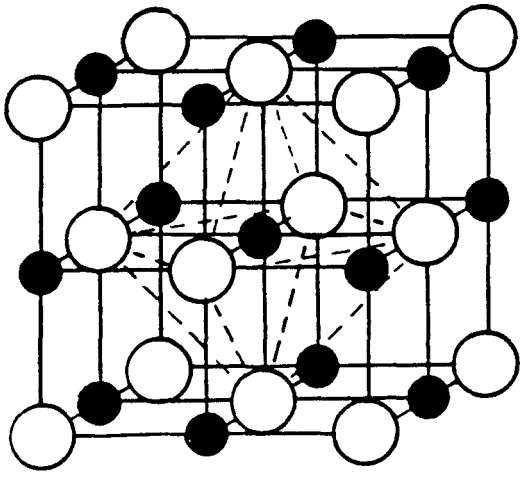

Figure 2.15. Structure of δ-VN.

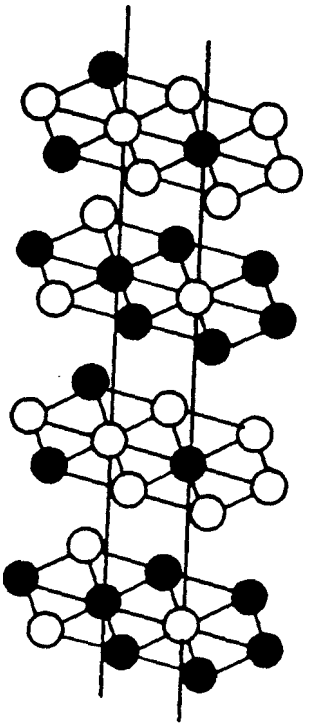

Figure 2.16. Nitrogen arrangement in β-V_2N[97].

Chapter 3. Experimental

In this study, thermogravimetric analysis (TGA) was used to monitor the reactions under investigation. The structures of the starting materials, reaction intermediates, and final products were determined by powder X-ray diffraction; powder patterns of the reaction intermediates were obtained in situ as the reactants were exposed to NH_3 at various temperatures. The surface areas of the reactants and products were measured using the BET method. In addition, the surface areas of the intermediates were measured as a function of temperature to determine which reaction steps contribute to the observed increase in surface area.

MATERIALS

Many of the materials used were purchased and used directly from the bottle without further purification: molybdenum trioxide MoO_3 (99.998%), vanadium (IV) oxide VO_2 (99+%), vanadium sesquioxide V_2O_3 (95+%), and vanadium monoxide VO (99%) were purchased from Alfa Chemicals; ammonium paramolybdate $(NH_4)_6Mo_7O_{24}\cdot 4H_2O$ (99.999%) and ammonium metavanadate NH_4VO_3 (99.995%) were purchased from Mallinckrodt, Inc.; and vanadium pentoxide V_2O_5 (99.995%) was purchased from Johnson Matthey

Chemicals. The other materials used for this study were synthesized by the procedures described below.

Molybdenum Trioxide

In addition to the molybdenum trioxide sample purchased from Alfa Chemicals, a molybdenum trioxide sample was synthesized using the method described by Fransen[100]. A 5-g sample of ammonium paramolybdate $(NH_4)_6Mo_7O_{24}\cdot 4H_2O$ was dissoved in 1/3 liter of distilled water at room temperature. Addition of 2/3 liter of acetone yielded a precipitate which was dried at 100°C for 18 hrs. This procedure produced anhydrous ammmonium molybdate $(NH_4)_6Mo_7O_{24}$, which was subsequently heated in air at 330°C for 24 hrs to form MoO_3 with a BET surface area of 5.2 m^2/g. This sample was designated MoO_3-AM.

Diammonium Molybdate

Diammonium molybdate, $(NH_4)_2MoO_4$, was synthesized by exposing MoO_3-AM to liquid ammonia in a dry ice-acetone bath for four hours or to gaseous ammonia at 25°C for one week. During the latter reaction, the sample weight was monitored using the Cahn RG microbalance. The final weight change corresponded to the uptake of two moles of NH_3 and one mole of H_2O. No H_2O was added to the NH_3 since the tank of high purity ammonia (Matheson, 99.99%) was contaminated with enough water to produce the desired product. The x-ray powder pattern showed that the final product was

homogeneous. It was not possible to obtain elemental analysis for $(NH_4)_2MoO_4$ because it rapidly lost ammonia upon exposure to air.

Hydrogen Molybdenum Bronzes

A series of molybdenum oxide hydroxides, or hydrogen molybdenum bronzes, of the general formula $MoO_{3-x}(OH)_x$ (or H_xMoO_3) were prepared by the reduction of MoO_3 with Zn metal and HCl as originally described by Glemser et al[30-33]. Approximately 1-5 g of MoO_3 was placed in 50-200 ml of 5.0N HCl. The Zn metal was added slowly; the amount of zinc used was based on the color of the final product, which is a rough indicator as to the amount of hydrogen uptake in the molybdenum trioxide. Once the desired product was obtained, the solution was filtered and the resulting powder was washed with water to remove zinc ions. The final product was then dried with a vacuum filter and allowed to dry completely overnight.

Hydrogen Vanadium Bronzes

Several hydrogen vanadium bronzes of the general formula $H_xV_2O_5$ were prepared using the hydrogen spillover method[73]. Samples of V_2O_5 were treated with an aqueous solution of chloroplatinic acid and dried under vacuum to yield samples containing about 2% by weight of acid. The samples were oxidized at 400°C for 4 hours to form PtO_2. On exposure to hydrogen at 90°C, the platinium oxide was reduced to Pt, which subsequently catalyzed the insertion of hydrogen into the oxide lattice.

TGA APPARATUS

A schematic flow diagram of the apparatus used to conduct the TGA and the BET experiments is shown in Figure 3.1. The apparatus is divided into three sections: (1) the gas handling system, (2) the reactor/balance system, and (3) the data acquisition system. Each of these three sections are discussed in detail below.

Gas Handling

Gas selection was accomplished with a network of three-way valves and toggle valves, as shown in Figure 3.1. The ammonia flow rate was controlled using a Matheson Series 601 rotometer equipped with a high accuracy needle valve; the Viton o-rings and packings were replaced with Buna-N o-rings and packings since ammonia attacks Viton. All other gases were controlled using a 1/8-inch micro-metering needle valve and the flow rates were measured with a 25-cm^3 soap film flowmeter. Oxygen and water were reduced to below 1 ppm from the helium, nitrogen, and argon gas streams using Matheson Model 6406 disposible gas purifiers, while the ammonia gas stream was purified of water using a Matheson Model 450 gas purifier.

Reactor/Balance

The reactor/balance configuration used in the TGA system is shown in Figure 3.2. The balance used was a Cahn Recording Gram (RG)

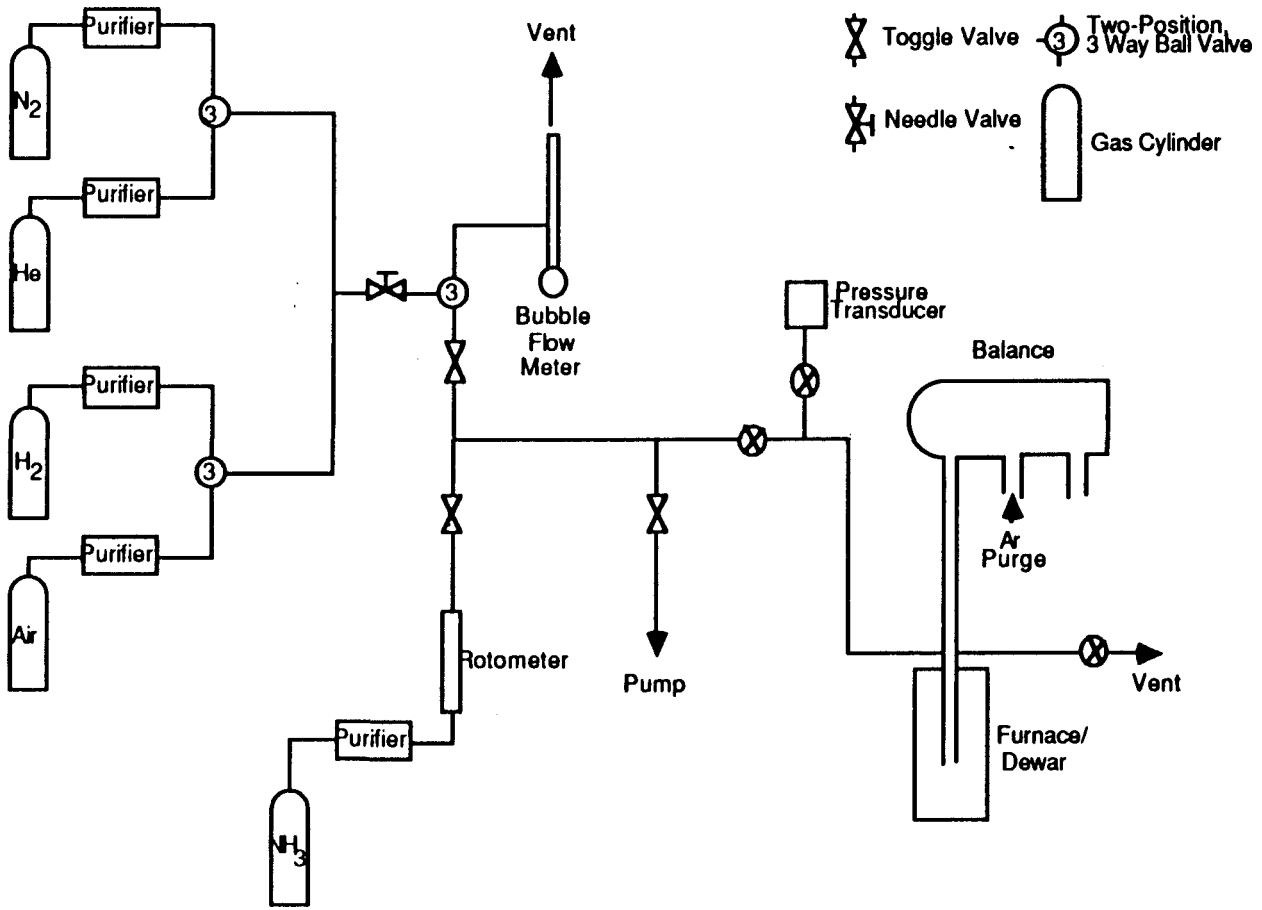

Figure 3.1: Flow diagram of the TGA/BET apparatus

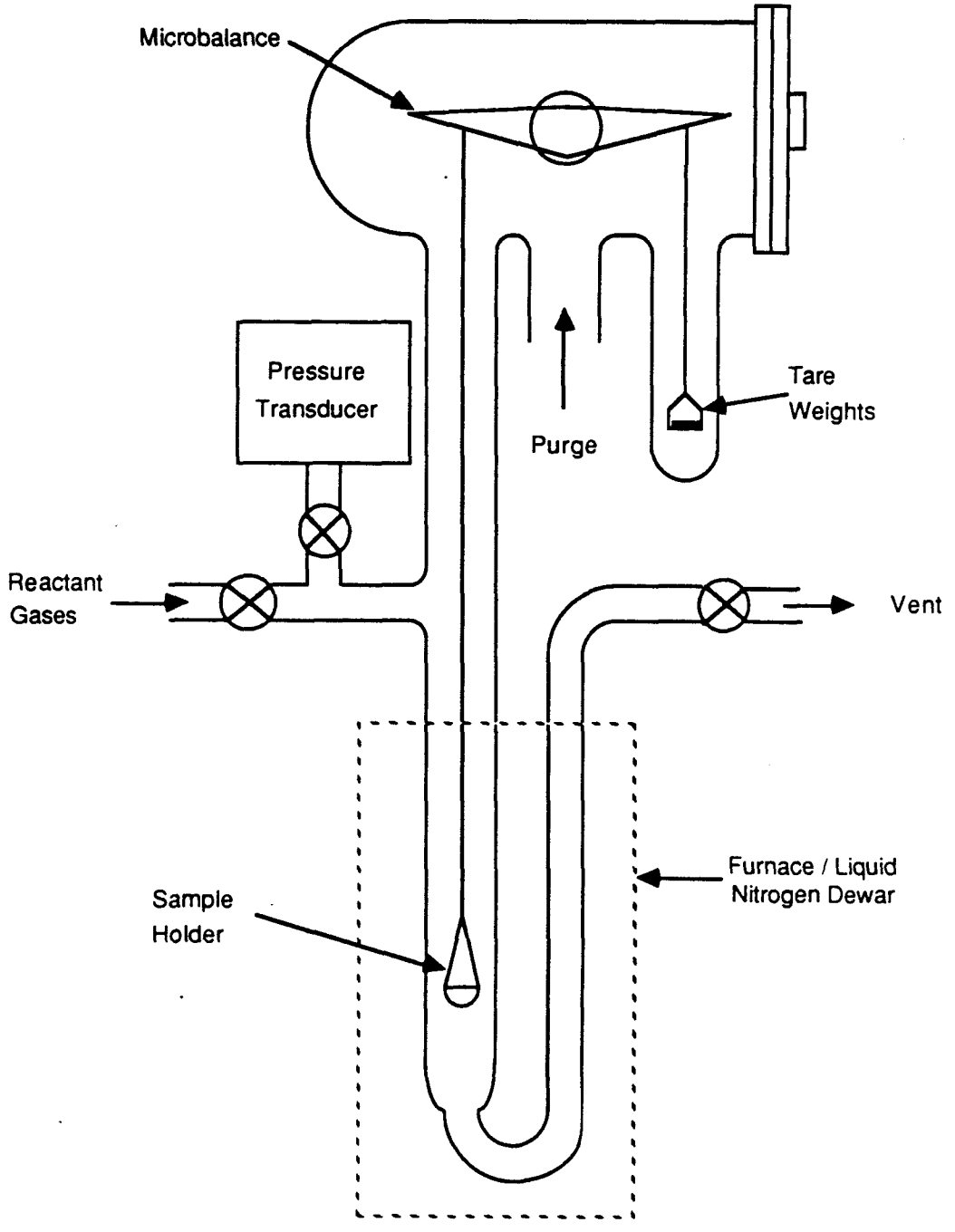

Figure 3.2. Schematic of TGA apparatus.

Electrobalance, a microbalance with a 2.5-g capacity and 10^{-7}-g sensitivity. The microbalance was housed in a Pyrex glass bottle. The bottle had a metal end cap with electrical feedthroughs and permitted operation of the balance in any controlled environment, including vacuum. The vacuum bottle was supported by a wood stand mounted to a rigid Unistrut structure. The wood stand was chosen for its ability to absorb minor vibrations that might induce error in the experimental measurements. An inlet for an argon purge stream was provided to protect the balance beam and weighing mechanism from corrosive gases during flow experiments.

The sample, in powdered form, was suspended in either an aluminum or quartz pan by a 30-cm long 0.1-mm diameter nichrome suspension wire. The quartz sample pan had a sample volume of 0.12 cm^3 and was used in experiments up to 1000°C. The aluminum sample pan had a larger sample volume of 0.28 cm^3, but the maximum operating temperature was limited by its melting point 660°C. The temperature of the sample was measured with a 60-cm- long sheathed chromel-alumel thermocouple, placed so that its tip was approximately 5 mm from the sample.

The sample was suspended in a 30-mm-o.d. flow-through reactor tube. The effluent gas line was designed to exit the furnace at the top, so that the furnace could easily be raised and lowered around the sample. The reactor tube was constructed of quartz with quartz-to-pyrex seals located near the teflon valves at both the inlet and exit gas lines. These valves allowed the sample to be isolated and maintained in a desired environment. In addition, a Type 600

Barocel Pressure Transducer with a 0-1000 Torr range was located at the inlet gas line.

To minimize the effect of static electricity, which can disturb the weight measurements by attraction between the reactor tube and the sample holder, the outside of the reactor tube was cleaned with Memorex X-PRF Anti-Static Record Cleaning Solution. In addition, the inside of the reactor tube was cleaned throughly with acetone after each experiment.

The furnace was constructed using a 2-3/8-inch-i.d. Thermocraft ceramic heater wired to a 110-volt source. The furnace was rated at 615 Watts and had a maximum temperature of 1200°C. An 8-inch-o.d., 9-1/2-inch-long galvanized steel cylinder housed the heater unit, and the furnace was supported with a standard laboratory jack with which it was raised and lowered around the reactor tube. A liquid nitrogen dewar could also be raised around the reactor tube and supported by a standard laboratory ring stand, thus allowing the sample to be cooled with liquid nitrogen for BET surface area measurements.

The furnace temperature was controlled with a Model 2010 LFE programmable temperature controller which was capable of ramping the temperature linearly in time up to 900°C at rates ranging from 0.005°C/s to 1°C/s. A variac was placed between the furnace and the controller to allow better control of the furnace temperature, thereby minimizing temperature overshoots at low temperatures. The control thermocouple (sheathed, ungrounded chromel-alumel) was placed between the reactor tube and the furnace elements; this thermocouple responded much faster to changes in the power input and was therefore used for feedback to the controller. Due to the

time lag associated with heat transfer through the reactor wall and to the sample, the thermocouple used for monitoring the sample temperature would create oscillations in the heating rate if it were used as the control thermocouple.

Data Acquisition

The output signals from the microbalance control unit and the Omega Model 660 digital thermometer were digitized with a Labmaster 12-bit A/D converter linked to a Fountain Turbo-XT computer; the overall system configuration is shown in Figure 3.3. Data aquisition was controlled with Hart Scientific "Q.E.D." data acquisition software. This program controlled the A/D converter, stored and displayed the data, and provided routines for rudimentary manipulation of data. Further details of the program are provided in Appendix A.

XRD

The system used for the X-ray diffraction experiments is depicted in Figure 3.4. The x-ray diffractometer used was a Picker Model 3488, capable of scanning at angles between 10^{o} and 90^{o} relative to the surface of the sample. The diffractometer used Cu-K radiation with an average wavelength of 1.5418

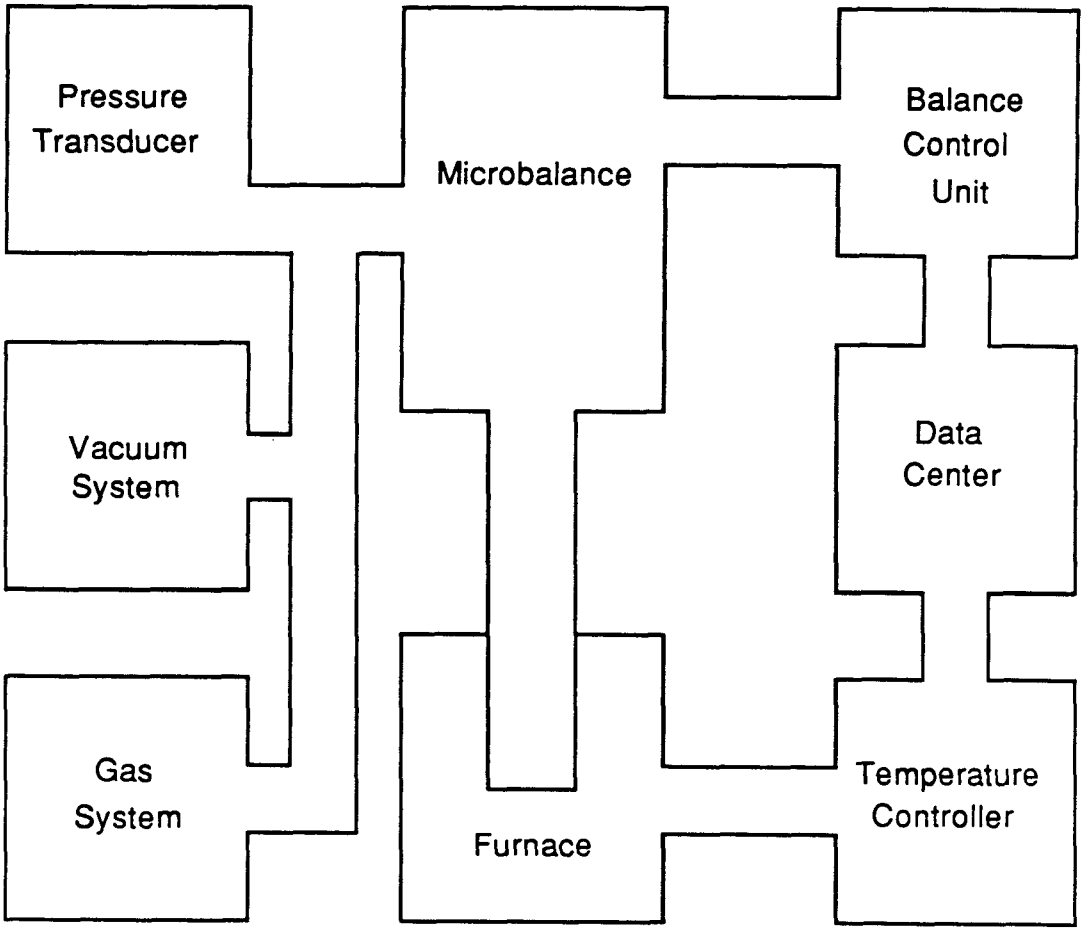

Figure 3.3. System configuration of theTGA/BET apparatus.

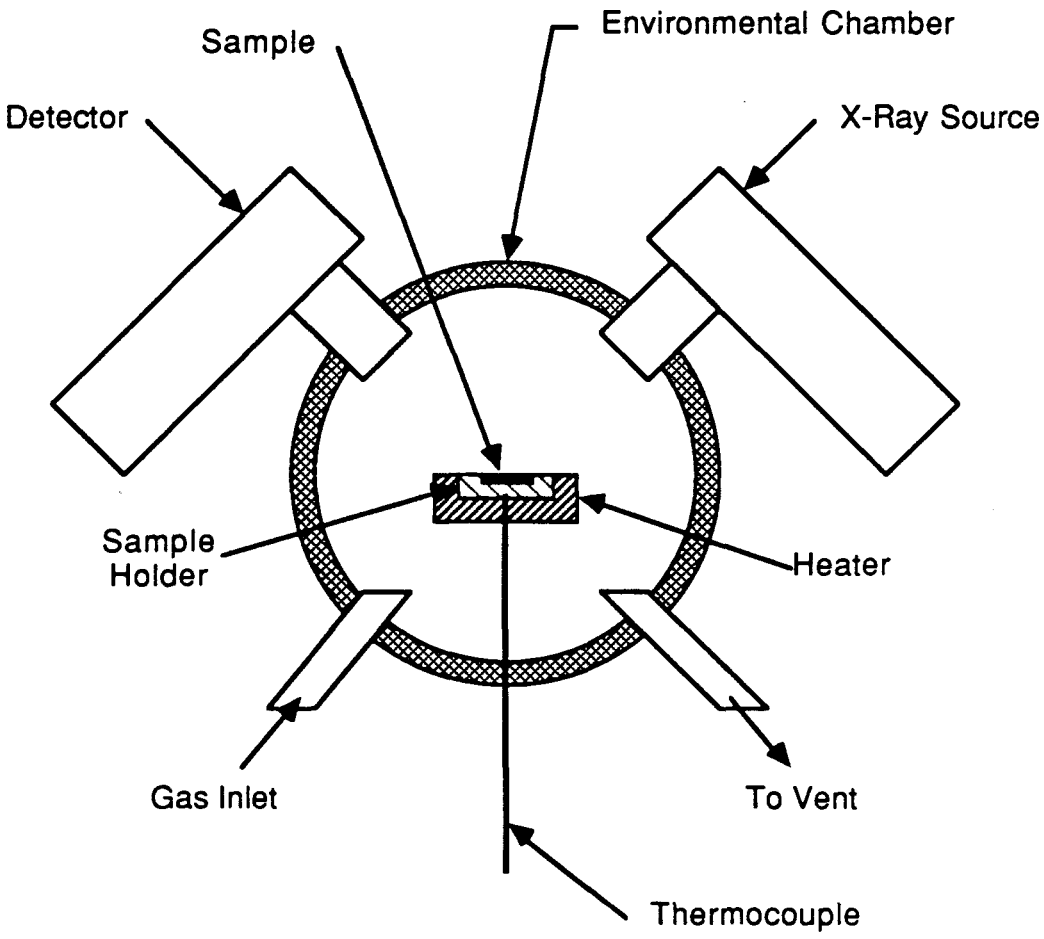

Figure 3.4. Diagram of XRD apparatus with hot-stage and environmental chamber.

angstroms. Diffraction patterns were recorded as intensity verses angle on a strip chart recorder.

The XRD apparatus was equipped with an environmental cell and sample heater which allowed the collection of diffraction patterns of the sample at elevated temperatures in controlled environments. The sample was placed in an aluminum sample holder located in the center of the ceramic heater. This heater was capable of raising the sample temperature to 1000^{o}C, although the experiments used in this study were limited by the melting point of the aluminum sample holder, 660^{o}C. The sample holder was positioned so that it was in direct contact with the chromel- alumel thermocouple but was not in contact with the heater element. Cooling water lines surrounded the chamber, allowing the selective heating of the sample. A leak-tight seal was provided by a viton o-ring at the front of the chamber. Power to the heater was controlled by a Model 2010 LFE programmable temperature controller which could raise the temperature of the sample as fast as 1^{o}C/min. The power to the furnace was fed through a variac to allow better control of the furnace temperature.

Water was removed from the ammonia gas using a Matheson Model 450 gas purifier. The ammonia flow rate was adjusted using a needle valve, and tygon tubing was used as the connection lines between the gas cylinder and the environmental chamber, and from the chamber to an existing vent duct.

Scanning Electron Microscopy (SEM)

Scanning electron microscopy, or SEM, was performed on several samples using a AMR 50 microscope made available through Lawrence

Berkeley Laboratory. Typical maginifications used for this study were 1000 to 5000x, although the equipment was capable of 20,000x.

Elemental Analysis

Elemental analyses of the reactants and products for nitrogen, hydrogen, carbon, and transition metals were performed by the Microanalytical Lab at the Department of Chemistry, University of California, Berkeley. Nitrogen, hydrogen, and carbon compositions were determined using a combustion method and analyzing the effluent gas. Transition metal analysis was performed by atomic adsorption.

The elemental analysis of the nitride products were influence by the adsorption of water and ammonia. During the cooling of the products in ammonia, an increase in weight of 1-5 wt% was observed, presumably due to the adsorption of ammonia. Additionally, the nitrides were air- and water-sensitive; upon exposure to air, a weight increase as high as 10 wt% was observed for some samples due to the adsorption of water and/or oxygen. These effects were highest for the high surface area samples. Therefore, elemental analysis was only used as a qualitative tool; the product compositions were determined from the final TGA weight and XRD.

EXPERIMENTAL PROCEDURE

TGA Experiments

A 50 to 200 mg sample was loaded into the sample pan and the sample chamber was either evacuated to 10^{-1} Torr or flushed with helium or nitrogen. The desired gas was subsequently flowed over the sample, while the temperature was raised linearly at 0.5-5°C/min; typical flow rates were 100-200 cm^3/min at STP. For the reactions with ammonia, a gas flow rate of 150 cm^3/min at STP and a heating rate of 1°C/min were used. During the reaction, both the sample weight and chamber temperature were monitored continuously. The sample was held at the final reaction temperature to insure complete reaction of the sample.

All the TGA data are expressed as weight per mole of metal atoms in the starting material. This normalization is convenient for two reasons. First, the normalized weight of a given intermediate does not depend on the gross or molecular weight of the starting material. Thus two TGA spectra coincide when two reactions yield the same product. Also, the normalized weight change between plateaus in a TGA spectrum can be related easily to the molecular weight of the species which are lost or gained during the reaction. For example, loss of one mole of NH_3 per mole of molybdenum in the sample results in a reduction of the normalized weight by 17 g/mol.

TGA spectra are also displayed in differential form, as differential thermograms (DTG). Maxima in a DTG correspond to inflection points in the corresponding TGA spectrum, at which the mass changes most rapidly.

Therefore, a DTG is more sensitive to changes in reaction rate than a TGA spectra.

BET Measurements

Measurement of the surface area of the sample was performed using the BET method[101] by nitrogen adsorption at 77.4 K. The sample was first evacuated to a pressure of 10^{-1} Torr and the weight of the sample was recorded. Next, the sample was cooled with liquid N_2 to 77.4 K. After sufficient time had elapsed for the sample temperature to equilibrate (typically 15-30 minutes as determined by the stability of the sample weight), a known pressure of nitrogen was introduced into the sample chamber. The sample gained weight as nitrogen was adsorbed; a constant weight was achieved after approximately 15 minutes. The sample weight and system pressure were recorded and the nitrogen partial pressure was increased for a second measurement for nitrogen partial pressures between 0.05 and 0.35 atm. The number of moles of nitrogen that were adsorbed at a given pressure was calculated from the weight change of the sample. The surface area of the sample was calculated using the BET equation and a nitrogen cross-section value of 0.162 nm^2. Buoyancy effects on the sample weight as the total pressure of the system was increased were significant for samples with low surface areas (<2 m^2/g) but were insignificant for samples with surface areas in excess of 10 m^2/g.

The evolution of surface area during reaction was determined by interrupting a TGA experiment at a particular temperature, cooling the sample

rapidly in flowing ammonia, and measuring the surface area by nitrogen adsoprtion at 77 K. Following the adsorption measurement, the sample was reheated in flowing ammonia to the previous reaction temperature, and the TGA experiment was continued to a higher temperature. This procedure was repeated at 25-100^{o}C intervals.

High Temperature (Hot-Stage) XRD Experiments

The structures of reaction intermediates were determined by high temperature X-ray diffraction. A sample was loaded into the aluminum sample holder and placed into the ceramic heater located in the environmental chamber of the X-ray diffractometer. The temperature was raised linearly in time at 1^{o}C/min while the ammonia gas stream flowed over the sample. The temperatures at which reaction intermediates formed were determined from the TGA data, and XRD patterns were obtained at these temperatures. Due to temperature gradients in the sample, it was difficult to prepare single-phase intermediates at elevated temperatures. Several intermediates were usually present, which neccessitated a series of XRD patterns over a temperature range to determine the order of formation of the phases. After the sample reached the desired temperature, the sample was allowed to equilibrate for 30 minutes. An X-ray pattern was obtained over the range of 10-80^{o} at a scan rate of 1^{o}/min. Upon completion of the scan, the sample temperature was raised to the next temperature of interest and the procedure was repeated. An X-ray diffraction pattern of the final product was obtained after allowing the sample to react at a final temperature of 625^{o}C for 12 hours.

Chapter 4. Synthesis of Molybdenum Nitrides

The reactions of molybdenum trioxide MoO_3, molybdenum dioxide MoO_2, ammonium paramolybdate $(NH_4)_6Mo_7O_{24}\cdot 4H_2O$, and diammonium molybdate $(NH_4)_2MoO_4$ with ammonia have been studied. As shown in Table 4.1 these reactions form both MoN and Mo_2N, and the phase and surface area of the nitride is sensitive to the starting material. Molybdenum trioxide reacts to form high surface area Mo_2N, while diammonium molybdate forms low surface area MoN. Both molybdenum dioxide and ammonium paramolybdate form a mixture of Mo_2N and MoN; the mixture formed by molybdenum dioxide has a low surface area, while ammonium paramolybdate forms a high surface area mixture.

The reactions of these materials with ammonia have been studied using TGA/DTG, high temperature XRD, BET surface area analysis, and SEM. It is shown below that molybdenum trioxide, ammonium paramolybdate, and diammonium molybdate all form the same oxynitride precursor to the nitrides; however, each compound produces different intermediates prior to forming this oxynitride. In each reaction, the precursor to the oxynitride is a layered material,; this species controls the surface area and the phase of the nitride product. In contrast, molybdenum dioxide does not form an oxynitride precursor to the nitride product and produces only a mixture of low surface area MoN and Mo_2N.

Starting Material	Final Product	Final Surface Area (m^2/g)
MoO_3	Mo_2N	57.2
MoO_2	Mo_2N + MoN	6.3
$(NH_4)_6Mo_7O_{24}\cdot 4H_2O$	Mo_2N + MoN	56.9
$(NH_4)_2MoO_4$	MoN	16.5

Table 4.1. Product of reactions of ammonia with molybdenum oxides and ammonium molybdates.

REACTION NETWORKS - FORMATION OF OXYNITRIDE INTERMEDIATE

Molybdenum Trioxide

Molybdenum trioxide forms two intermediates in its reaction with ammonia to form molybdenum nitride. As shown by the TGA/DTG results in Figure 4.1, the reaction begins above 375°C and proceeds in tow steps at 460°C and 595°C, forming an intermediate at approximately 535°C. A smaller third DTG peak is present at 695°C. At 750°C, the final weight loss after several hours of reaction is 28.1%, very close to the theoretical weight loss of 28.5% expected for the formation of Mo_2N. High-temperature XRD indicates the presence of MoO_2 between 375 and 620°C; these data are summarized in Appendix C. Based on the thermogravimetric and XRD data, we propose that the reaction of MoO_3 with ammonia proceeds through the following reaction pathway:

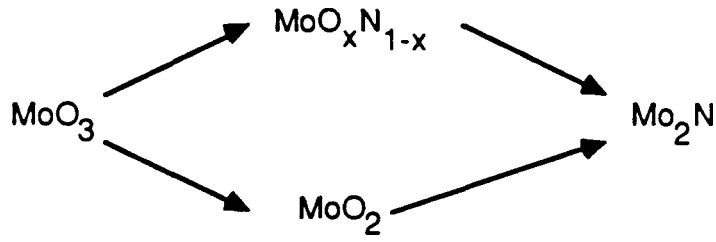

The high temperature XRD results presented in Appendix C indicate that the main reaction of MoO_3 with NH_3 to form Mo_2N is accompanied by a side reaction, the partial reduction of the trioxide to molybdenum dioxide. TGA of the

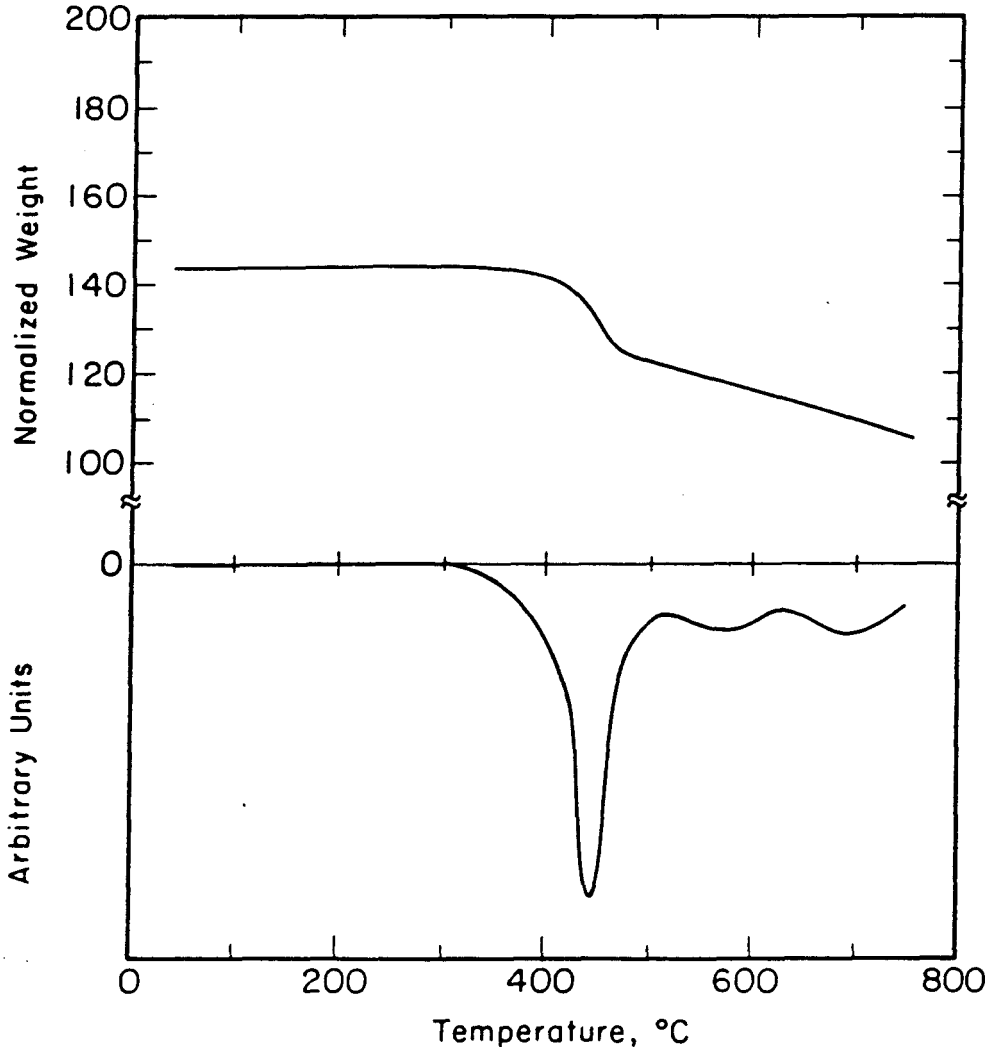

Figure 4.1 TGA/DTG of the reaction of molybdenum trioxide with ammonia (heating rate = 1°C/min, 150 cm^3/min NH_3 at STP).

direct reaction of MoO_2 with ammonia, presented in Figure 4.2, shows that MoO_2 does not begin to lose weight until 688°C, and continues to lose weight appreciably at the final reaction temperature of 750°C. XRD shows that the final product is a mixture of Mo_2N and MoN. This shows that MoO_2 converts directly to a nitride product, and suggests that the high-temperature DTG peak in Figure 4.1 corresponds to the nitridification of MoO_2. Therefore, DTG peaks in the MoO_3/NH_3 reaction below 688°C are not produced by reaction of MoO_2, and molybdenum dioxide plays only a spectator role at temperatures below 688°C.

The intermediate formed at 535°C is a mixture of MoO_2 and a fcc compound, as shown by the XRD patterns in Appendix C. This fcc phase could be Mo_2N or the oxynitride MoO_xN_{1-x}. From the TGA weight at 625°C, the amount of MoO_2 formed through the side reaction can be calculated to be approximately 15 wt%. Back-calculation of the sample composition at 535°C shows that the fcc intermediate still contains oxygen. The reaction of this oxynitride to form the nitride is represented by the DTG peak at 595°C; MoO_2 does not react with ammonia until above 688°C. For this reason, it is concluded that MoO_3 forms a fcc oxynitride intermediate prior to forming fcc Mo_2N.

The formation of an oxynitride intermediate is consistent with the results of Lyutaya[60], who determined the activation energies of formation of MoO_xN_{1-x} and Mo_2N for the MoO_3/NH_3 reaction. The formation of the oxynitride has a lower energy of activation (16.8 kcal/mole) than the activation energy for the formation of the nitride Mo_2N (22.2 kcal/mole), which indicates

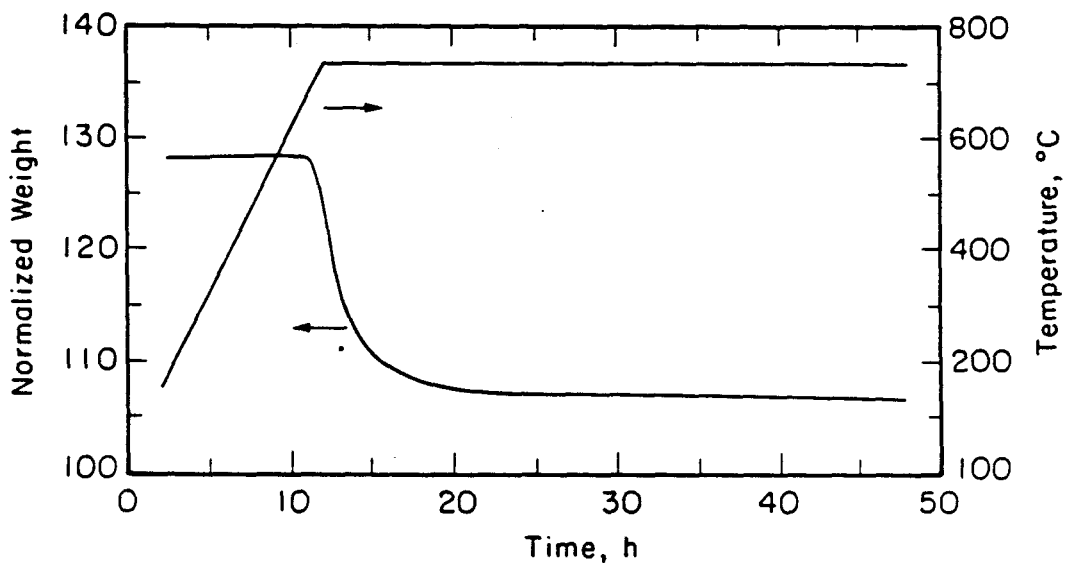

Figure 4.2. TGA of the reaction of molybdenum dioxide with ammonia (heating rate = 1°C/min, 150 cm^3/min NH_3 at STP).

that at lower temperatures the formation of an oxynitride intermediate should be favored over the nitride.

Diammonium Molybdate

Diammonium molybdate, $(NH_4)_2MoO_4$, reacts with ammonia through a different reaction pathway than molybdenum trioxide yet still forms the same fcc-oxynitride MoO_xN_{1-x} as a precursor to the nitride product. The TGA/DTG results shown in Figure 4.3 indicate a reaction pathway with four reaction steps, resulting in the formation of three reaction intermediates. These steps are represented by DTG peaks at 150, 210, 305, and 350°C, while intermediates I, II, and III are formed at 165, 225, and 330°C, repectively. The normalized weights of intermediates I, II, and III to the starting material are 165.83, 162.10, and 126.04, respectively, while the final weight of 108.00 is close to the theoretical value of 109.96 for a pure MoN product. Based on the TGA/DTG and high-temperature X-ray diffraction results, the following reaction pathway is proposed:

$$(NH_4)_2MoO_4 \text{ ====> } (NH_3)_{0.23}H_2MoO_4 \text{ ====> } MoO_3{\cdot}H_2O$$

$$\text{====> } MoO_xN_{1-x} \text{ ====> } MoN$$

The intermediates formed during the reaction of $(NH_4)_2MoO_4$ with NH_3 were identified using powder X-ray diffraction at reaction temperatures and are listed in Table 4.2. The weight loss at 225°C, which is associated with the first

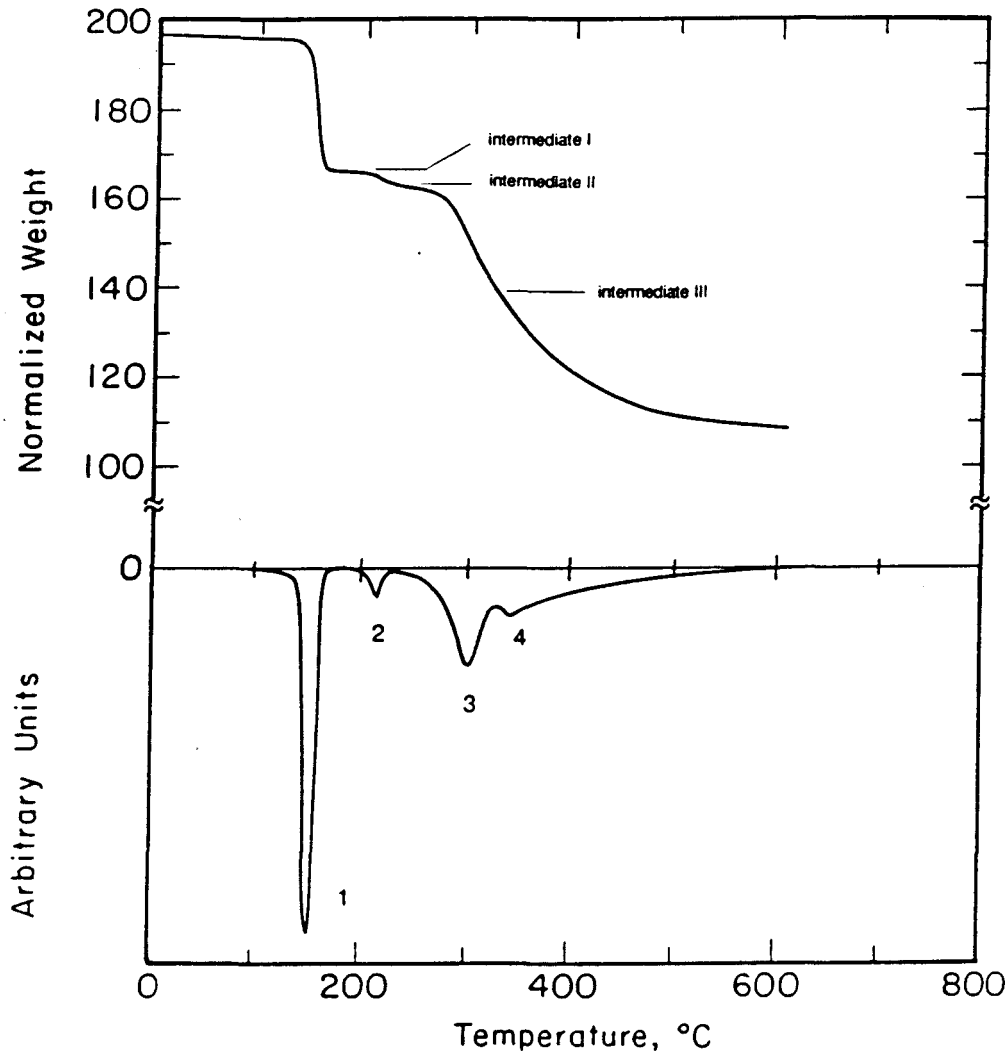

Figure 4.3. TGA/DTG of the reaction of diammonium molybdate with ammonia (heating rate = 1°C/min, 150 cm^3/min NH_3 at STP).

Intermediate	XRD Structure	TGA Temp, ^{o}C	Normalized Wt Actual	Theor.
I	*	165	165.83	----
II	$MoO_3 \cdot H_2O$	225	162.10	161.95
III	MoO_xN_{1-x}	330	----	----

* No XRD pattern was obtained for this intermediate, but its stoichiometry was determined from its weight to be $(NH_3)_{0.23}MoO_3 \cdot H_2O$.

Table 4.2. Proposed reaction intermediates in the reaction of diammonium molybdate with ammonia.

two reaction steps, corresponds to the loss of two moles of NH_3 per mole of $(NH_4)_2MoO_4$. The X-ray diffraction patterns at both 175°C and 275°C are a mixture of those of the starting material, $(NH_4)_2MoO_4$, and H_2MoO_4. An XRD pattern of the first intermediate formed was not obtained; it is possible that the material is amorphous. Above 245°C, the H_2MoO_4 reacts to form intermediate III, which exhibits diffraction lines which are characteristic of the fcc structure; this intermediate could be either MoO_xN_y or Mo_2N. However, the weight loss is not sufficient to be Mo_2N. Since the intermediate is single phase and still contains oxygen, it is concluded that this is the fcc oxynitride MoO_xN_{1-x}. The XRD of the final product indicates that it is hexagonal MoN.

Ammonium Paramolybdate

The reaction of ammonium paramolybdate, $(NH_4)_6Mo_7O_{24}\cdot 4H_2O$, with ammonia involves a more complex reaction pathway. This reaction is complicated by the sequential loss of ammonia and water in several steps. However, the same fcc-oxynitride intermediate is formed as the precursor to the nitride product, similar to the molybdenum trioxide and diammonium molybdate reactions with ammonia.

The reaction involves seven reaction steps, represented by DTG peaks at 120, 155, 175, 220, 275, 370, and 500°C; the TGA/DTG results are shown in Figure 4.4. This results in the formation of six intermediate phases at 140, 165, 185, 245, 300, and ~450°C. Identification of these intermediates was made using high temperature XRD and/or TGA intermediate weights; the XRD results are presented in Appendix C, while the intemediates are listed in Table 4.3.

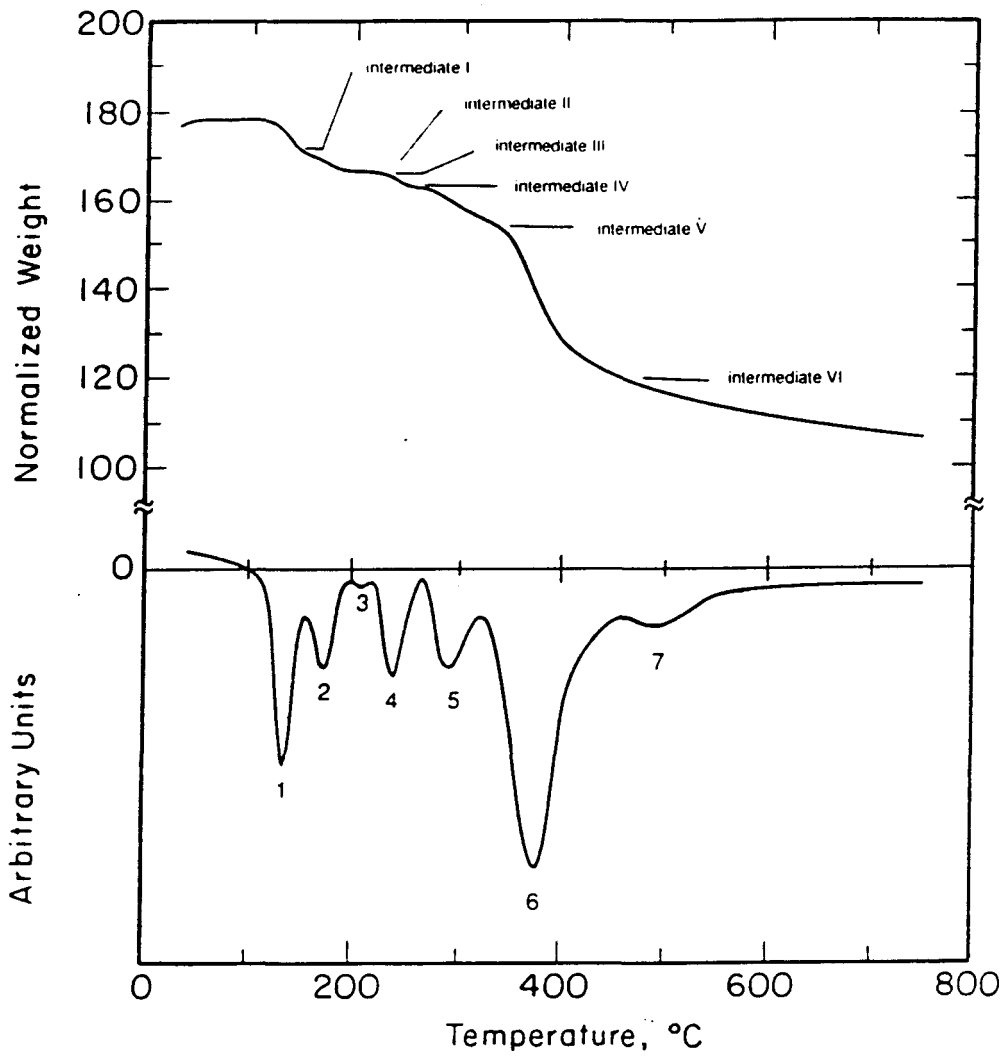

Figure 4.4. TGA/DTG of the reaction of ammonium paramolybdate with ammonia (heating rate = 1°C/min, 150 cm^3/min NH_3 at STP).

Intermediate	XRD Structure	TGA Temp, °C	Normalized Wt Actual	Theor.
I	$(NH_4)_6Mo_7O_{24}\cdot 2H_2O^*$	140	171.96	171.43
II	$(NH_4)_6Mo_7O_{24}$	165	165.96	166.31
III	$(NH_4)_8Mo_{10}O_{34}$	185	164.72	164.72
IV	$(NH_4)_2O\cdot 3MoO_3$	245	160.13	161.37
V	$(NH_4)_4Mo_8O_{26}$	300	156.78	156.95
VI	MoO_xN_{1-x}	450	----	----

* Not identified by XRD but proposed based on its weight.

Table 4.3. Proposed reaction intermediates for the reaction of ammonium paramolybdate with ammonia.

Based on these results, the following reaction pathway is proposed:

$$(NH_4)_6Mo_7O_{24}\cdot 4H_2O \text{ ====> } (NH_4)_6Mo_7O_{24}\cdot 2H_2O \text{ ====> } (NH_4)_6Mo_7O_{24}$$

$$\text{===> } (NH_4)_2O\cdot 2.5MoO_3 \text{ ====> } (NH_4)_2O\cdot 3MoO_3 \text{ ====>} (NH_4)_2O\cdot 4MoO_3$$

$$\text{====> } MoO_xN_{1-x} \text{ ====> } MoN + Mo_2N$$

The failure of x-ray diffraction to confirm the presence of the dihydrate, $(NH_4)_6Mo_7O_{24}\cdot 2H_2O$, is probably due to the overlap of the two weight loss steps, indicating that a stable intermediate with uniform composition is not formed. The TGA/DTG results, however, do suggest the formation of the dihydrate intermediate; the DTG clearly shows the presence of two reaction peaks before the formation of intermediate II, and the weight loss associated with the minimum between these peaks is consistent with the weight loss expected for the formation of the dihydrate. TGA and XRD confirm that the starting material loses four water molecules to form intermediate II, $(NH_4)_6Mo_7O_{24}$. This loss of water in two equal steps at 120°C and 155°C agrees with previous reports that two of the four water molecules of hydration act as a "bridge" between a pair of ammonium ions lying between adjacent heptamolybdate ions. The other two water molecules are situated elsewhere, each bonded to a pair of cations, and are not as strongly bonded in the structure[40]. This loss of water in two stages was also observed for potassium

heptamolybdate tetrahydrate, $K_6Mo_7O_{24}\cdot 4H_2O$, which is isomorphous with ammonium paramolybdate[40].

After the initial loss of the four water molecules of hydration, the reaction proceeds through several molybdate intermediates. This reaction pathway is similar to the polycondensation reactions observed for the decomposition of several molybdates to form molybdenum trioxide[42-53]; the sample loses ammonia and water simultaneously in the ratio 2:1[49]. The two ammonia and one water molecules have been shown to be bonded together as $(NH_4)_2O$ groups between the heptamolybdate ions in ammonium paramolybdate[40]. The final molybdate structure detected before the formation of the oxynitride intermediate is ammonium octamolybdate, $(NH_4)_4Mo_8O_{26}$. In comparison, when ammonium paramolybdate decomposes in air, it does not lose the four waters of hydration in a separate series of reactions; rather, it decomposes directly to ammonium decamolybbdate, $(NH_4)_6Mo_{10}O_{34}$, which is the third intermediate formed in the reaction with ammonia[53].

Above 325°C, $(NH_4)_4Mo_8O_{26}$ reacts to form a fcc crystal structure before hexagonal MoN is formed. Although the proposed fcc oxynitride MoO_xN_{1-x} has the same X-ray diffraction pattern as the fcc nitride Mo_2N, the temperature at which this intermediate is detected by XRD corresponds to a sample weight which is much too high for the bulk of the sample to be Mo_2N. It is therefore concluded that the intermediate still contains oxygen. As the temperature is increased, the sample loses weight continuously. At temperatures above 625°C, the hexagonal hcp MoN phase is present in the XRD patterns.

CONTROL OF NITRIDE PHASE

The reactions of molybdenum trioxide, ammonium paramolybdate, and diammonium molybdate react to form different nitride phases or mixtures of phases, although each reaction involves the same fcc oxynitride intermediate. The temperature at which this oxynitride is formed, however, depends on the reaction pathway and in particular on the oxynitride precursor. Since in each case the oxynitride reacts readily to form the nitride product, it is the temperature of formation of the oxynitride which influences the final nitride phase. Table 4.4 summarizes these results.

The temperature-dependence of the reaction of the oxynitride to form different nitride products is consistent with the results of Lyutaya[60]. He showed that the nitridification of activated Mo metal with ammonia at 450°C formed MoN, while reacting at 700°C formed Mo_2N. A similar trend is present in the nitridification of the fcc oxynitride: at 325°C, MoN is formed; at 535°C, Mo_2N is formed; and in betwwn a mixture of the nitrides is formed. Attempts to convert Mo_2N to MoN in ammonia from 450 to 750°C were unsuccessful. Additionally, the MoN product from the diammonium molybdate/ammonia reaction is not converted to Mo_2N at temperatures below 750°C. Therefore, the two nitrides must be produced from the oxynitride in parallel, with the relative rates of reaction depending upon the temperature.

The ratio of the two nitride phases in the final product depends upon the final reaction temperature, implying that the ratio of the two nitride phases can be controlled by altering this temperature. In the ammonium

Starting Material	Oxynitride Precursor	Oxynitride Formation Temp, ^{o}C	Ultimate Product
MoO_3	MoO_3	535	Mo_2N
$(NH_4)_6Mo_7O_{24}\cdot 4H_2O$	$(NH_4)_4Mo_8O_{26}$	450	Mo_2N + MoN
$(NH_4)_2MoO_4$	$MoO_3\cdot H_2O$	325	MoN

Table 4.4. Dependence of molybdenum nitride stoichiometry and phase on the precursor and formation temperature of the oxynitride intermediate.

paramolybdate/ammonia reaction, the XRD patterns of the nitride at final reaction temperatures of 625°C and 750°C contained both crystal structures, with the 750°C product containing a higher Mo_2N/MoN ratio than 625°C. Based on the final weights of the products, it can be calculated that the product at 625°C contained 32.1 mole% Mo_2N and 67.9 mole% MoN, while the product at 750°C contained 72.5 mole% Mo_2N and 27.5 mole% MoN. Also, the presence of a higher concentration of MoN in the product at 625°C is supported by the XRD data, based on the ratio of the [202] diffraction peak of MoN to the [200] peak of Mo_2N. These two peaks were chosen since they do not overlap, thereby presenting a fair representation of the relative (but not absolute) concentrations of the two phases. This ratio, $MoN_{[202]}/Mo_2N_{[200]}$, was 0.89 at 625°C and dropped to 0.32 at 750°C.

CONTROL OF SURFACE AREA

Influence of Oxynitride Formation

Figure 4.5 shows the development of the surface area during the reaction of these three starting materials with ammonia. In the reactions of molybdenum trioxide and ammonium paramolybdate with ammonia, the large increase in surface area occurs during the formation of the oxynitride. In the case of diammonium molybdate, which forms the same oxynitride intermediate, a low surface area product is formed (<20 m^2/g). The structure of the oxynitride

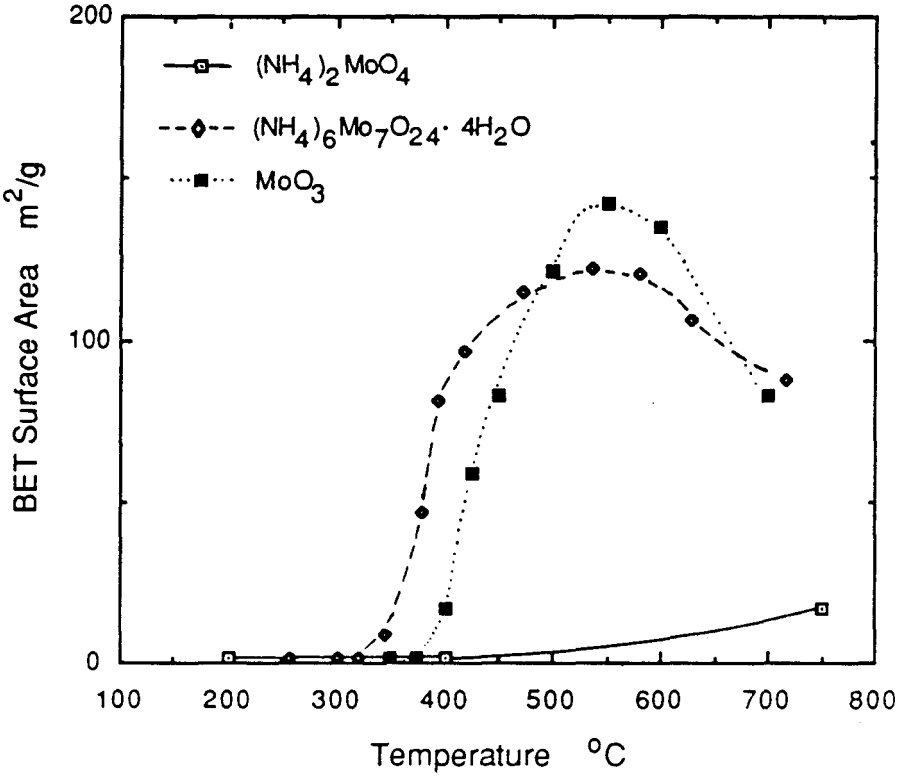

Figure 4.5. Surface area development during the synthesis of molybdenum nitrides from MoO_3, ammonium paramolybdate, and diammonium molybdate.

precursor appears to play a key role in the surface area development of the nitride product.

The BET isotherm indicates that the high surface area nitrides develop a pore structure. A typical BET isotherm is shown in Figure 4.6. This isotherm is best described as a type IV isotherm. The small type B adsorption-desorption hysteresis indicates the formation of a pore structure with slit-shaped pores or plate-like particles[9]. The oxynitride intermediates formed in the reactions of MoO_3 and the paramolybdate with ammonia also exhibit this hysteresis. From the SEM photographs, it was determined that the particle sizes remained constant for the high surface area nitrides.The large increase in surface area is therefore due to the development of a pore structure which occurs during the formation of the oxynitride.

Pseudomorphism of Reactants and Products

The high surface area nitrides formed from molybdenum trioxide and ammonium paramolybdate are both pseudomorphous with their starting materials. SEM photographs of ammonium paramolybdate and the nitride product in Figures 4.7 and 4.8 show that the product exhibited the same fracturing along layers which was present in ammonium paramolybdate, even though MoN is not a layered material. Previous studies of the molybdenum trioxide/ammonia reaction by Boudart[9] show that the final product also retains the particle morphology of the starting material. Although SEM photographs for diammonium molybdate could not be obtained due to loss of ammonia upon placement in the vacuum chamber, photographs of the nitride product were

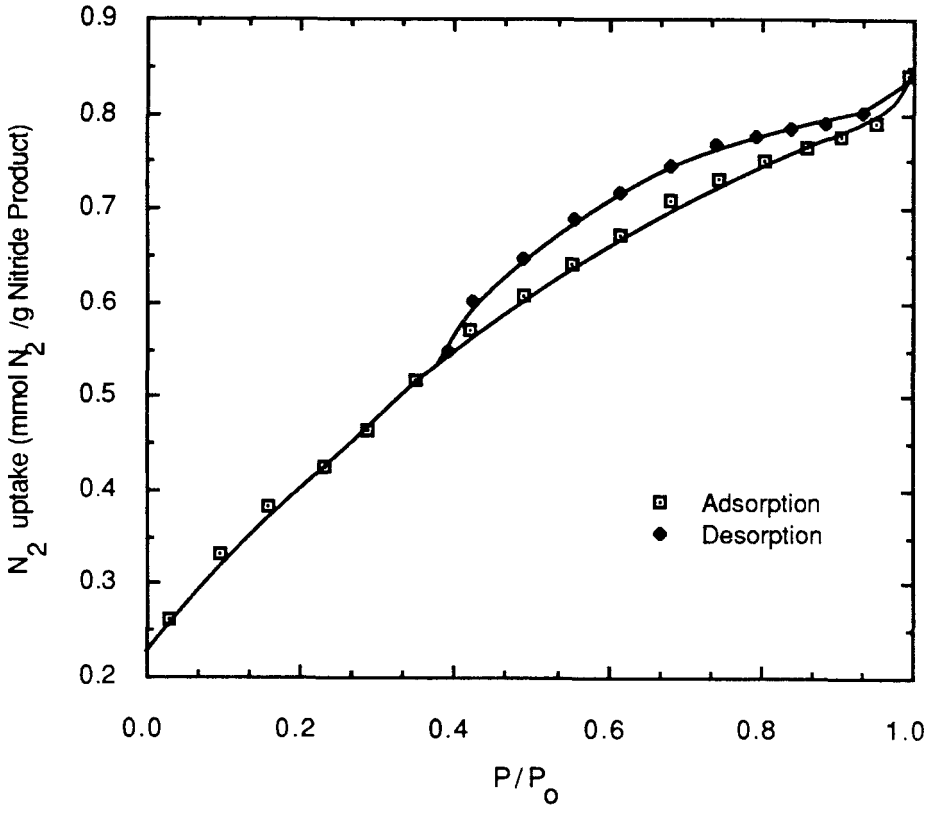

Figure 4.6. BET isotherm of the MoN/Mo_2N Mmxture formed by reacting ammonium paramolybdate with ammonia.

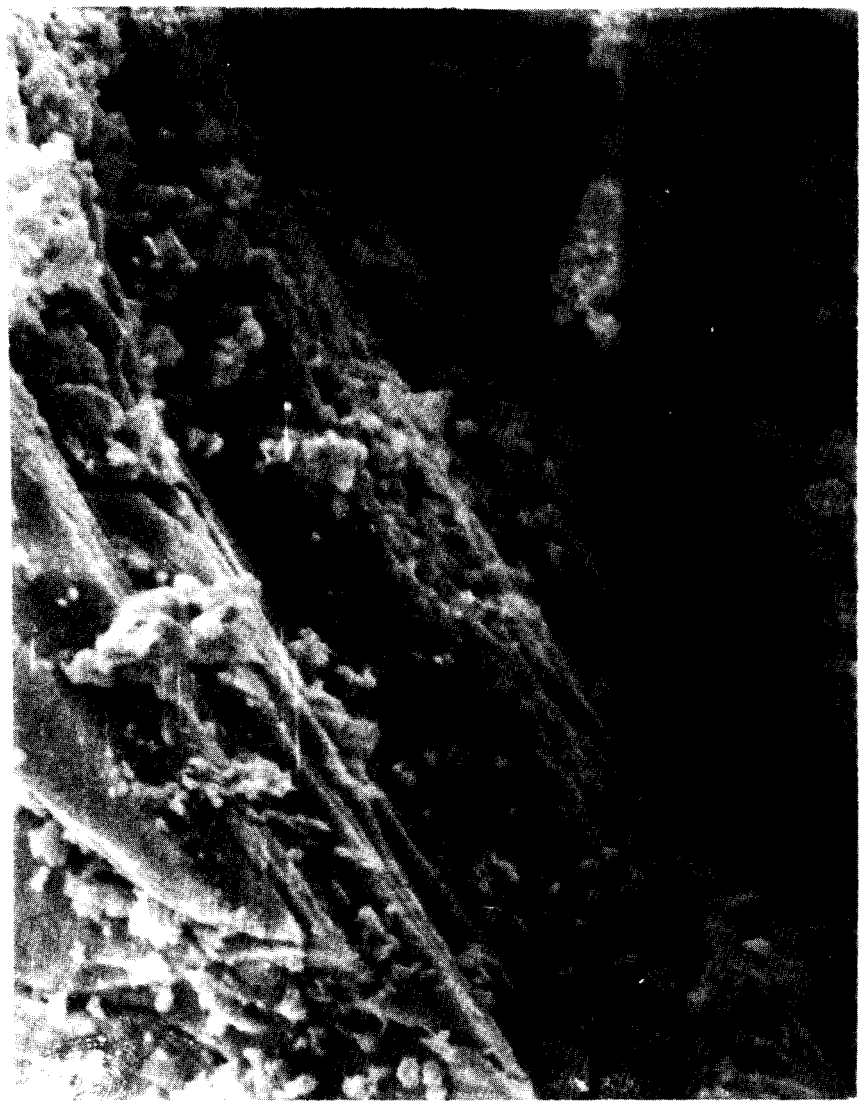

Magnification = 2000 X

Figure 4.7. SEM of Ammonium Paramolybdate.

Magnification = 2000 X

Figure 4.8. SEM of Product from Ammonium Paramolybdate/Ammonia Reaction.

obtained and are shown in Figure 4.9. By comparison to the high surface area nitrides, it is evident that the particles have totally different morphologies.

The pseudomorphism of the starting materials and the final products during the synthesis of molybdenum nitrides apparently contributes to the high surface area. During the reactions of molybdenum trioxide and ammonium paramolybdate with ammonia, the density of the sample increases 400-500%. However, the gross particle size and shape is unchanged. Therefore, these materials must develop cracks to accomodate this increase in density, and this forms the pore structures which are responsible for the increased surface areas observed in the BET isotherms. This pseudomorphism is due to a reaction mechanism in which the molybdenum atoms are constrained during formation of the oxynitride intermediate.

Previous work suggested that the reaction between MoO_3 and NH_3 is topotactic[9]. This is incorrect, as the bonding in MoO_3 is totally disrupted as it forms the nitride. However, topotacticity is not a necessary condition for surface area generation. The combination of pseudomorphism and a large increase in sample density appears to be sufficient to create a high surface area product.

In contrast to the results of molybdenum trioxide and ammonium paramolybdate, the reaction of diammonium molybdate with ammonia produces a low surface area nitride product (<20 m^2/g). The surface area generation is continuous during the development of the oxynitride and nitride phase, and there is no evidence of a pore structure in the BET isotherm. Comparison of the reactions of molybdenum trioxide and diammonium molybdate with ammonia shows several differences. First, the reaction of molybdenum trioxide is

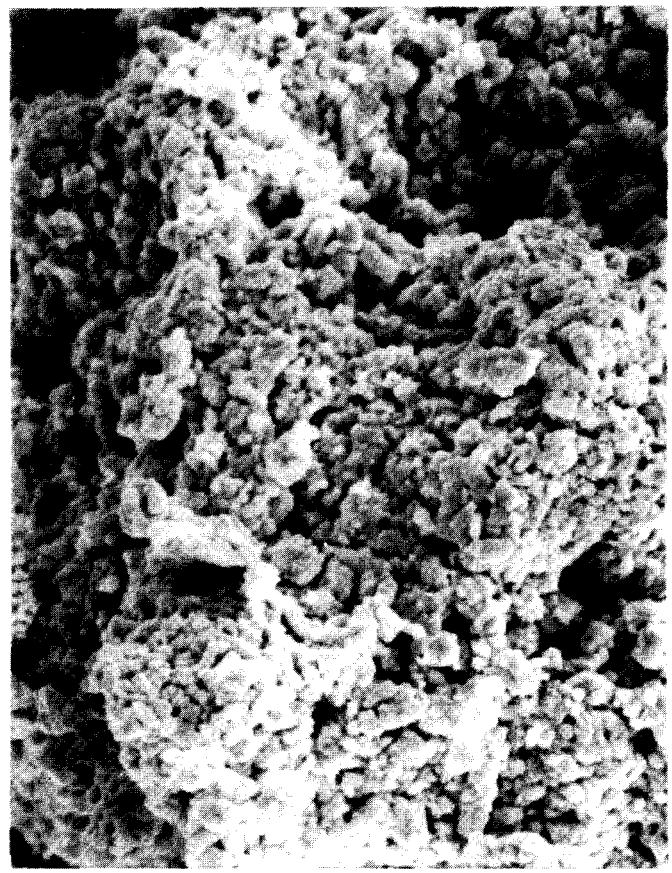

Magnification = 2000 X

Figure 4.9. SEM of MoN Product From Diammonium Molybdate/Ammonia Reaction.

pseudomorphous, while the reaction of diammonium molybdate is not. Secondly, the oxynitride precursors for the two reactions, MoO_3 and $MoO_3 \cdot H_2O$, differ in the structure of their layers; molybdenum trioxide consists of double-thick layers of MoO_6 octahedra held loosely together by Van der Waals interactions, while hydrated molybdenum trioxide has monolayers of MoO_6 octahedra. From this, it is speculated that the bilayers of molybdenum trioxide constrain the movement of the Mo atoms enough to produce a pseudomorphous transformation to a high surface area oxynitride. In contrast, the Mo atoms in the monolayers of hydrated molybdenum trioxide are not strongly constrained and can rearrange during the reaction to form a low surface area oxynitride.

The possibility that this low surface area results from hydrothermal sintering caused by the interlayer water molecules in the hydrated molybdenum oxide intermediate has been ruled out. Varying the flow rates and heating rates to reduce the gas-phase water concentration had no effect on the product surface area. In addition, the temperature region in which the oxynitride forms, 325-500^{o}C, is too low for hydrothermal sintering to result[102].

The reaction of molybdenum dioxide with ammonia involves a completely different reaction mechanism than molybdenum trioxide and the ammonium molybdates. Unlike these compounds, the dioxide does not intercalate or react with ammonia at low temperatures, nor does it form the oxynitride intermediate. Instead, it reacts directly to form the nitride at high temperatures. This is analogous to typical high temperature synthesis routes which yield low surface area products[8].

Maximum in Surface Area Generation

From Figure 4.5, it can be seen that the surface areas of the molybdenum trioxide and ammonium paramolybdate samples pass through a maximum at 550°C. The temperature dependence of the product surface area is listed in Table 4.5. The decrease in surface area is attributed to hydrothermal sintering at high temperatures, since water is formed as a product of these reactions. This conclusion is supported by the observation that if the heating rate is raised from 1°C/min to 5°C/min, the surface area of the products is dramatically reduced; increasing the heating rate increase the water production rate and should thereby accellerate sintering. Similarly, the surface area is flow rate dependent; it was neccessary to keep the ammonia flow rate high enough for water removal. This study did not quantify these effects, nor did it attempt to optimize the reaction conditions. Other authors discuss hydrothermal sintering[102], and Oyama et al[7] discuss the importance of superficial gas velocity in the synthesis of transition metal nitrides.

CONCLUSIONS

The synthesis of molybdenum nitrides from oxide and ammonium oxide precursors can be summarized as follows:

(1) An oxynitride intermediate MoO_xN_{1-x} with a fcc structure is formed during the reactions of molybdenum trioxide, ammonium paramolybdate, and

Starting Material	Oxynitride Precursor	$S_{g,max}$, T_{max} (m^2/g, ^oC)	$S_{g,final}$, T_{final} (m^2/g, ^oC)
MoO_3	MoO_3	141.9, 550	57.2, 750
$(NH_4)_6Mo_7O_{24}\cdot 4H_2O$	$(NH_4)_4Mo_8O_{26}$	132.4, 550	56.9, 750
$(NH_4)_6Mo_7O_{24}\cdot 4H_2O$	$(NH_4)_4Mo_8O_{26}$	132.4, 550	123.0, 625
$(NH_4)_2MoO_4$	$MoO_3\cdot H_2O$	—	16.5, 625
MoO_2	—	—	6.3, 750

Table 4.5. Temperature-dependence of product surface areas.

diammonium molybdate with ammonia; this oxynitride converts directly to the nitride product. In contrast, molybdenum dioxide reacts directly to form a molybdenum nitride product. It is the formation of this oxynitride intermediate which is important for the development of surface area; therefore, the structure of the oxynitride precursor is more important than the structure of the starting material in determining the surface area of the product.

(2) The temperature at which the oxynitride reacts to form the nitride determines the phase of the nitride: fcc Mo_2N is formed at temperatures higher than those at which hexagonal MoN is formed.

(3) The mechanisms of the reaction of molybdenum trioxide and ammonium paramolybdate with ammonia both involve constraint of the molybdenum atoms, resulting in pseudomorphous formation of nitrides with high surface areas. In contrast, the mechanisms for the reactions of diammonium molybdate and molybdenum dioxide with ammonia are significantly different, and result in low surface area nitrides.

(4) The surface area of the product is influenced by the final reaction temperature due to hydrothermal sintering at the higher temperatures.

Chapter 5. Synthesis of Vanadium Nitride

Like molybdenum trioxide, vanadium pentoxide is a layered material with the layers held loosely together in comparison to the intralayer bonding[63]; it also reacts with ammonia to form ammonium metavanadates[76,89-92]. The previous chapter showed that layering and NH_3 "mobility" is important as it allows for lower reaction temperatures and is apparently necessary for generation of high surface area nitrides. For this reason, the reaction of ammonia with vanadium oxides was studied to determine whether the results in Chapter 4 can be generalized to other transition metals.

This chapter investigates the reactions of ammonium metavanadate NH_4VO_3, vanadium pentoxide V_2O_5, vanadium dioxide VO_2, and vanadium sesquioxide V_2O_3 with ammonia to form vanadium nitride, VN. The reactions were monitored using TGA/DTG, and the products were analyzed for surface area, structure, and composition. The weights of the intermediates during the TGA experiments were compared to known intermediate compounds and previous studies on these reactions; a detailed study of the reaction intermediates, however, was not performed since other authors have already studied these reaction steps[65-66,79,81-88].

REACTION NETWORKS - REDUCTION TO LOWER OXIDES

The reactions of V_2O_5, VO_2, and V_2O_3 with ammonia involve the formation of lower oxide intermediates before forming a similar oxynitride product, VO_xN_{1-x}. Ammonium metavanadate, NH_4VO_3, loses all of its ammonia in two steps before decomposing through several vanadium oxide intermediates, followed by the formation of a similar oxynitride product. In all of the reactions, it is the oxide V_2O_3 which nitrides to form the product. These reactions are discussed in greater detail below.

Vanadium Pentoxide

The reaction of vanadium pentoxide with ammonia involves four reaction steps with the formation of three reaction intermediates, as illustrated in Figure 5.1. The DTG peaks associated with these reaction steps are present at 371, 401, 468, and 578°C. Based on the TGA intermediate weights, the reaction intermediates were identified; a summary of these results are presented in Table 5.1. The XRD pattern of the final product indicated a cubic structure which could be either VO or VN; the lattice parameters obtained from the pattern were between the two values of the pure components, indicating a solid solution of both VO and VN. Also, the final TGA weight indicated that the product still contained oxygen. From these results, it is concluded that the reaction proceeds through the following pathway:

$$V_2O_5 \text{ ====> } V_4O_9 \text{ ====> } VO_2 \text{ ====> } V_2O_3 \text{ ====> } VO_xN_{1-x}$$

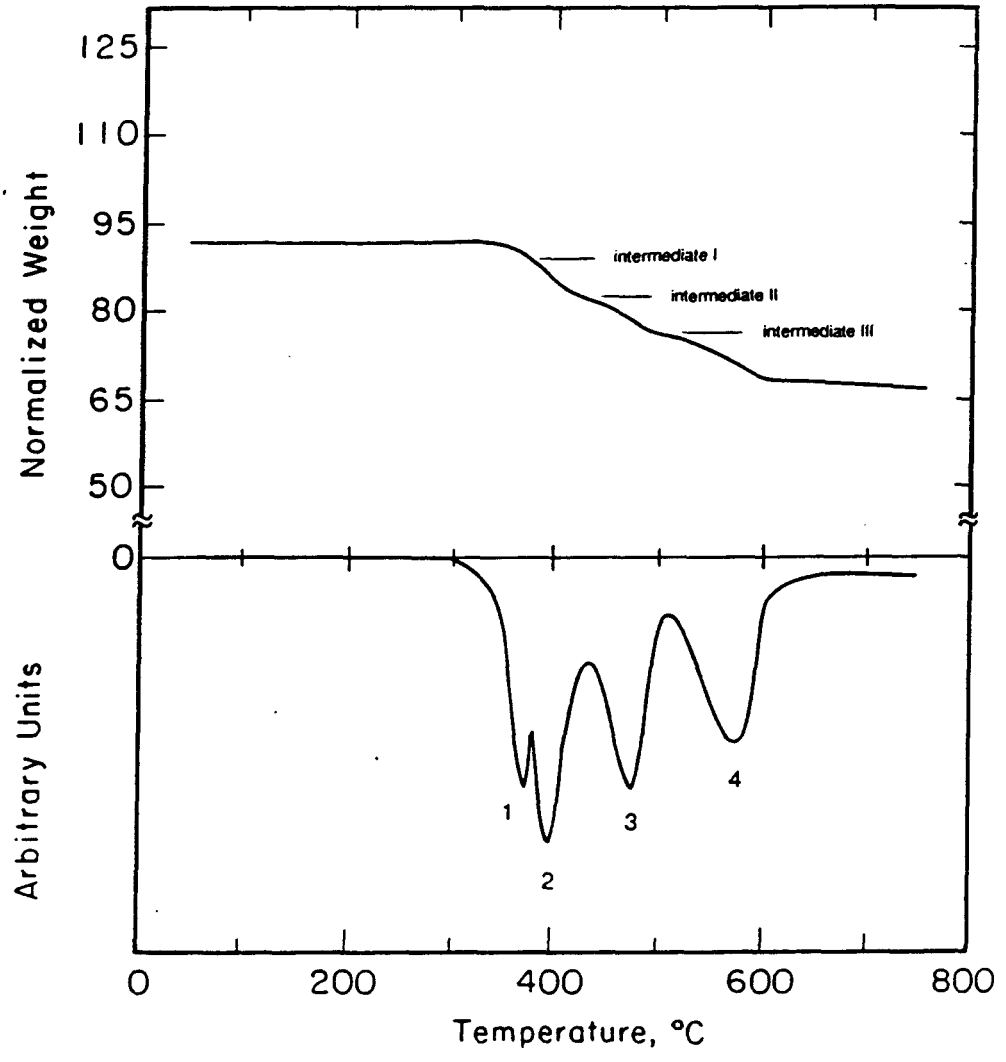

Figure 5.1. TGA/DTG of the reaction of vanadium pentoxide with ammonia (heating rate = 1°C/min, 150 cm^3/min NH_3 at STP).

Starting Material	Proposed Reaction Intermediate	Normalized Wt Theoretical	Actual
V_2O_5	V_4O_9	86.94	87.39
	VO_2	82.94	81.39
	V_2O_3	74.93	75.48
V_2O_4	V_2O_3	74.98	75.64
NH_4VO_3	$(NH_4)_2V_6O_{16}$	99.67	99.43
	VO_2	82.94	80.71
	V_2O_3	74.98	75.10

Table 5.1. Comparison of theoretical to actual intermediate weights for proposed reaction intermediates.

Most authors agree with the formation of VO_2 and V_2O_3 as intermediates in the reaction of V_2O_5 with NH_3[79]. However, the formation of V_4O_9 has not been reported previously, although the formation of V_6O_{13} during the reduction of V_2O_5 with hydrogen has been proposed based on TPR results[66]. Some discrepency in the weights of the intermediates is present due to the overlap of the DTG peaks, making the assignment of exact temperatures of formation of these intermediates difficult; however, the DTG results clearly show the presence of an intermediate oxide before the formation of vanadium dioxide. At 750°C, the sample still contained oxygen, as indicated by the final TGA weight and XRD. This oxynitride product was formed by the nitrification of V_2O_3.

Vanadium Dioxide

The reaction of VO_2 with ammonia proceeds through the same reaction pathway as that of V_2O_5; the starting oxide reduces to lower oxide intermediates before the final product is formed. Based on the TGA/DTG results in Figure 5.2, the reaction involves two reaction steps with one intermediate. The DTG peaks associated with the two reaction steps are at 450 and 625°C. From the TGA/DTG results, the following reaction pathway is proposed:

$$VO_2 \text{ ====> } V_2O_3 \text{ ====> } VO_xN_{1-x}$$

The reaction intermediate was identified by its TGA weight; a comparison to the theoretical weight is shown in Table 5.1. At the final reaction temperature of 750°C, the sample still contains oxygen. Like the reaction of vanadium

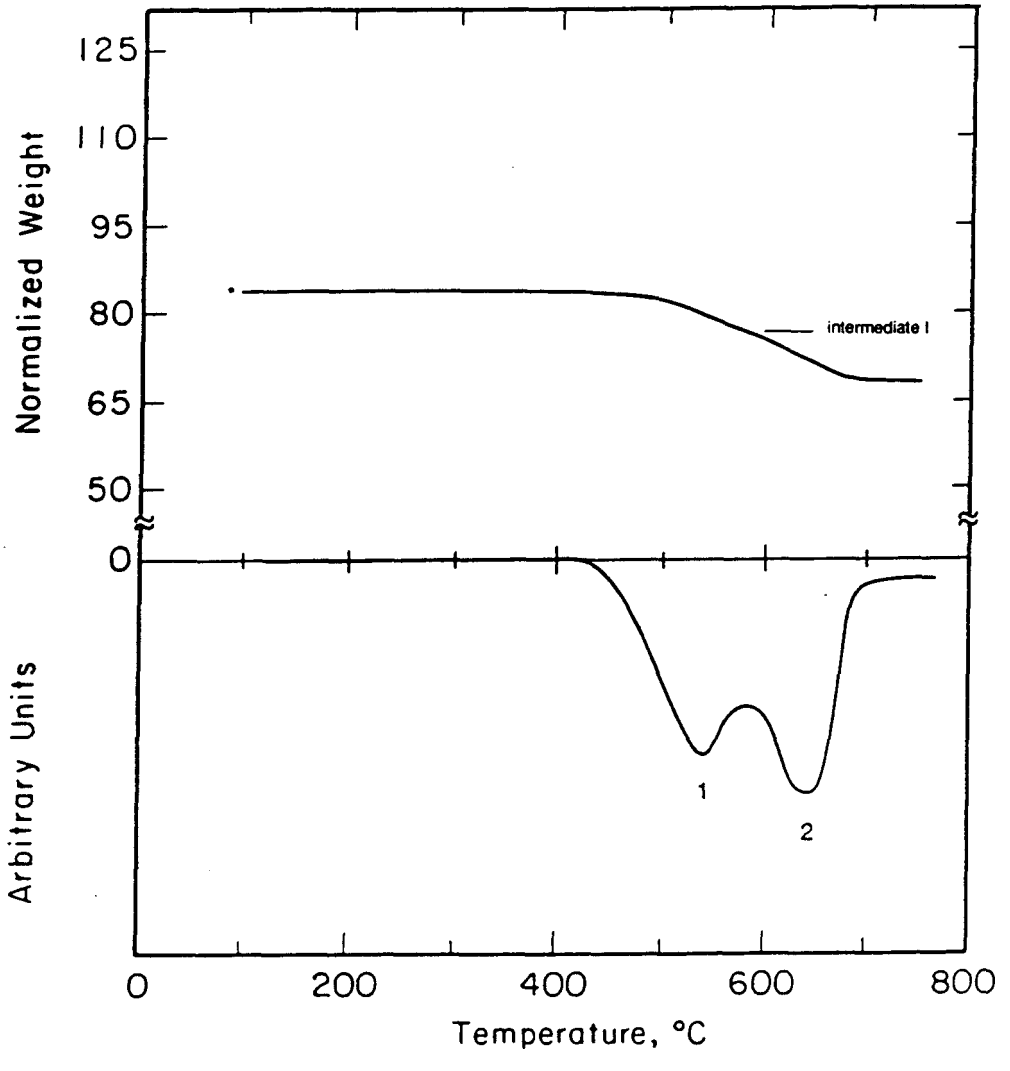

Figure 5.2. TGA/DTG of the reaction of vanadium dioxide with ammonia (heating rate = 1°C/min, 150 cm^3/min NH_3 at STP).

pentoxide with ammonia, the oxynitride product formed by this reaction is the result of the nitridification of V_2O_3.

Vanadium Sesquioxide

Vanadium sesquioxide, V_2O_3, reacts directly to form the oxynitride product as shown by the TGA/DTG results in Figure 5.3. The DTG peak associated with this reaction is present at 650°C. At the final reaction temperature of 750°C, the sample still contains oxygen, as indicated by the final TGA weight and the XRD pattern.

Ammonium Metavanadate

The TGA/DTG results for the reaction of ammonium metavanadate, NH_4VO_3, with ammonia show the presence of four reaction steps and the formation of three reaction intermediates, as depicted in Figure 5.4. These DTG peaks associated with the reaction steps are present at 225, 305, 410, and 549°C. The intermediate phases were identified from their TGA weights; the proposed intermediates and weights are shown in Table 5.1, along with their theoretical values. The discrepency between actual and theoretical values for some intermediates is a result of the difficulty in assigning a weight value for an intermediate when two DTG reaction peaks overlap; the values used were those at the minima between the two peaks. Based on the TGA/DTG results, the following reaction pathway is proposed:

$$NH_4VO_3 \text{ ====> } (NH_4)_2V_6O_{16} \text{ ====> } V_2O_4 \text{ ====> } V_2O_3 \text{ ====> } VO_xN_{1-x}$$

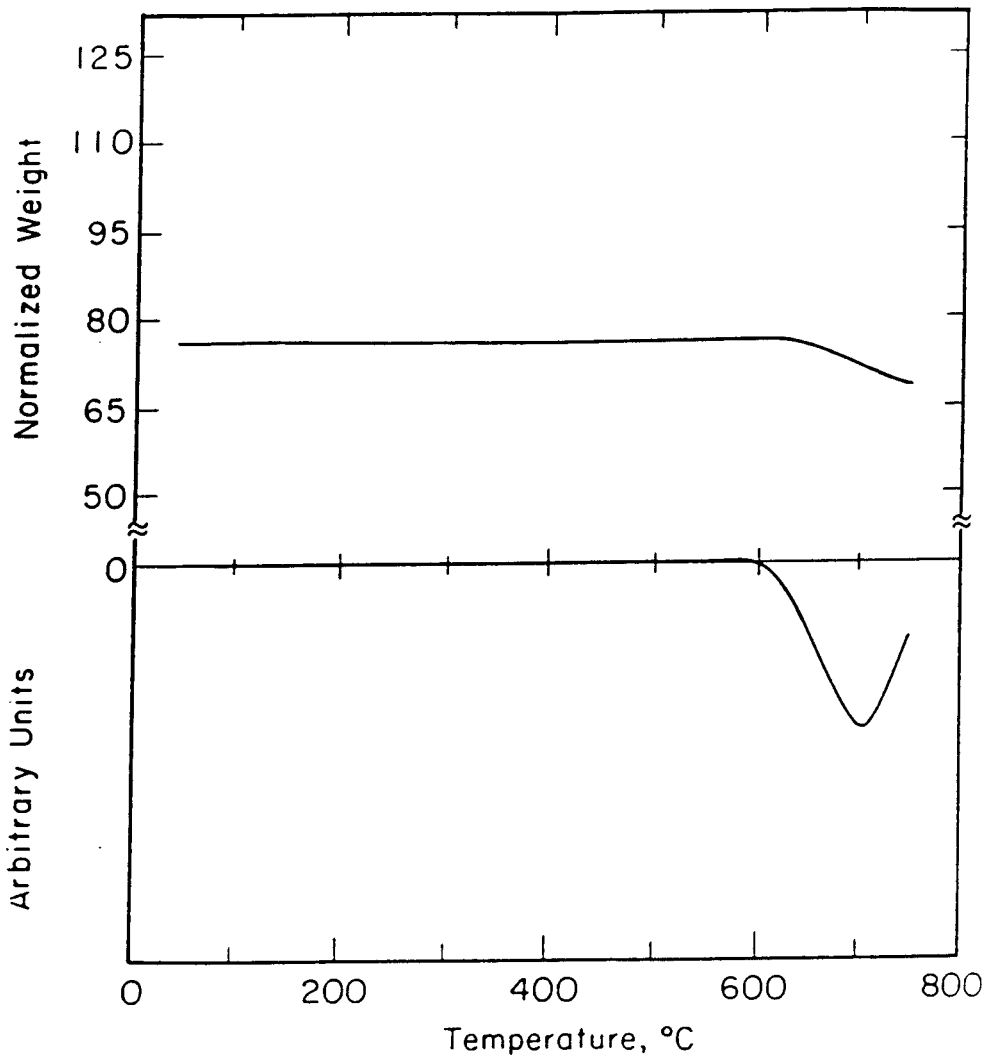

Figure 5.3. TGA/DTG of the reaction of vanadium sesquioxide with ammonia (heating rate = 1°C/min, 150 cm^3/min NH_3 at STP).

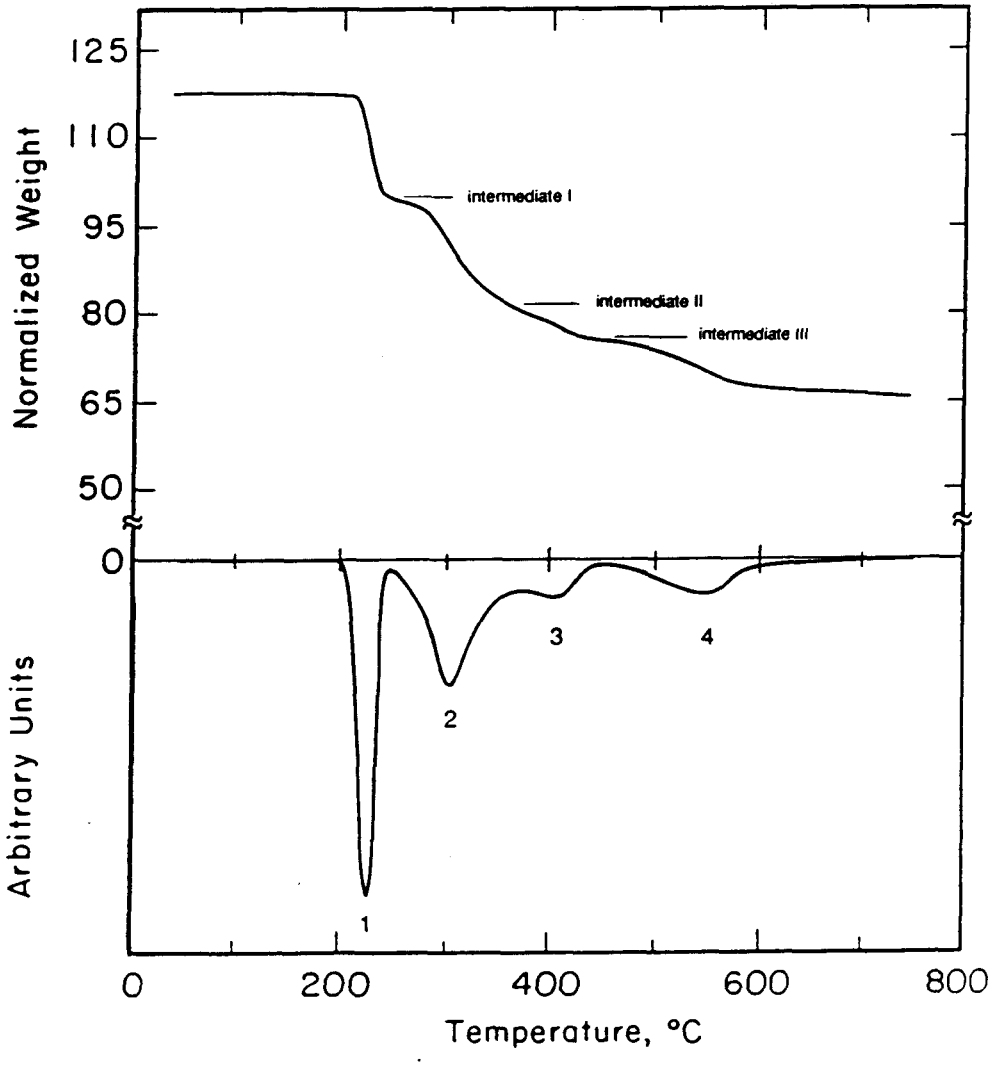

Figure 5.4. TGA/DTG of the reaction of ammonium metavanadate with ammonia (heating rate = 1°C/min, 150 cm^3/min NH_3 at STP).

Previous authors[81-83,85,88-89] have reported that the hexavanadate, $(NH_4)_2V_6O_{16}$, decomposes to form vanadium pentoxide, V_2O_5, before the dioxide is formed; the TGA/DTG results, however, do not indicate that the pentoxide is produced. As in the previous reactions, an oxynitride is produced by nitridification of V_2O_3; this product retained oxygen at 750°C.

FORMATION OF OXYNITRIDE PRODUCT

The products formed from the reactions of V_2O_5, V_2O_4, V_2O_3, and NH_4VO_3 with ammonia at a final reaction temperature of 750°C are vanadium oxynitrides, designated as VO_xN_{1-x}. X-ray diffraction of the final products indicate that they are single-phase; their compositions were determined based on the final sample weights during the TGA experiments, and are listed in Table 5.2. Based on the results, it is concluded that the products all contain a substantial amount of oxygen (>5 mole%).

The vanadium oxynitride, VO_xN_{1-x}, is a solid solution of VO and VN with a varying O:N ratio. Both VO and VN exist in the NaCl structure, with the lattice parameter varying linearly from 4.08 Å to 4.129 Å as the O:N ratio decreases[98]. The formation of vanadium nitride does not occur on the completion of the reduction of the vanadium oxides to VO, but simultaneously with it[79]. At temperatures in excess of 1000°C, pure VN can be formed; however, at the final TGA reaction temperature of 750°C, some of the oxygen still remains.

No conclusions can be made as to the control of the O:N ratio of the product. Table 5.2 lists the compositions of the products, based on the final TGA weights. Small inaccuracies in the final weights and purity of the starting materials can induce large errors in the apparent O:N ratio due to the similarities in the molecular weights of VO and VN (66.941 and 64.948 g/gmol, respectively). It is interesting to note, however, that the oxynitride formed from ammonium metavanadate contains the least amount of oxygen; this suggests that by lowering the oxynitride formation temperature that the oxygen may be able to be removed completely at lower temperatures.

PRODUCT SURFACE AREA

The surface area of the oxynitride products for all of the reactions were below 20 m^2/g, as shown in Table 5.2. The results indicate that all of the oxides first reduce to V_2O_3 before they begin to nitride. This lower oxide is isotropic and does not retain the layered structure of V_2O_5. The last oxide intermediate in each case, therefore, is a three-dimensional network of VO_6 octahedra[68-69]. This is similar to the reaction of MoO_2 with ammonia, which requires much higher temperatures than the layered MoO_3 to react and forms a low surface area product.

In the reaction of vanadium pentoxide with ammonia, V_2O_5 is reduced to lower oxides before nitriding at higher temperatures. Since the nitriding of the oxide is accomplished by the decomposition products of ammonia rather than

Starting Material	Composition of Final Product	Final BET S_g (m^2/g)
V_2O_5	$VO_{0.40}N_{0.60}$	19.4
V_2O_5/Pt	$VO_{0.50}N_{0.50}$	9.9
V_2O_4	$VO_{0.70}N_{0.30}$	6.8
V_2O_3	$VO_{0.35}N_{0.65}$	6.3
NH_4VO_3	$VO_{0.10}N_{0.90}$	12.6

Table 5.2. Comparison of the final products of the reactions of vanadium oxides and ammonium metavanadate with ammonia.

ammonia itself[60], it is hypothesized that nitridification is limited by ammonia decomposition. It may therefore be possible to react the layered vanadium pentoxide directly if the decomposition of ammonia could be catalyzed at a temperature before the first reduction step occurs. One possibility is the addition of platinum to the vanadium pentoxide to catalyze this decomposition. Such a reaction scheme could result in a high surface area vanadium nitride, based on the results for molybdenum trioxide.

The TGA/DTG of the reaction of V_2O_5/Pt with ammonia is compared to the reaction of V_2O_5 in Figure 5.5. The use of Pt to catalyze the decomposition of ammonia did not alter the reaction pathway, but did lower the reaction temperatures of each step. These results are summarized in Table 5.3. This implies that the decomposition of ammonia is the rate-limiting step in the reduction of vanadium pentoxide to form lower oxides and not just for the nitridification of V_2O_5.

CONCLUSIONS

(1) V_2O_5, VO_2, V_2O_3, and NH_4VO_3 are reduced through similar pathways sequentially to lower oxides by ammonia before nitridification begins. In all cases, the oxide which nitrides is V_2O_3. The nitridification of V_2O_3 results in a low surface area product (<20 m^2/g).

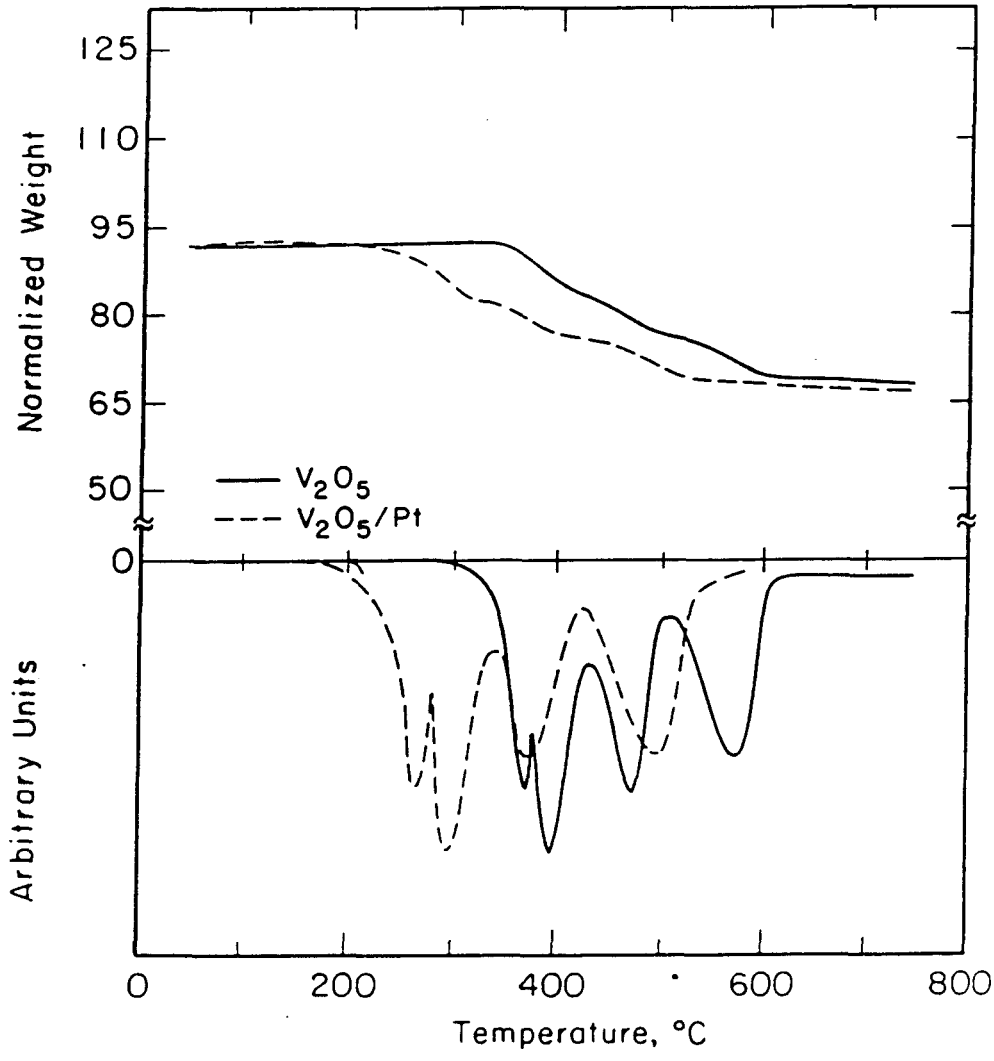

Figure 5.5. Comparison of TGA/DTG of the reactions of V_2O_5 and V_2O_5/Pt with ammonia (heating rate = 1°C/min, 150 cm^3/min NH_3 at STP).

Starting Material	DTG Peak Temperature (°C)				Normalized Wt Intermediate			
	1	2	3	4	I	II	III	Product
V_2O_5	371	401	468	578	87.39	81.39	75.48	65.75
V_2O_5/Pt	273	298	384	501	86.85	80.94	75.48	65.93

Table 5.3. Comparison of DTG reaction peaks and intermediates for Pt catalyzed and uncatalyzed V_2O_5/NH_3 reactions.

(2) The product formed at 750°C is a solid solution of VO and VN, designated as VO_xN_{1-x}.

(3) Catalyzing the decomposition of ammonia reduces the temperature of reduction of vanadium pentoxide to lower oxides, but does not alter the reaction pathway.

Chapter 6. Reactions of Hydrogen Bronzes With Ammonia

The reactions of ammonia with hydrogen molybdenum bronzes and hydrogen vanadium bronzes offer an interesting comparison with the reactions of MoO_3 and V_2O_5 with ammonia. Hydrogen molybdenum bronzes, H_xMoO_3 ($0<x<2.0$), and hydrogen vanadium bronzes, $H_xV_2O_5$ ($0<x<3.77$), have crystal structures similar to the parent MoO_3 and V_2O_5, respectively; hydrogen is inserted topotactically between the loosely held layers. The hydrogen reduces the metal atom without altering the structure of the parent oxide significantly. Due to their structural similarities with the parent oxides, the bronzes allow the study of the effect of partially reducing the metal atoms by insertion of hydrogen into the oxide lattice on the reaction temperature and product surface area.

The reduction of the metal atom is an important part of the formation of the nitride products from the oxide precursors. During the reaction of MoO_3 and V_2O_5 with ammonia, the Mo and V atoms are reduced from oxidation states of +6 and +5 to 0, respectively. The effect of reducing the metal atom by the insertion of hydrogen without significantly altering the structure may promote the reaction at lower temperatures, and this may reduce the sintering of the high surface area molybdenum nitrides observed at higher reaction temperatures.

The reduction of the layered oxides with hydrogen may also avoid the reduction to lower oxides that occurs in the reactions of MoO_3 and V_2O_5 with ammonia. The reaction of MoO_3 with ammonia to form Mo_2N is accompanied by the reduction of MoO_3 to MoO_2; the subsequent nitridification of MoO_2

occurs only above 688°C. However, at temperatures above 550°C the surface area is reduced from 141.9 m^2/g at 550°C to 57.2 m^2/g at 750°C. If this side reaction can be avoided by reducing the Mo atom through the insertion of hydrogen into the trioxide lattice, it may allow lower reaction temperatures and therefore higher surface areas.

A similar effect may be possible with V_2O_5. During the reaction of vanadium pentoxide with ammonia, V_2O_5 reduces to form V_2O_3, a non-layered oxide, prior to nitridification; the result is a low surface area product (<20 m^2/g). Based on the results of the molybdenum oxide system, it is the layered materials which react with ammonia to form high surface area nitrides. If vanadium pentoxide could react with ammonia to form the oxynitride in one step, it might be possible to form a high surface area vanadium nitride.

REACTION NETWORKS - INFLUENCE OF HYDROGEN INSERTION

A comparison of the reactions of the hydrogen bronzes with ammonia to those of their parent oxides shows that the reaction pathways are not altered by hydrogen insertion. Based on the TGA results, the reactions proceed through the same steps, but at lower temperatures. As the hydrogen content is increased in the hydrogen molybdenum bronzes, this temperature shift increases.

Hydrogen Molybdenum Bronze

A series of hydrogen molybdenum bronzes, H_xMoO_3 with x = 0, 0.04, 0.13, 0.31, and 0.80, were reacted with ammonia, and the TGA/DTG of these reactions are compared in Figure 6.1. From the figure, it is obvious that as the hydrogen content is increased, the samples react at lower temperatures. The reactions of molybdenum trioxide and the bronzes with x<0.31with ammonia are characterized by two DTG peaks associated with the formation of the oxynitride MoO_xN_{1-x} and its subsequent reaction to form the nitride Mo_2N. Table 6.1 lists the temperatures of these peaks for the trioxide and the bronzes. As the hydrogen content is increased, the bronzes react at lower temperatures and the DTG peaks shift to lower temperatures. The characteristics of the products formed by reacting at a final temperature of 750°C are listed in Table 6.2.

The reaction of $H_{0.80}MoO_3$ with ammonia differs from the other bronzes as it exhibits three DTG peaks. The first peak is associated with the formation of the oxynitride MoO_xN_{1-x}. The last two peaks are associated with the formation of MoN and Mo_2N from the oxynitride, respectively; the formation of both nitride phases is confirmed by XRD. The formation of the hexagonal MoN phase is not surprising, based on the results in Table 6.1; the formation of the oxynitride occurs at a significantly lower temperature than for the lower hydrogen content bronzes, and previous results show that the MoN phase is formed at lower temperatures.

The reaction of hydrogen molybdenum bronzes with ammonia eliminates the formation of MoO_2. As Figure 6.1 shows, the DTG peak at 695°C for the

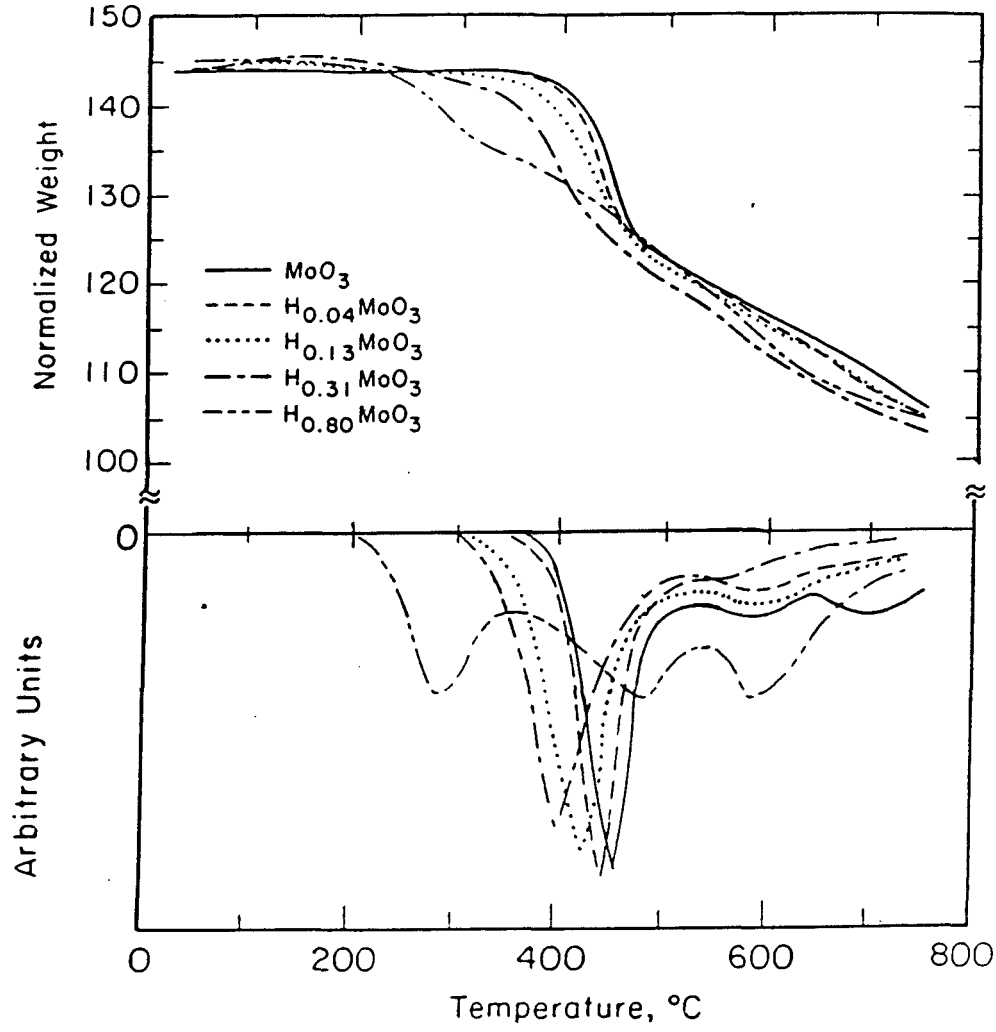

Figure 6.1. Comparison of TGA/DTG of the reactions of hydrogen molybdenum bronzes with ammonia (heating rate = 1°C/min, 150 cm^3/min NH_3 at STP).

Starting Material	T_{onset}, °C	DTG Peaks, °C			
		1	2a	2b	3
MoO_3	375	460	---	595	695
$H_{0.04}MoO_3$	350	440	---	590	---
$H_{0.13}MoO_3$	310	425	---	590	---
$H_{0.31}MoO_3$	300	405	---	550	---
$H_{0.80}MoO_3$	205	285	495	595	---

Reaction 1: H_xMoO_3 ===> MoO_xN_{1-x}

Reaction 2a: MoO_xN_{1-x} ===> MoN

Reaction 2b: MoO_xN_{1-x} ===> Mo_2N

Reaction 3: MoO_2 ===> Mo_2N

Table 6.1. Reaction temperatures of the reactions of MoO_3 and H_xMoO_3 with NH_3.

Starting Material	Final Product (XRD)	Final Surface Area m^2/g
MoO_3	Mo_2N	57.2
$H_{0.04}MoO_3$	Mo_2N	57.5
$H_{0.13}MoO_3$	Mo_2N	65.0
$H_{0.31}MoO_3$	Mo_2N	65.5
$H_{0.80}MoO_3$	Mo_2N + MoN	83.8

Table 6.2. Product of the reactions of hydrogen molybdenum bronzes with ammonia at 750°C.

reaction of MoO_3 with ammonia is not present for the bronzes; this peak is associated with the reaction of MoO_2 with ammonia. Additionally, X-ray diffraction patterns obtained at 500°C during the reaction of $H_{0.31}MoO_3$ with ammonia do not show the presence of MoO_2. This result suggests that it is possible to fully nitride the bronzes at lower temperatures than MoO_3, and this should reduce the sintering that occurs at higher temperatures.

Hydrogen Vanadium Bronze

A hydrogen vanadium bronze of composition $H_{3.05}V_2O_5$ was reacted with ammonia; its TGA is compared to that of V_2O_5 in Figure 6.2. The hydrogen bronze initially loses its hydrogen, and then produces the same intermediates as V_2O_5. The reaction temperatures for the formation of the lower oxide intermediates shift to lower temperatures, but the temperature at which the last oxide, V_2O_3, nitrides is not changed significantly; Table 6.3 lists the DTG peak temperatures for the two compounds. The reaction pathway is not changed by the insertion of the hydrogen into the material as first hoped; only the reaction temperatures are lowered.

DEVELOPMENT OF SURFACE AREA

Hydrogen Molybdenum Bronze

The reaction of the molybdenum bronzes with ammonia produces higher surface area nitrides then that produced by the reaction of MoO_3 with ammonia.

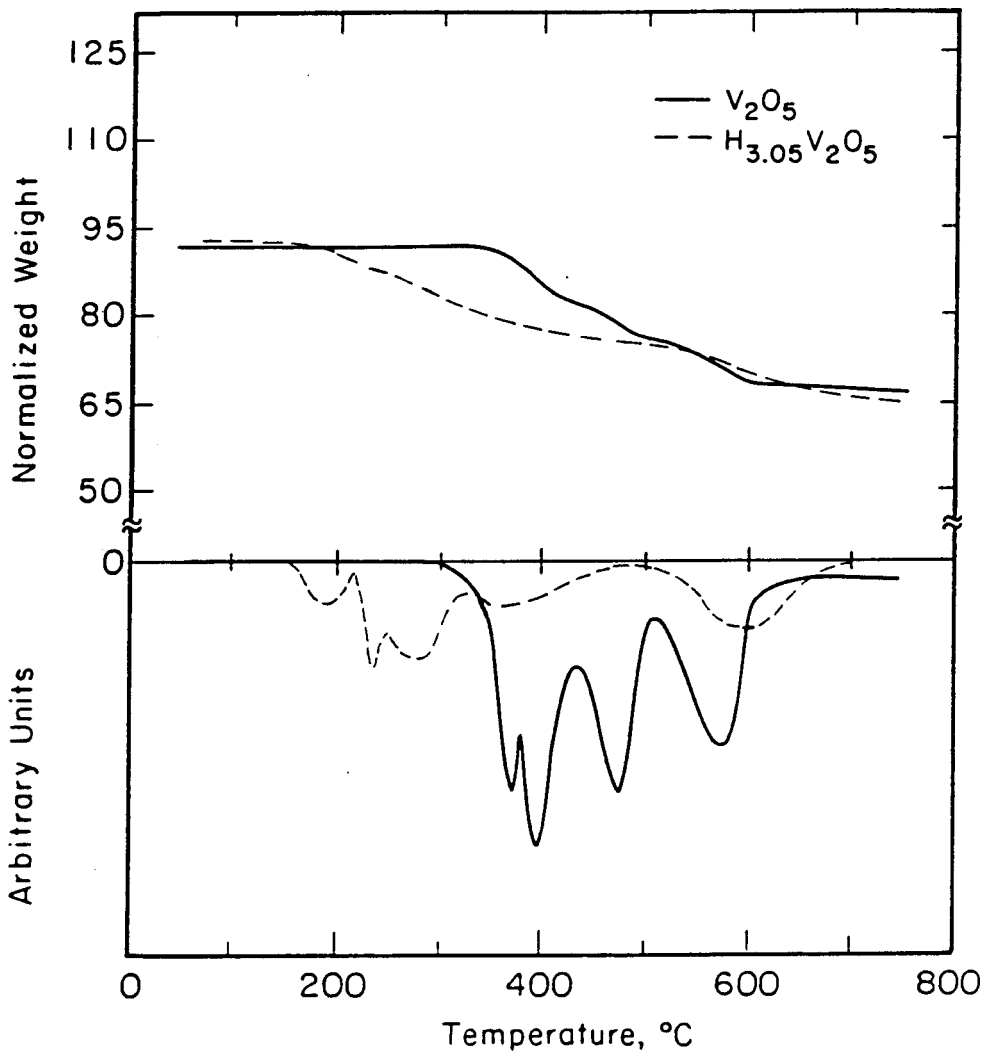

Figure 6.2. Comparison of TGA/DTG of the reaction of V_2O_5 and $H_{3.05}V_2O_5$ with ammonia (heating rate = 1°C/min, 150 cm^3/min NH_3 at STP).

Starting Material	DTG Peaks, °C				Product Composition	BET S_g m^2/g
	1	2	3	4		
V_2O_5	371	401	468	578	$VO_{0.40}N_{0.60}$	19.4
$H_{3.05}V_2O_5$	240	275	360	600	$VO_{0.57}N_{0.43}$	12.5

Table 6.3. Reaction temperatures and product characteristics of the reactions of V_2O_5 and $H_{3.05}V_2O_5$ with NH_3.

As Table 6.2 shows, the surface area of the nitride product increases from 57.2 m^2/g for MoO_3 to 83.8 m^2/g for $H_{0.80}MoO_3$. The development of the surface area during the reaction with ammonia is compared in Figure 6.3 for MoO_3 and $H_{0.80}MoO_3$. The bronze exhibits a higher maximum in surface area due to the decrease in the temperature of oxynitride formation, indicated by the first DTG peak. At the lower temperatures, the mobility of the molybdenum atoms is reduced. Since the molybdenum atoms are constrained to a higher degree at lower temperatures, the material cannot compensate as much for the large change in density, thereby resulting in a higher surface area material. The effect of hydrothermal sintering at higher temperatures is apparent in both cases.

Hydrogen Vanadium Bronze

The use of hydrogen vanadium bronze to form vanadium nitrides does not result in an increase in the surface area of the product. This reflects the fact that addition of hydrogen does not alter the reaction pathway, nor does it change the nitriding temperature for the oxynitride precursor V_2O_3.

CONCLUSIONS

Based on the results, the following conclusions can be made:

(1) The insertion of hydrogen into MoO_3 and V_2O_5 to form hydrogen

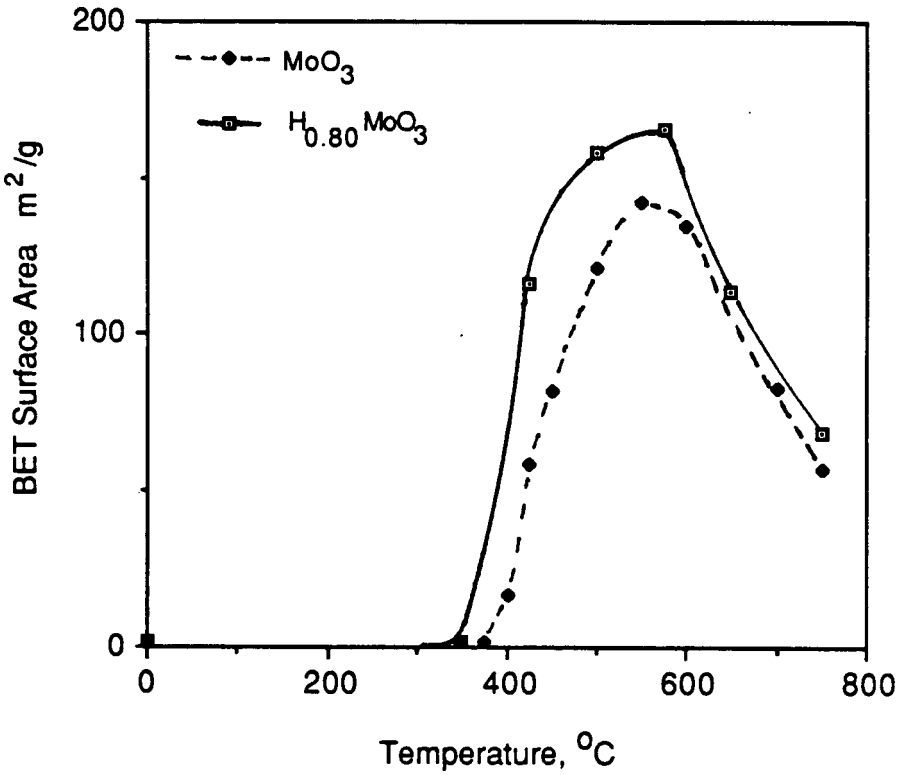

Figure 6.3. Surface area development during the reactions of MoO_3 and $H_{0.80}MoO_3$ with ammonia.

bronzes results in the lowering of the initial and intermediate reaction temperatures in the reaction with ammonia.

(2) Hydrogen molybdenum bronzes do not form MoO_2 when they react with ammonia and therefore can be fully nitrided at lower temperatures than MoO_3. The lower nitridification temperature of the bronzes also reduces the effect of hydrothermal sintering on the ultimate surface area of the the nitride.

(3) The nitridification of hydrogen vanadium bronzes produces the same intermediates as that of V_2O_5 and forms a relatively low surface area oxynitride.

Chapter 7. Summary

SELECTION OF STARTING MATERIALS

The synthesis of high surface area nitrides in this study are accompanied by a large increase in density and the formation of pseudomorphous products. These two characteristics, when coupled together, result in the formation of a pore structure and an increase in surface area. From this information, some insight as to the selection of nitride precursors can be obtained.

Starting compounds which are significantly less dense than the desired nitride product are a prerequisite for the formation of high surface area nitrides. In addition, materials which allow the formation of pseudomorphous products by constraining the movement of the metal atoms during the reaction are also necessary. This can be facilliated by the use of layered materials, although the degree of constraint necessary is difficult to quantify; the double-thick layers of MoO_3 formed a high surface area nitride, while the single layers of $MoO_3 \cdot H_2O$ formed a low surface area nitride. Three-dimensional materials with isotropic bonding such as MoO_2 or V_2O_3 do not form high surface area products.

In addition, since formation of high surface area materials is unfavorable at high temperatures, an additional criterion for the selection of starting materials is the ability to intercalate or react with ammonia at temperatures below approximately 300°C. Again, layered oxides appear to be well suited as

starting materials because of their reactivity with ammonia

Although these characteristics aid in the choice of a starting material, it is the intermediate compound which nitrides that controls the quality of the product. The reaction pathway is therefore significant, since many of these compounds react through several intermediates before nitriding. These reaction pathways are impossible to predict, although the mechanism of decomposition may provide a hint of likely intermediates in the reaction with ammonia.

In the particular case of molybdenum nitride, where the reactions of the oxnitride to form both Mo_2N and MoN are competing reactions in the temperature range of 450-700^{o}C, the temperature of formation of the oxynitride is important. This temperature is lowered as the NH_3:MoO_3 ratio increases. Also, it may be possible to control the nitride phase formed by altering the final reaction temperature or the heating rate.

SUGGESTIONS FOR FUTURE RESEARCH

The selection of nitride precursors for the formation of high surface area products might be simplier if the reaction mechanism of nitridification were known. Unfortunately, the determination of solid-state reaction mechanisms is difficult, and few are known. Additional information could be obtained, however, if the nature of the reaction of ammonia with the oxide lattice could be determined. In particular, it would be useful to determine what decomposition

products of ammonia are responsible for the nitridification and how these species are bonded to the solid before they react. Spectroscopic techniques are likely tools to answer these questions. Unfortunately, IR spectroscopy is not useful because the nitrides and oxynitride are IR-opaque. One possibility, however, is ^{15}N NMR.

A model for the pore structure of high surface area nitrides could also yield information about the nature of the reaction with ammonia. This study has concentrated on the synthesis of high verses low surface area nitrides, and has not characterized the pore structures in terms of size, shape, pore size distribution, or degree of interconnection between pores. A model for the pore structure of these nitrides, when compared to the starting materials, may assist in the determination of how the pores are formed in the materials. Also, the slit-like nature of the pores, along with the layered nature of the nitride precursors, indicates that these pores may be formed between the layers of the starting materials. Determination of this is not possible using SEM due to its resolution. However, transmission electron microscopy (TEM) could be used to image individual pores. By using an environmental chamber with a hot-stage on the TEM apparatus, it may be possible to observe the morphological changes in situ. This could yield interesting clues about the developement of pores in an initially non-porous material.

REFERENCES

1. Mittasch, A., Adv. Catal. Rel. Subj. **2**, 81 (1980).
2. Saito, M. and Anderson, R.B., J. Catal. **63**, 438 (1980).
3. Ibid, **67** 296 (1977).
4. Shigehara, Y., Nippon Kagaku Kaishi **4**, 474 (1977).
5. Ibid, **10** 1438 (1977).
6. Kharlamov, A.I.. Teor. Eksp. Khim. **15** .468.
7. Schlatter, J.C., Oyama, S.T., Metcalfe, J.E., and Lambert, J.M., Ind. Eng. Chem. Res., in press.
8. Toth, L.E., "Transition Metal Carbides and Nitrides", Academic Press, New York, 1971, pp. 12-13.
9. Boudart, M. and Volpe, L., J. Solid State Chem. **59**, 332 (1985).
10. Remy, F., Mercier, R., Keowkamnerd, K. and Hantzpergue, J.J., C.R. Acad. Sci., Ser. C. **275(14)**, 733 (1972).
11. Rosenheim, A. and Jacobson, F., Z. anorg. allgem. Chem. **50**, 297 (1906).
12. Watt, G.W. and Davies, D.D., J. Amer. Chem. Soc. **70**,2041 (1948).
13. Kihlborg, L., Hagerstrom, G., and Ronnquist, A., Acta Chem. Scand. **23**, 1187 (1961).
14. Chang, L.L.Y. and Phillips, B., J. Am. Ceram. Soc. **52**, 527 (1969).
15. "CRC Handbook of Chemistry and Physics, 65th Edition", ed. by R.C. Weast, CRC Press, Inc., Boca Raton, Florida, 1984, pp. B116-117.
16. Johnson, J.W.; Jacobson, A.J.; Rich, S.M.; Brody, J.F., J. Amer. Chem. Soc. **103**, 5246 (1981).

17. Kihlborg, L. and Magneli, A., Acta Chem. Scand. **9**, 471 (1955).

18. Kennedy, M.J. and Bevan, S.C., Climax First International Conference on the Chemistry and Uses of Molybdenum, ed. by P.C.H. Mitchell, Climax Moly. Co., LTD, London, 1973.

19. Solonin, Yu.M., Soviet Powder Metallurgy and Metal Ceramics **3**, 217 (1979).

20. Bond, G.C. and Tripathi, J.B.P., Climax First Int. Conf. on the Chem. and Uses of Moly., ed. by P.C.H. Mitchell, Climax Moly. Co., LTD, London, 1973.

21. Magneli, A. and Andersson, G., Acta Chem. Scand. **9(8)**, 1378 (1955).

22. Magneli, A., Arkiv. Kemi, Mineral. Geol. **A24**, (1946) No.2.

23. Schollhorn, R., Angew. Chem. Int. Ed. Engl. **19**, 983 (1980).

24. Volpe, L. and Boudart, M., Catal. Rev.-Sci. Eng. **27(4)**, 515 (1985).

25. Dickens, P.G., Kay, S.A., Crouch-Baker, S. and Claridge, D.A., Solid State Ionics **23**, 9 (1987).

26. Johnson, J.W., Jacobson, A.J., Rich, S.M. and Brody, J.F., J. Am. Chem. Soc. **103(17)**, 5246 (1981).

27. Krebs, B.,Acta Cryst. B **28**, 2222 (1972).

28. Gunter, J.R., J. Solid State Chem. **5**, 354 (1972).

29. Oswald, H.R., Gunter, J.R., and Dubler, E., J. Solid State Chem. **13**, 330 (1975).

30. Glemser, O. and Lutz, G., Z. anorg. u. allgem. Chem. **264**, 17 (1951).

31. Glemser, O., Hauschild, U. and Lutz, G., Z. anorg. u. allgem. Chem. **269**, 93 (1952).

32. Glemser, O., Nachr. Akad. Wiss. Gottingen, Math.-physik.- Kl., Abt. IIa, 121 (1955).

33. Glemser, O., Lutz, G. and Meyer, G., Z. anorg.u. allgem. Chem. **285**, 173 (1956).

34. Birtill, J.J. and Dickens, P.G., Mat. Res. Bul. **13**, 311 (1978).

35. Dickens, P.G., Birtill, J.J., and Wright, C.J., J. Solid State Chem. **28**, 185 (1979).

36. Ritter, C., Muller-Warmuth, W., Schollhorn, R., J. Chem. Phys. **83**, 6130 (1985).

37. Dickens, P.G. and Hibble, S.J., Solid State Ionics **22**, 69 (1986).

38. Schollhorn, R., Schulte-Nolle, T. and Steinhoff, G., J. Less Common Metals **71**, 210 (1980).

39. Gatehouse, B.M., Leverett, P., J. Chem. Soc. A. **5**, 849 (1969).

40. Evans, H.T., Gatehouse, B.M., and Leverett, P. ,J. Chem. Soc., Dalton, 505 (1975).

41. Lindquist, I., Arkiv. Kemi **2**, 325 (1950).

42. Kiss, A.B., Gado, P., Asztalos, I. and Hegedus, A.J. ,Acta Chim. Acad. Sci. Hungaricae **66**, 235 (1970).

43. Schwing-Weill, M.-J., Bull. Soc. Chim. Fr. **10**, 3795 (1967).

44. Duval, C. "Inorganic Thermogravimetric Analysis", Elsevier, Amsterdam 96, 426 (1963).

45. Funaki, K., Sevgewa, T., J. Electrochem. Soc. Japan **18**, 152 (1950).

46. Rode, E.J., Tverdokhledov, V.N., Zh. neorg. Khim. **3**, 2343 (1958).

47. Ma, E., Bull. Chem. Soc. Japan **37**, 171 (1964).

48. Ma, E., Bull. Chem. Soc. Japan **37**, 648 (1964).

49. Onchi, M. and Ma, E., J. Phys. Chem. **67(10)**, 2240 (1963).

50. Louisy, A. and Dunoyer, J.-M., J. Chim. Phys. **67**, 1390 (1970).

51. Hegedus, A.J., Acta Chim. Acad. Sci. Hung. **66**, 235 (1970).

52. Hanafi, Z.M., Khilla, M.A. and Askar, M.H., Thermochimica Acta **45**, 221 (1981).

53. Fuchs, J., Hartl, H., Hunnius, W.-D. and Mahjour, S., Angew. Chem. internat. Edit. **14(5)**, 644 (1975).

54. Lindquist, I., Arkiv. Kemi **2**, 349 (1950).

55. Carpenter, K.H. and Hallada, C.J., Climax Third International Conference on the Chemistry and Uses of Molybdenum, ed. by P.C.H. Mitchell, Climax Moly. Co., LTD, London, 1979.

56. Hagg, G., Z. Phys. Chem., Abt. **B7**, 339 (1930).

57. Schonberg, N., Acta Chem. Scand. **8**, 204 (1954).

58. Toth, L.E., "Transition Metal Carbides and Nitrides", Academic Press, New York, 1971, p.36.

59. Hegedus, A.J., Sasvari, K. and Neugebauer, J., Z. Anorg. Chem. **293**, 56 (1957).

60. Lyutaya, M.D., Soviet Powder Metallurgy and Metal Ceramics **3**, 190 (1979).

61. Bliznakov, G., Piperov, B. and Tsolovski, I., Izv. Khim. **8(4)**, 614 (1975).

62. Stringer, J., J. Less-Common Metals **8**, 1 (1965).

63. Bachmann, H.G., Ahmed, F.R. and Barnes, W.H., Z. Krist. **115**, 110 (1961).

64. Nat. Bur. Standards Circ. **8**, 539 (1959).

65. Tarama, K., Teranishi, S. and Miyazaki, T., Kogyo Kagaku Zasshi **55**, 68 (1952).

66. Bosch, H., Kip, B.J., van Ommen, J.G. and Gellings, P.J., J. Chem. Soc., Faraday Trans. 1 **80**, 2479 (1984).

67. Andersson, G., Acta Chem. Scan. **10(4)**, 623 (1956).

68. Newnham, R.E. and de Haan, Y.M., Z. Krist. **117**, 235 (1962).

69. Prewitt, C.T., Shannon, R.D., Rogers, D.B., and Sleight, A.W., Inorg. Chem. **8(9)**, 1985 (1969).

70. Dickens, P.G., Chippendale, A.M., Hibble, S.J. and Lancaster, P., Mater. Res. Bull. **19**, 319 (1984).

71. Hibble, S.J., Chippendale, A.M. and Dickens, P.G., J. Electrochem. Soc. **132**, 2668 (1985).

72. Tinet, D., Legay, M.H., Gatineau, L. and Fripiat, J., Phys. Chem. **90**, 948 (1986).

73. Bond, G.C., Sermon, P.A. and Wright, C.J., Mater. Res. Bull. **19**, 701 (1984).

74. Tinet, D. and Fripiat, J.J., Rev. Chim. Miner. **19**, 612 (1982).

75. Selim, S.A., Philip, Ch.A., and Mikhail, R.Sh., Thermochim. Acta **36**, 287 (1980).

76. Hawthorne, F.C. and Calvo, C., J. Solid State Chem. **22**, 157 (1977).

77. Sata, T., Komada, E., and Ito, Y., Kogyo Kagaku Zasshi **71**, 643 (1968).

78. Sata, T. and Ito, Y., Kogyo Kagaku Zasshi **71**, 647 (1968).

79. Epelbaum, V. and Brager, A., Acta Physiochim. USSR **13**, 595 (1940).

80. Epelbaum, V. and Brager, A., Acta Physicochimica USSR **13**, 600 (1940).

81. Trau, J., Roczniki Chem. **36**, 1365 (1962).

82. Trau, J., Zeszyty Nauk. Politech. Krakow **21**, 113 (1966).

83. Lamure, J. and Colin, G., Compt. Rend. Acad. Sci. Paris **258**, 6433 (1964).

84. Satava, V., Collect. Czech. Chem. Commun. **24**, 2172 (1959).

85. Taniguchi, M. and Ingraham, T.R., Can. J. Chem. **42(11)**, 2467 (1964).

86. Brown, M.E. and Stewart, B.V., J. Therm. Anal. **2** 287, (1970).

87. Brown, M.E., Glasser, L., and Stewart, B.V., Prog. Vac. Microbalance Tech. **2**, 125 (1973).

88. Selim, S.A., Philip, Ch.A., and Mikhail, R.Sh., Thermochim. Acta **39**, 267 (1980).

89. Levanto, U.-M., Acta Polytech. Scand. **82**, 8 (1969).

90. Bachmann, H.G., Ahmed, F.R. and Barnes, W.H., Z. Krist. **115**, 215 (1961).

91. Evans, H.T, and Block, S., Inorg. Chem. **5(10)**, 1808 (1966).

92. Kelmers, A.D., J. Inorg. Nucl. Chem. **21**, 45 (1961).

93. Evans, H.T. and Mrose, M.E., Acta Cryst. **11**, 56 (1958).

94. Brauer, G. and Schnell, W.D., J. Less-Common Metals **6**, 326 (1964).

95. Hahn, H., Z. anorg. allg. Chem. **258**, 58 (1949).

96. Toth, L.E., Wang, C.P. and Yen, C.M., Acta Met. **14**, 1403 (1966).

97. Toth, L.E. "Transition Metal Carbides and Nitrides", Academic Press, New York, 1971, p.46.

98. Epelbaum, V. and Brager, A., Acta Physiochim. **21(4)**, 764 (1946).

99. Epelbaum, V. and Ormont, B., Acta Physiochim. **22(2)**, 319 (1947).

100. Fransen, T., van Berge, P.C., and Mars, P. ,React. Kinet. Catal. Lett. 5(4), 445 (1976).

101. Satterfield, C.N., "Heterogeneous Catalysis in Practice", McGraw-Hill, New York, 1980, p.102.

102. Anderson, P.J. and Morgan, P.L., Trans. Farad. Soc. 60 930 (1964).

APPENDIX A: COMPUTER PROGRAM FOR DATA ACQUISITION

This appendix contains a description of the computer program used for data acquisition during TGA experiments. It utilizes the block system of building programs provided with the Q.E.D. software; this system is described in more detail in the instruction manuel provided with the software.

The program "TGA" utilizes five different block operations, as described below:

(1) **Acquire** blocks, which take the raw data from the A/D converter and scale it as specified by the user as signal verses time (in nanoseconds).

(2) **Mnp**, or manipulation blocks, which perform specified operations on the inputed data. For this program, three different manipulation operations are used: (a) select manipulations, which either take one part of the data and route it to another manipulation block for further operations, or recombine data after manipulations have been performed; (b) con, or constant manipulations, which output a constant specified by the user for other manipulation purposes, and (c) div, or divide manipulations, which divide two numbers.

(3) **File** blocks, which store the raw data in files labled "weight" and "temp".

(4) **Window** blocks, which plot the data as specified by the user.

(5) **Display** blocks, which display the plots from the window blocks.

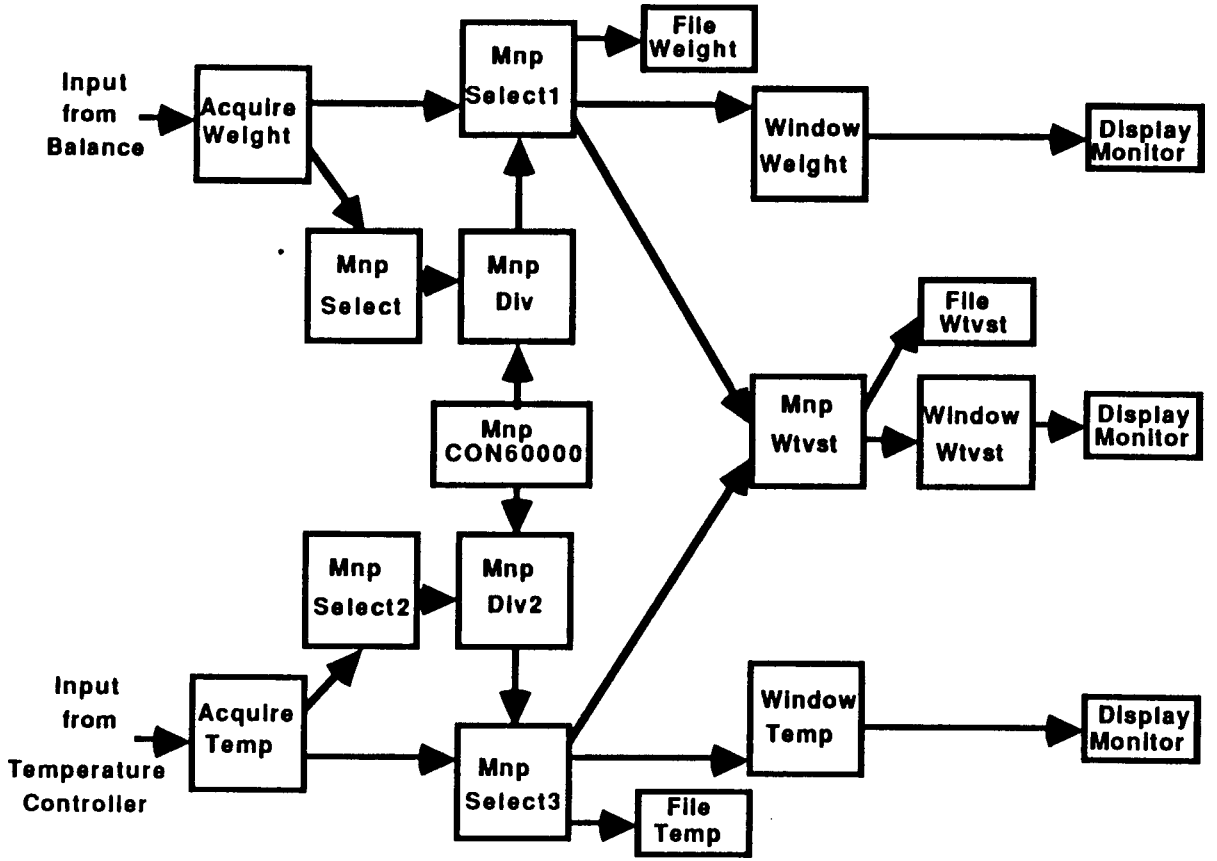

Figure A.1. Flow Diagram of Data Acquisition Program "TGA".

Display:monitor blocks show the graphs on the computer monitor, while display:printer blocks output the graphs to a printer. The program "TGA" performs the following routine. It (1) acquires the raw weight verses time and temperature verses time data, (2) converts the time from nanoseconds to hours, (3) stores the data in files labled "weight" and "temp", and displays the data on the computer monitor. It also combines the two sets of data into a weight verses temperature file; a later version of the program, however, "TGA2", does not perform this last function.

For the program to be run, the user must specify (a) the frequency of data collection, in data points per second, for each acquire block; (b) the window parameters for each window block; and (c) the duration of data collection. The user may also wish to change the default file names "weight" and "temp" to file names that are specific to that sample; this eliminates renaming the files later, and reduces the chance of writing over data.

APPENDIX B: XRD PATTERNS OF REACTANTS AND PRODUCTS

This appendix contains the X-ray diffraction patterns and tables of d-spacings for the reactants and products. The XRD for molybdenum trioxide, ammonium paramolybdate, and diammonium molybdate, however, can be found with the high-temperature XRD results. No pattern is included for molybdenum dioxide, as it was characterized by TGA and not XRD.

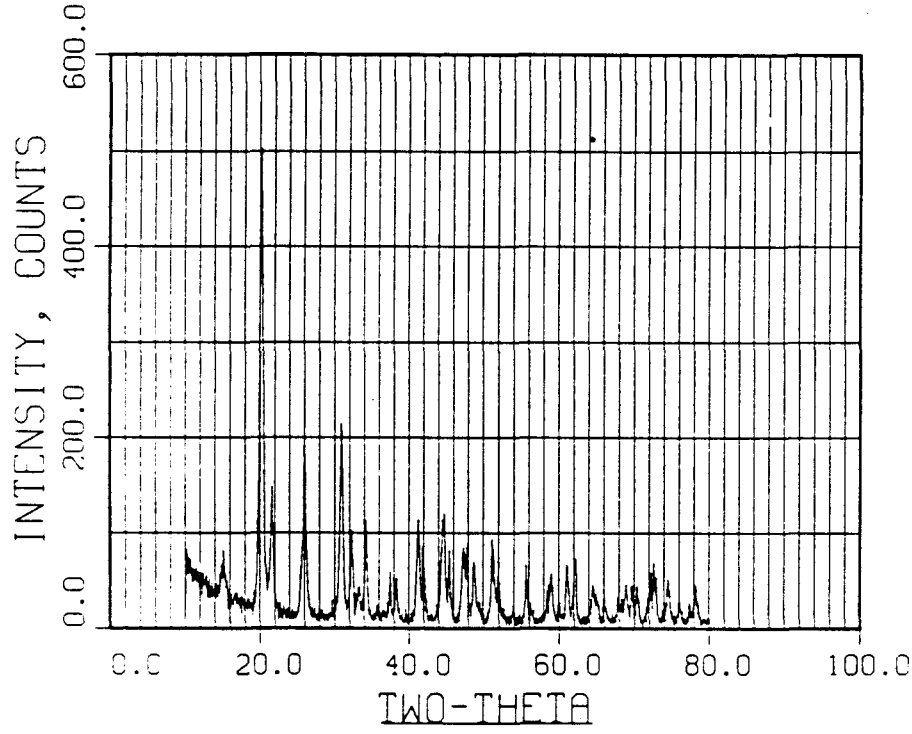

Figure B.1. XRD pattern of vanadium pentoxide starting material.

d-spacing, Å	I/I_o	Assignment	d-spacing, Å	I/I_o	Assignment
5.866	16	*	1.760	11	*
4.395	100	*	1.653	13	*
4.114	29	*	1.565	11	*
3.427	38	*	1.542	6	*
2.898	43	*	1.518	13	*
2.771	20	*	1.490	14	*
2.682	9	*	1.444	9	*
2.344	10	*	1.370	6	*
2.186	23	*	1.362	9	*
2.156	17	*	1.349	9	*
2.025	24	*	1.335	6	*
1.995	16	*	1.301	14	*
1.920	17	*	1.273	10	*
1.901	17	*	1.252	6	*
1.866	14	*	1.233	5	*
1.786	19	*	1.222	9	*

* V_2O_5

Table B.1. D-spacings for vanadium pentoxide starting material.

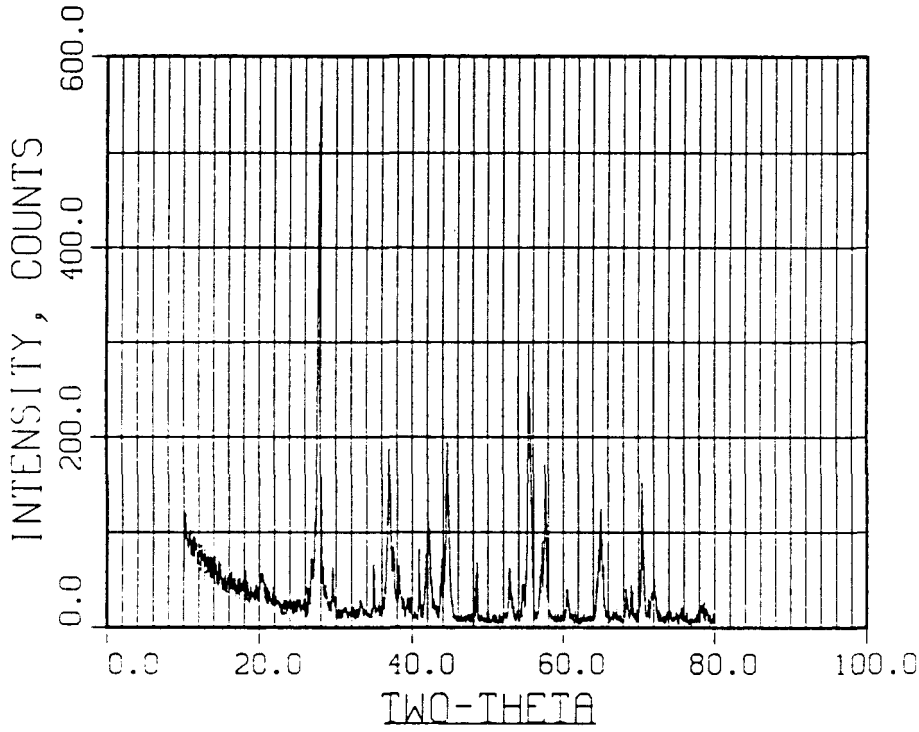

Figure B.2. XRD of vanadium dioxide starting material.

d-spacing, Å	I/I_o	Assignment	d-spacing, Å	I/I_o	Assignment
4.353	10	*	1.875	12	*
3.326	13	*	1.734	11	*
3.203	100	*	1.682	8	*
3.022	11	*	1.655	44	*
2.570	12	*	1.612	16	*
2.432	34	*	1.601	31	*
2.401	15	*	1.529	7	*
2.353	12	*	1.435	23	*
2.206	15	*	1.372	7	*
2.151	21	*	1.360	8	*
2.064	13	*	1.336	28	*
2.031	35	*	1.311	9	*

* VO_2

Table B.2. D-spacings for vanadium dioxide starting material.

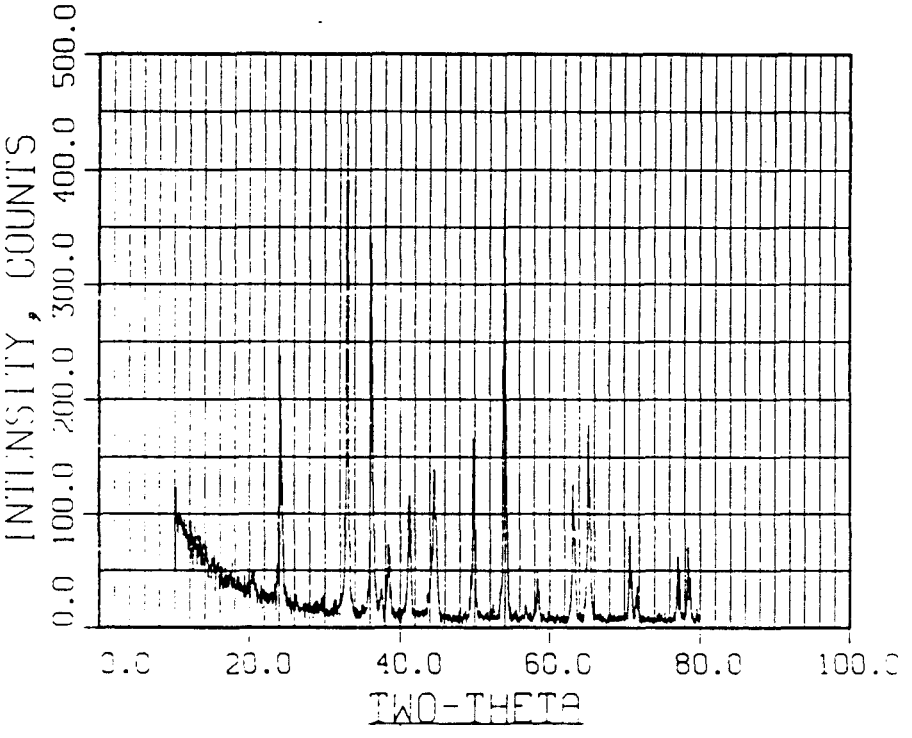

Figure B.3. XRD pattern for vanadium sesquioxide starting material.

d-spacing, Å	I/I_o	Assignment	d-spacing, Å	I/I_o	Assignment
3.685	53	*	1.580	12	*
2.718	100	*	1.472	28	*
2.481	75	*	1.431	40	*
2.398	8	*	1.331	18	*
2.338	16	*	1.315	8	*
2.186	26	*	1.238	14	*
2.033	31	*	1.220	16	*
1.832	37	*	1.216	10	*
1.699	85	*			

* V_2O_3

Table B.3. D-spacings for vanadium sesquioxide starting material.

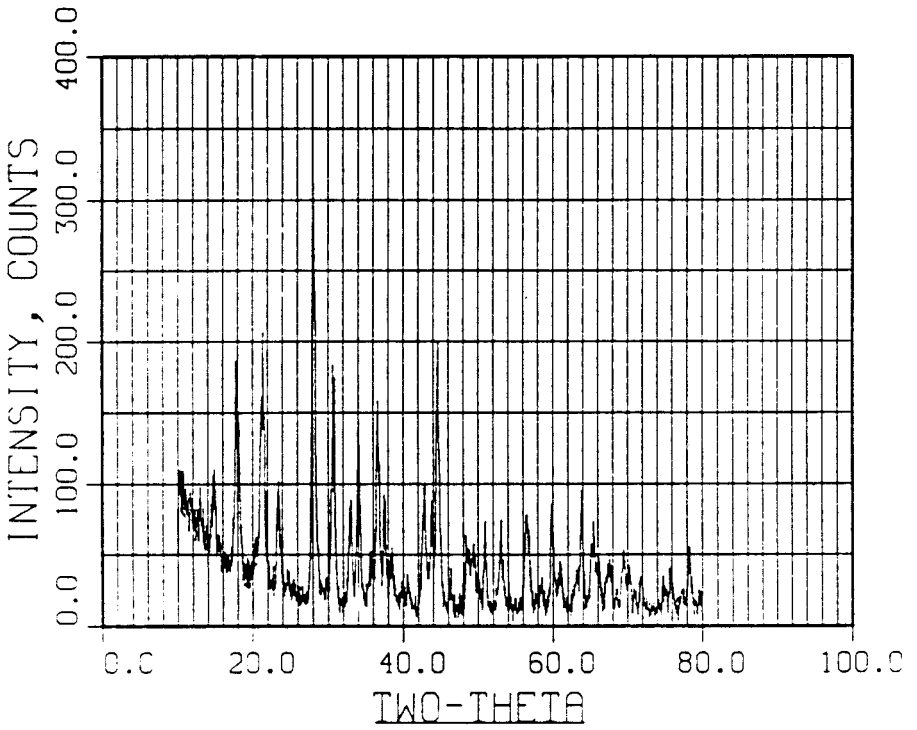

Figure B.4. XRD pattern of ammonium metavanadate starting material.

d-spacing, Å	I/I_0	Assignment	d-spacing, Å	I/I_0	Assignment
5.965	34	*	1.882	19	*
4.996	57	*	1.843	17	*
4.180	49	*	1.792	22	*
4.152	63	*	1.724	23	*
3.785	31	*	1.627	24	*
3.186	100	*	1.576	10	*
2.916	56	*	1.546	26	*
2.898	53	*	1.519	14	*
2.710	27	*	1.459	29	*
2.636	50	*	1.427	22	*
2.515	16	*	1.415	15	*
2.455	48	*	1.387	16	*
2.401	28	*	1.353	16	*
2.338	17	*	1.341	13	*
2.224	11	*	1.315	10	*
2.110	31	*	1.270	11	*
2.069	27	*	1.253	14	*
2.031	61	*	1.220	17	*
1.959	12	*			

* NH_4VO_3

Table B.4. D-spacings for ammonium metavanadate starting material.

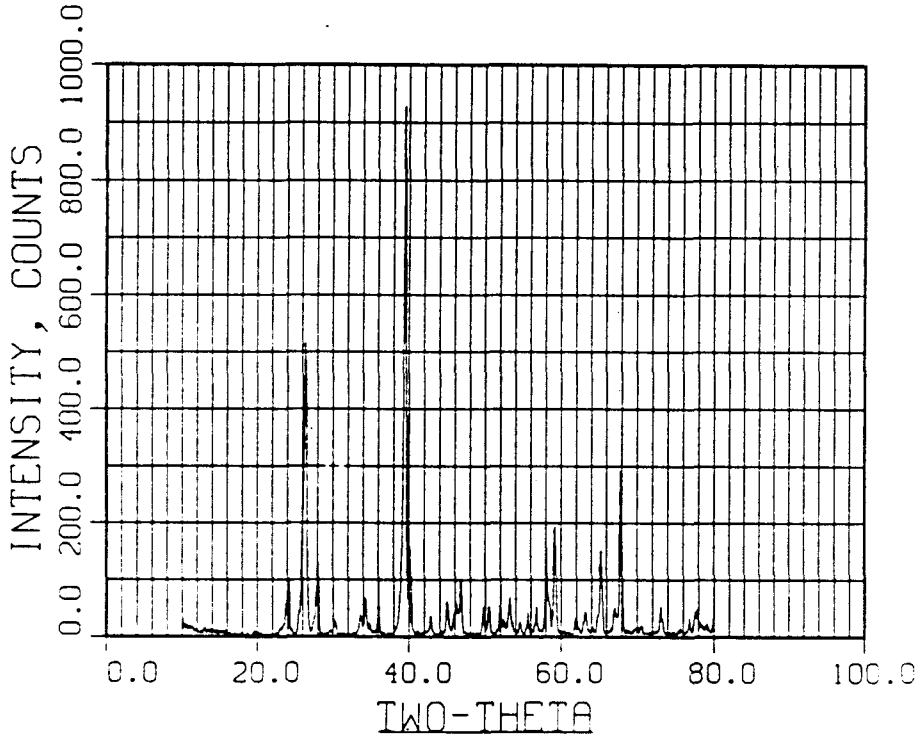

Figure B.5. XRD pattern for $H_{0.04}MoO_3$ starting material.

d-spacing, Å	I/I_o	Assignment	d-spacing, Å	I/I_o	Assignment
3.677	11	*	1.746	3	*
3.376	55	*	1.721	7	*
3.186	14	*	1.710	3	*
3.017	1	*	1.683	3	*
2.959	3	*	1.653	4	*
2.667	4	*	1.623	6	*
2.614	7	*	1.587	17	*
2.578	3	*	1.561	21	*
2.494	8	*	1.497	4	*
2.281	100	*	1.471	5	*
2.112	4	*	1.429	16	*
2.018	7	*	1.395	5	*
1.965	6	*	1.382	31	*
1.945	11	*	1.294	6	*
1.834	6	*	1.241	3	*
1.807	6	*	1.227	5	*

* $H_{0.04}MoO_3$

Table B.5. D-spacings for $H_{0.04}MoO_3$ starting material.

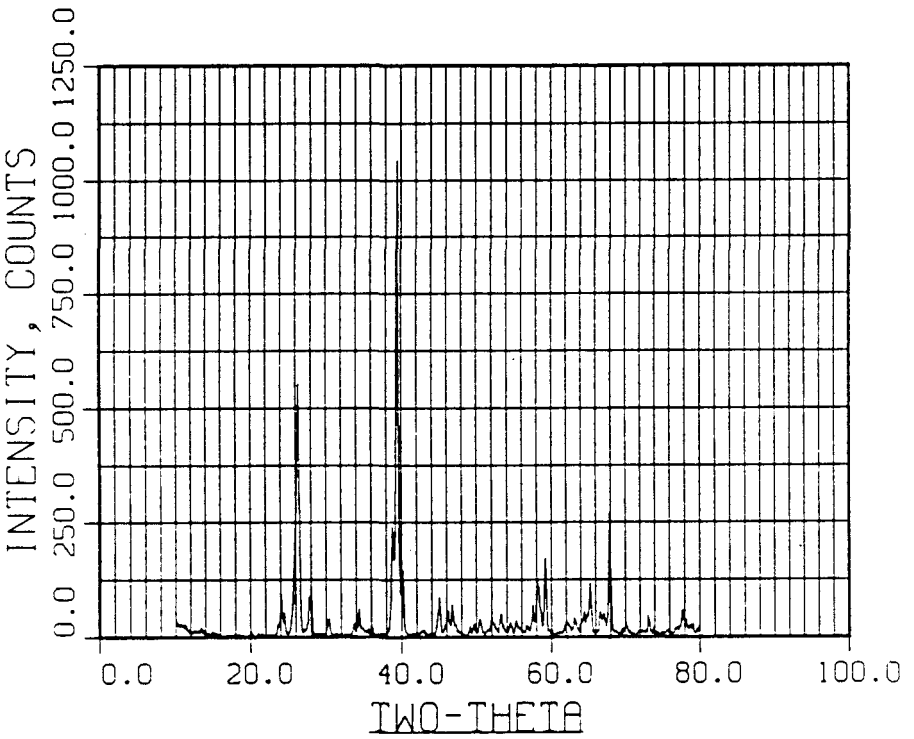

Figure B.6. XRD pattern for $H_{0.13}MoO_3$ starting material.

d-spacing, Å	I/I_o	Assignment	d-spacing, Å	I/I_o	Assignment
3.692	9	*	1.683	3	*
3.663	5	*	1.66	3	*
3.376	53	*	1.650	2	*
3.220	8	*	1.626	2	*
3.186	11	*	1.621	2	*
2.940	4	*	1.603	7	*
2.659	3	*	1.587	12	*
2.607	6	*	1.561	16	*
2.570	2	*	1.497	3	*
2.521	2	*	1.473	4	*
2.494	3	*	1.469	3	*
2.321	23	*	1.444	5	*
2.281	100	*	1.437	5	*
2.243	14	*	1.429	11	*
2.108	2	*	1.404	5	*
2.023	5	*	1.395	5	*
1.973	5	*	1.380	26	*
1.965	5	*	1.346	2	*
1.945	7	*	1.294	4	*
1.855	2	*	1.229	5	*
1.838	3	*	1.222	4	*
1.810	4	*	1.214	3	*
1.758	4	*	1.211	3	*
1.721	5	*			

* $H_{0.13}MoO_3$

Table B.6. D-spacings for $H_{0.13}MoO_3$ starting material.

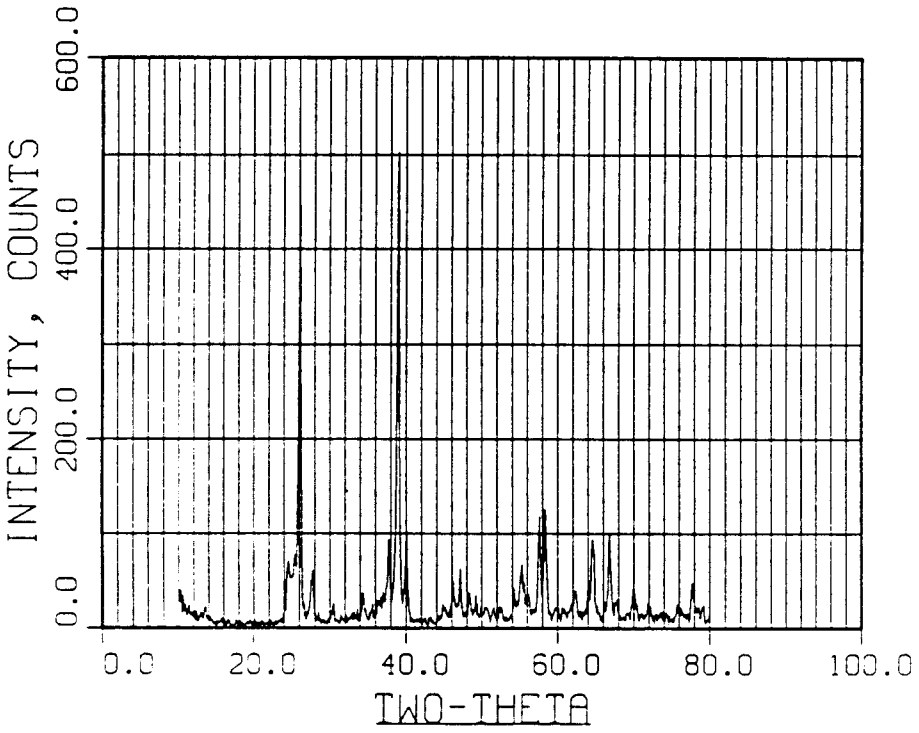

Figure B.7. XRD pattern for $H_{0.31}MoO_3$ starting material.

d-spacing, Å	I/I_o	Assignment	d-spacing, Å	I/I_o	Assignment
3.692	4	*	1.692	8	*
3.618	14	*	1.661	13	*
3.506	15	*	1.653	9	*
3.414	89	*	1.636	7	*
3.220	12	*	1.600	23	*
2.930	5	*	1.582	15	*
2.607	7	*	1.549	4	*
2.386	18	*	1.539	4	*
2.309	100	*	1.521	4	*
2.023	5	*	1.488	8	*
1.969	10	*	1.455	9	*
1.929	12	*	1.442	19	*
1.884	7	*	1.411	5	*
1.852	7	*	1.400	20	*
1.845	5	*	1.387	5	*
1.827	4	*	1.382	6	*
1.810	4	*	1.344	8	*
1.804	4	*	1.313	5	*
1.771	4	*	1.255	5	*
1.746	5	*	1.229	9	*
1.740	4	*	1.209	5	*

* $H_{0.31}MoO_3$

Table B.7. D-spacings for $H_{0.31}MoO_3$ starting material.

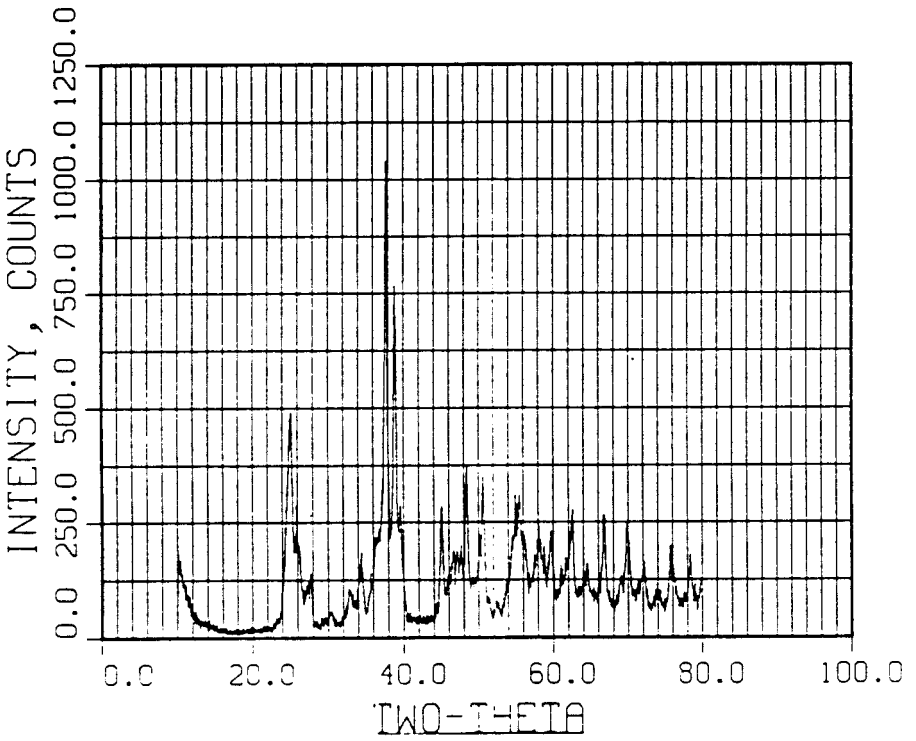

Figure B.8. XRD pattern for $H_{0.80}MoO_3$ starting material.

d-spacing, Å	I/I_o	Assignment	d-spacing, Å	I/I_o	Assignment
3.540	47	*	1.671	30	*
3.440	28	*	1.655	30	*
2.935	6	*	1.636	21	*
2.734	10	*	1.589	24	*
2.592	14	*	1.570	19	*
2.383	100	*	1.549	22	*
2.276	27	*	1.485	27	*
1.949	18	*	1.443	15	*
1.929	18	*	1.401	26	*
1.908	19	*	1.360	13	*
1.879	36	*	1.347	24	*
1.812	20	*	1.309	16	*
1.802	34	*	1.282	11	*
1.746	8	*	1.256	19	*
1.682	21	*	1.220	17	*

* $H_{0.80}MoO_3$

Table B.8. D-spacings for $H_{0.80}MoO_3$ starting material.

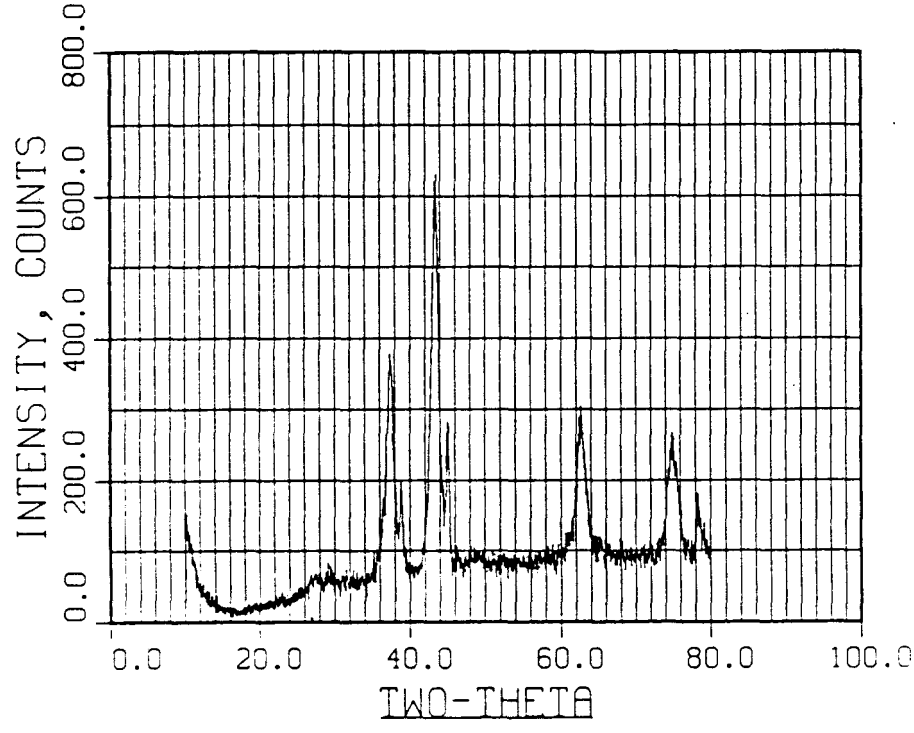

Figure B.9. XRD pattern for product of MoO_3/NH_3 reaction at 750°C.

d-spacing, Å	I/I_o	Assignment
2.404	62	1
2.321	----	*
2.085	100	1
2.014	----	*
1.484	50	1
1.268	44	1
1.221	----	*

1 = Mo_2N

* = Aluminum Sample Holder

Table B.9. D-spacings for product of MoO_3/NH_3 reaction at 750°C.

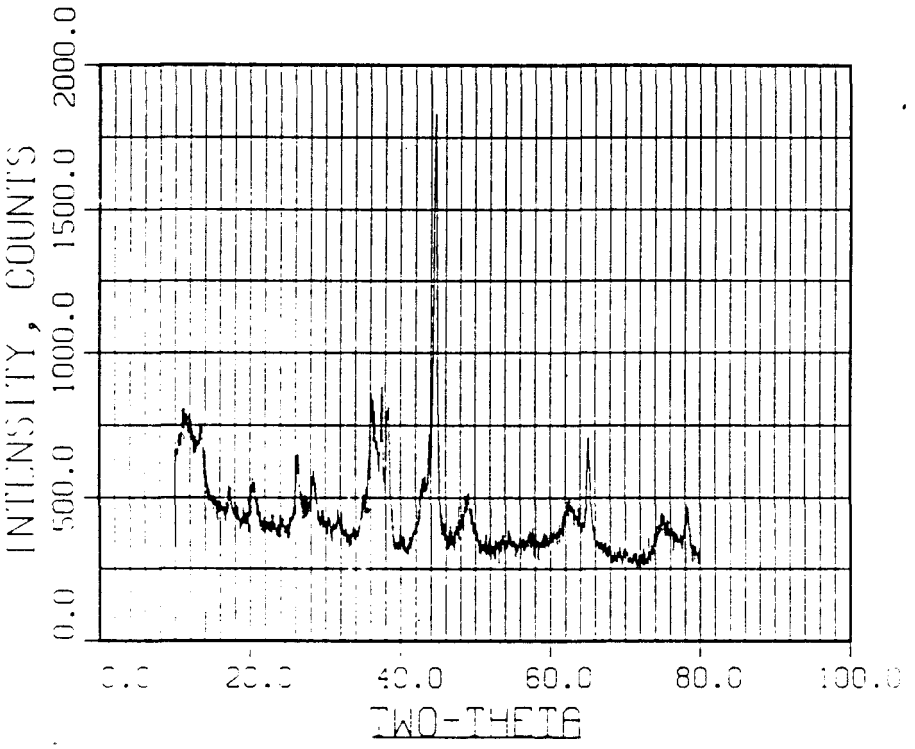

Figure B.10. XRD pattern for product of ammonium paramolybdate/NH_3 reaction at 625°C.

d-spacing, Å	I/I_o	Assignment
3.382	----	*
2.484	97	2
2.395	100	1
2.092	65	1
2.031	----	*
1.853	58	2
1.485	57	1
1.433	80	2
1.268	51	2
1.222	53	2,*

1 = Mo_2N
2 = MoN
* = Aluminum Sample Holder

Table B.10. D-spacings for product of ammonium paramolybdate/NH_3 reaction at 625°C.

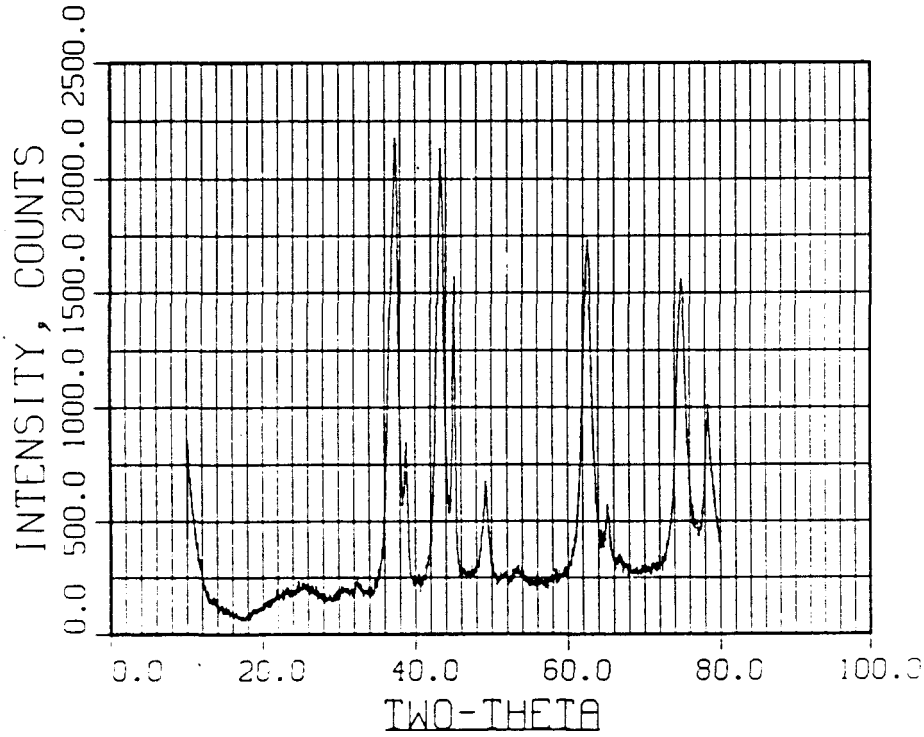

Figure B.11. XRD pattern for product of ammonium paramolybdate/NH_3 reaction at 750°C.

d-spacing, Å	I/I_o	Assignment
2.407	100	1
2.318	----	*
2.089	98	1
1.852	31	2
1.484	80	1
1.432	26	2
1.269	72	1,2
1.220	47	2,*

1 = Mo_2N
2 = MoN
* = Aluminum Sample Holder

Table B.11. D-spacings for product of ammonium paramolybdate/NH_3 reaction at 750°C.

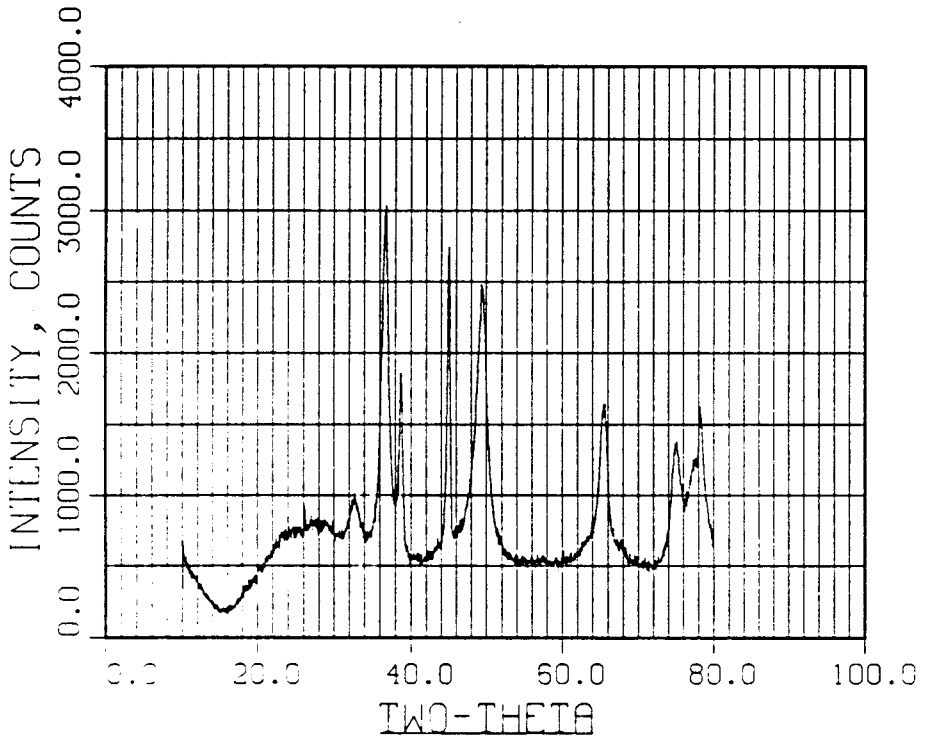

Figure B.12. XRD pattern for product of diammonium molybdate/NH_3 reaction at 625°C.

d-spacing, Å	I/I_o	Assignment
2.738	33	2
2.442	100	2
2.329	----	*
2.014	----	*
1.848	82	2
1.426	----	*
1.265	45	2
1.230	42	2
1.222	----	*

1 = Mo_2N
2 = MoN
* = Aluminum Sample Holder

Table B.12. D-spacings for product of diammonium molybdate/NH_3 reaction at 625°C.

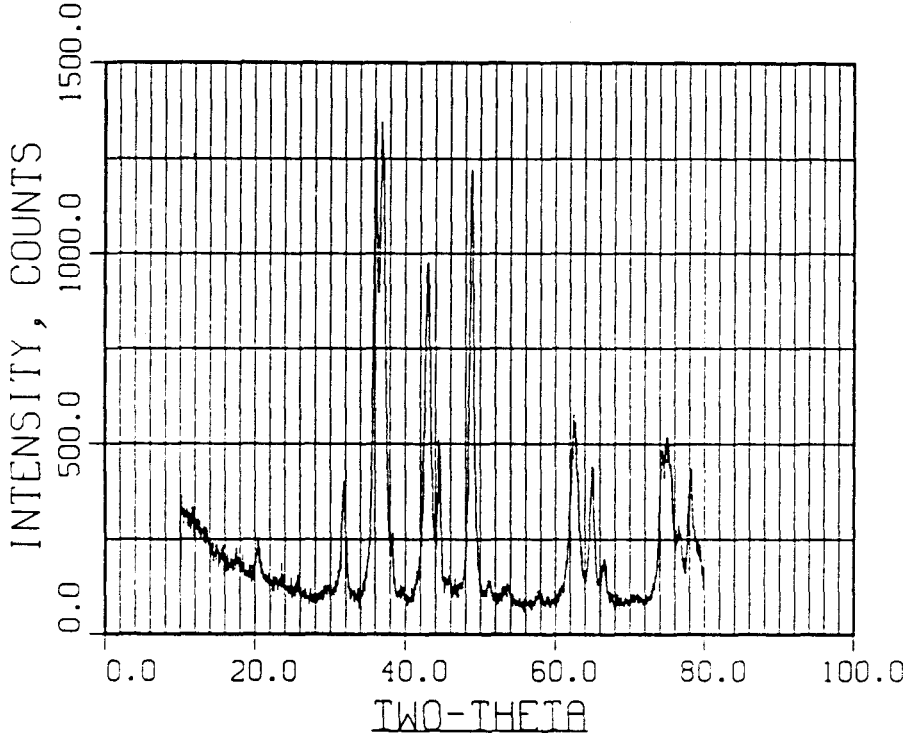

Figure B.13. XRD pattern for product of MoO_2/NH_3 reaction at 750°C.

d-spacing, Å	I/I_0	Assignment
2.814	29	2
2.494	100	2
2.432	94	1
2.347	----	*
2.103	71	1
2.040	----	*
1.866	89	2
1.487	42	1
1.436	32	2
1.277	35	2
1.266	38	1
1.244	21	*
1.224	32	2
1.209	18	1

1 = Mo_2N
2 = MoN
* = Aluminum Sample Holder

Table B.13. D-spacings for product of MoO_2/NH_3 reaction at 750°C.

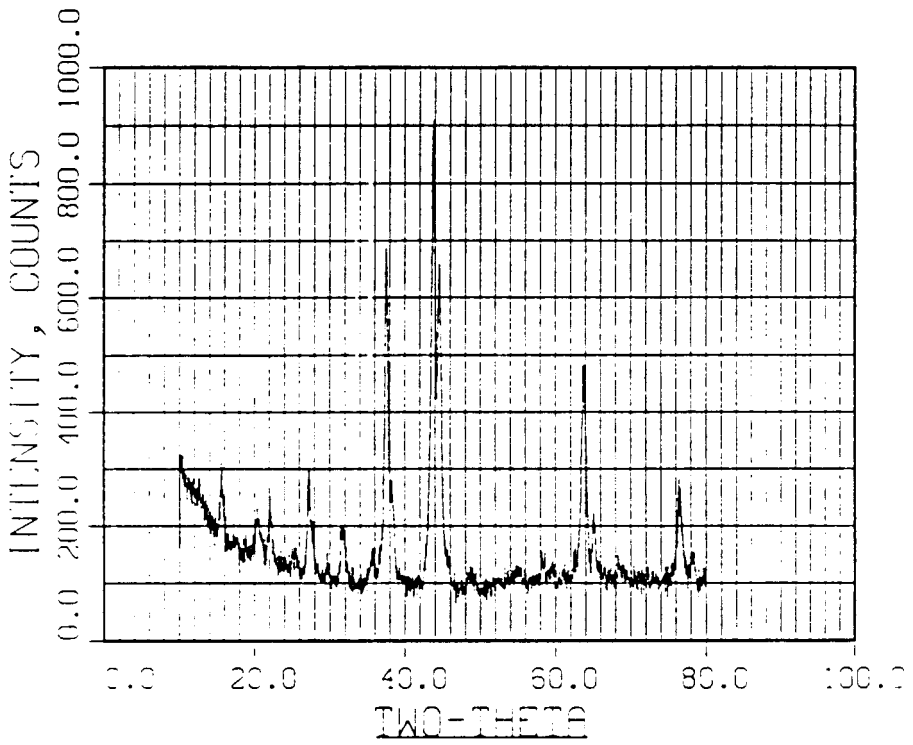

Figure B.14. XRD pattern for product of V_2O_5/NH_3 reaction at 750°C.

d-spacing, Å	I/I_o	Assignment
2.398	76	1
2.353	31	*
2.064	100	1
2.033	----	*
1.462	53	1
1.434	----	*
1.246	31	1

1 = VN

* = Aluminum Sample Holder

Table B.14. D-spacings for product of V_2O_5/NH_3 reaction at 750°C.

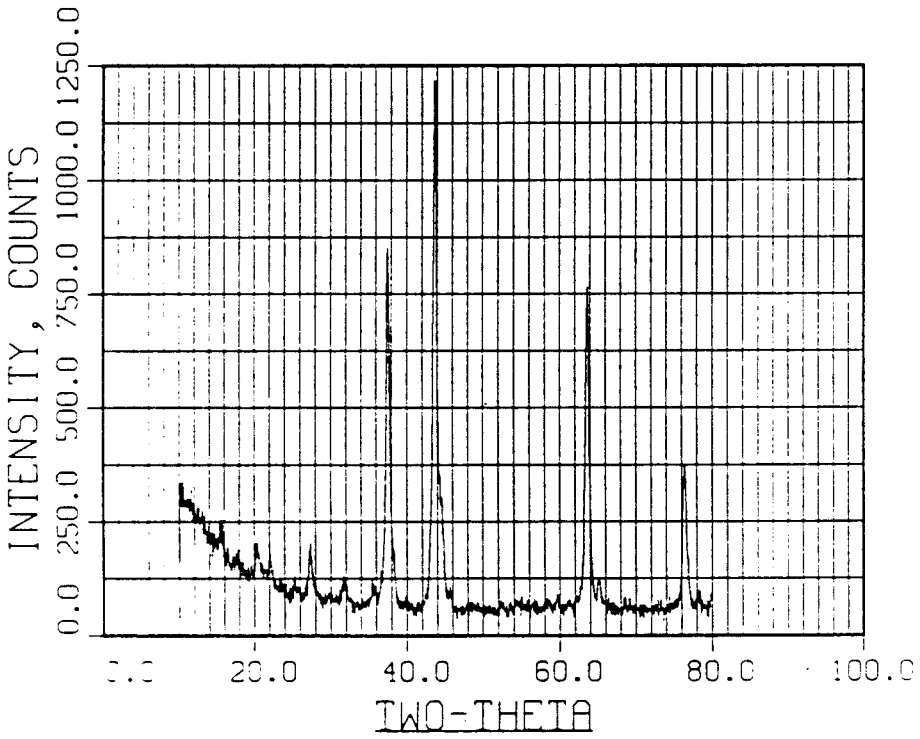

Figure B.15. XRD pattern for product of VO_2/NH_3 reaction at 750°C.

d-spacing, Å	I/I_0	Assignment
2.398	70	1
2.073	100	1
1.462	63	1
1.247	31	1

1 = VN

* = Aluminum Sample Holder

Table B.15. D-spacings for product of VO_2/NH_3 reaction at 750°C.

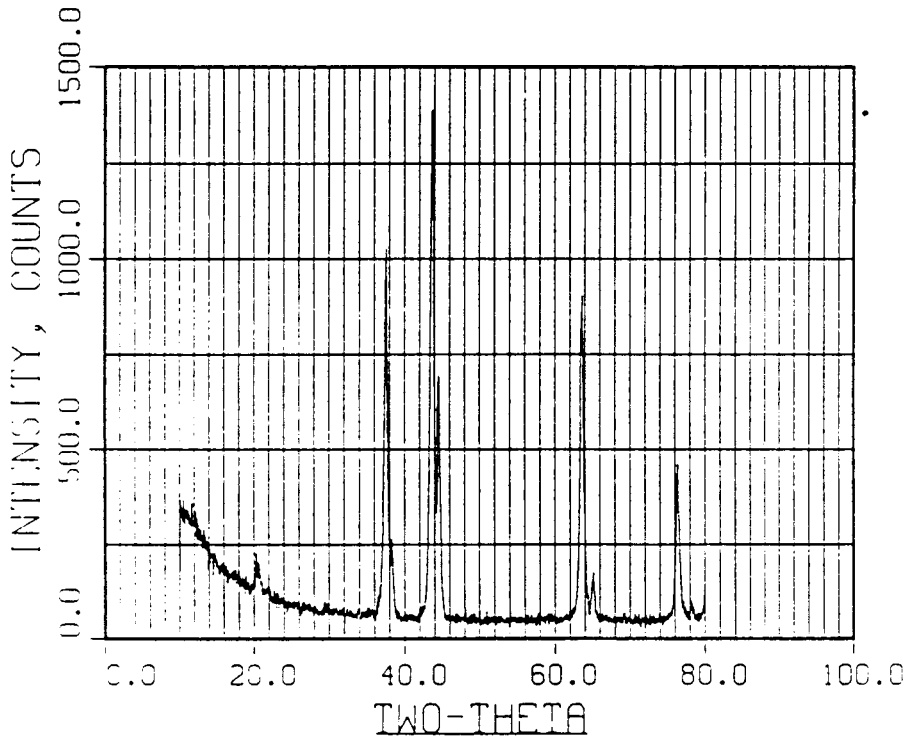

Figure B.16. XRD pattern for product of V_2O_3/NH_3 reaction at 750°C.

d-spacing, Å	I/I_0	Assignment
2.395	74	1
2.350	----	*
2.073	100	1
2.033	----	*
1.463	65	1
1.433	----	*
1.247	33	1

1 = VN

* = Aluminum Sample Holder

Table B.16. D-spacings for product of V_2O_3/NH_3 reaction at 750°C.

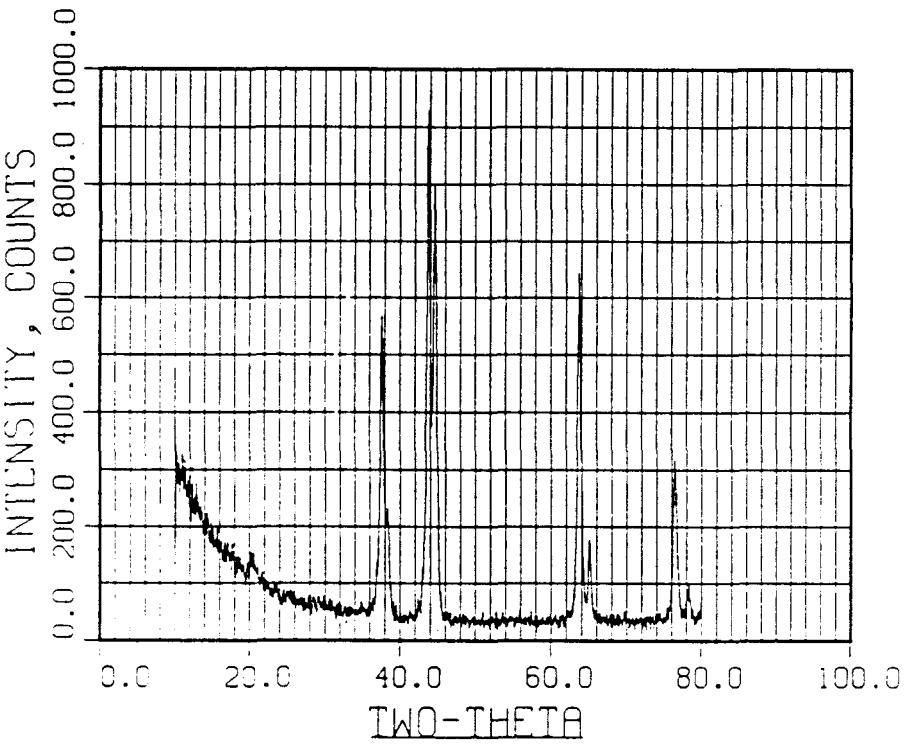

Figure B.17. XRD pattern for product of ammonium metavanadate/NH_3 reaction at 750°C.

d-spacing, Å	I/I_0	Assignment
2.395	61	1
2.347	----	*
2.069	100	1
2.031	----	*
1.462	69	1
1.434	----	*
1.246	34	1
1.221	----	*

1 = VN

* = Aluminum Sample Holder

Table B.17. D-spacings for product of ammonium metavanadate/NH_3 reaction at 750°C.

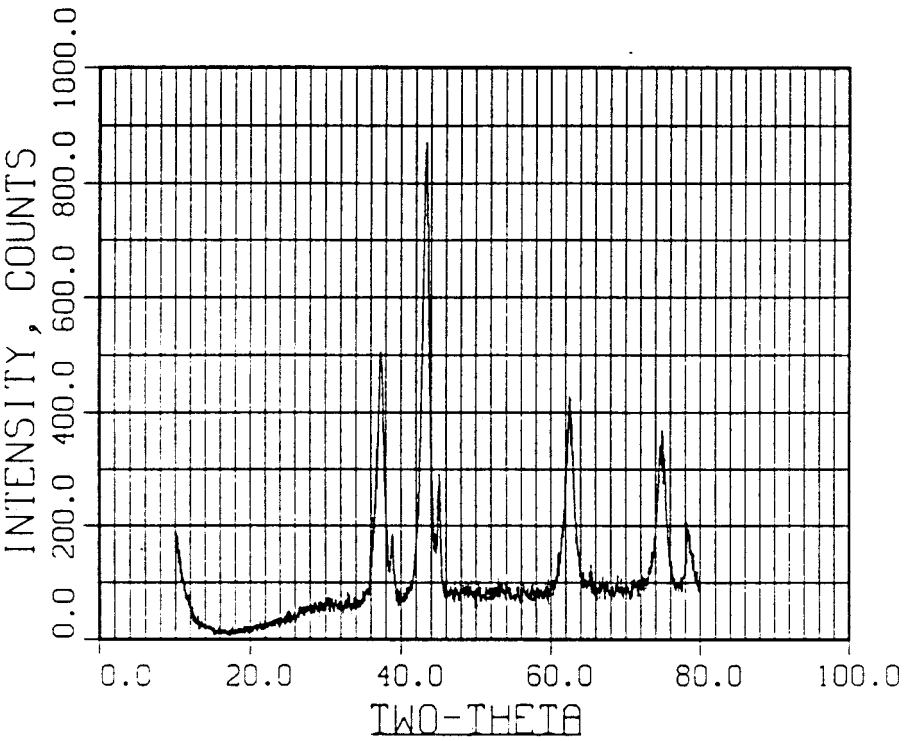

Figure B.18. XRD pattern for product of $H_{0.04}MoO_3/NH_3$ reaction at 750°C.

d-spacing, Å	I/I_o	Assignment
2.410	58	1
2.318	----	*
2.087	100	1
2.012	---	*
1.483	49	1
1.266	41	1
1.222	----	*

1 = Mo_2N
2 = MoN
* = Aluminum Sample Holder

Table B.18. D-spacings for product of $H_{0.04}MoO_3/NH_3$ reaction at 750°C.

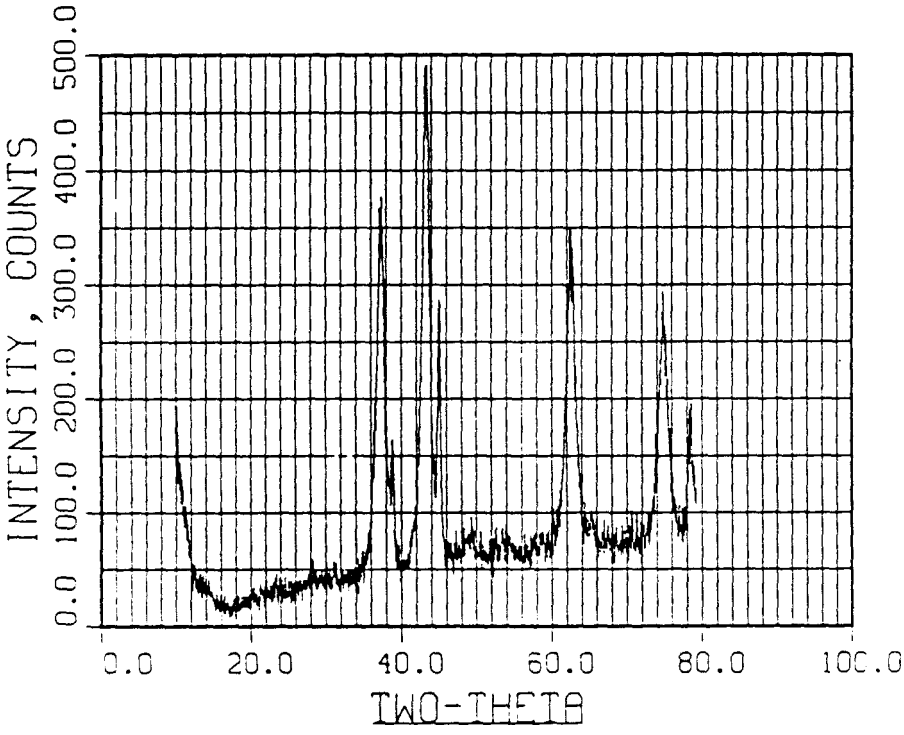

Figure B.19. XRD pattern for product of $H_{0.13}MoO_3/NH_3$ reaction at 750°C.

d-spacing, Å	I/I_o	Assignment
2.407	78	1
2.318	----	*
2.087	100	1
2.012	----	*
1.488	73	1
1.269	61	1
1.218	----	*

1 = Mo_2N
2 = MoN
* = Aluminum Sample Holder

Table B.19. D-spacings for product of $H_{0.13}MoO_3/NH_3$ reaction at 750°C.

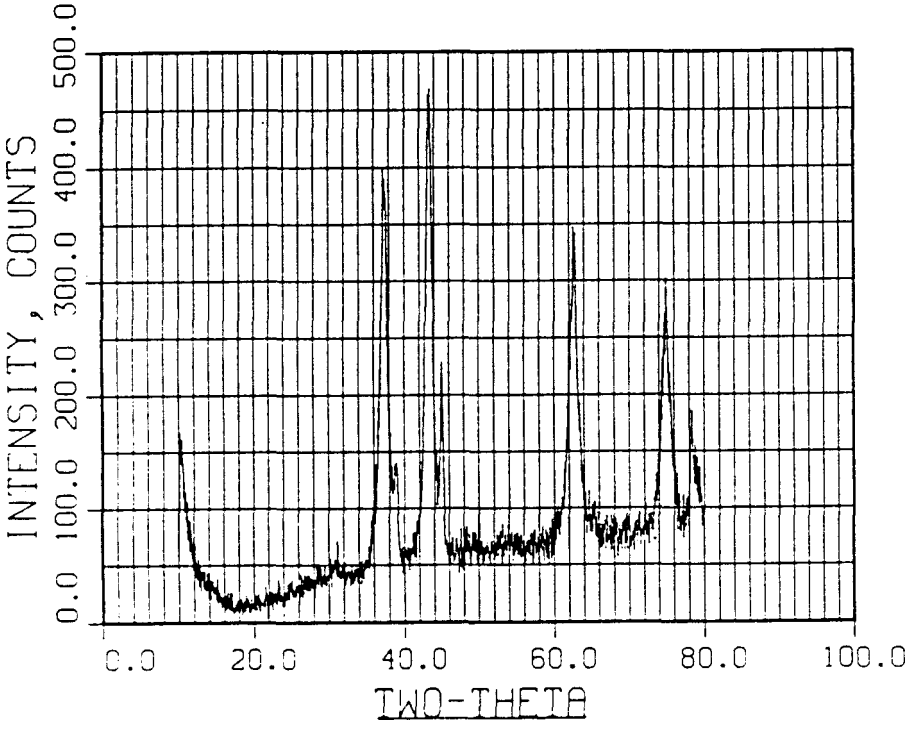

Figure B.20. XRD pattern for product of $H_{0.31}MoO_3/NH_3$ reaction at 750°C.

d-spacing, Å	I/I_o	Assignment
2.407	78	1
2.318	----	*
2.087	100	1
2.012	----	*
1.488	73	1
1.269	61	1
1.218	----	*

1 = Mo_2N
2 = MoN
* = Aluminum Sample Holder

Table B.20. D-spacings for product of $H_{0.31}MoO_3/NH_3$ reaction at 750°C.

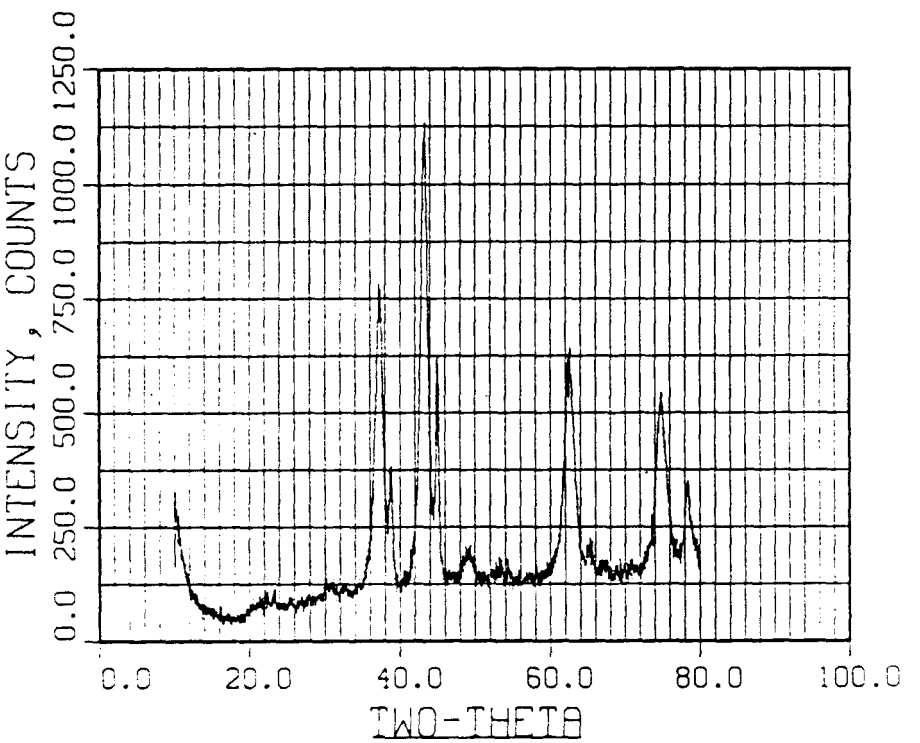

Figure B.21. XRD pattern for product of $H_{0.80}MoO_3/NH_3$ reaction at 750°C.

d-spacing, Å	I/I_o	Assignment
2.417	69	1
2.326	----	*
2.089	100	1
2.014	----	*
1.859	17	2
1.484	57	1
1.430	----	*
1.269	48	1
1.219	----	*

1 = Mo_2N
2 = MoN
* = Aluminum Sample Holder

Table B.21. D-spacings for product of $H_{0.80}MoO_3/NH_3$ reaction at 750°C.

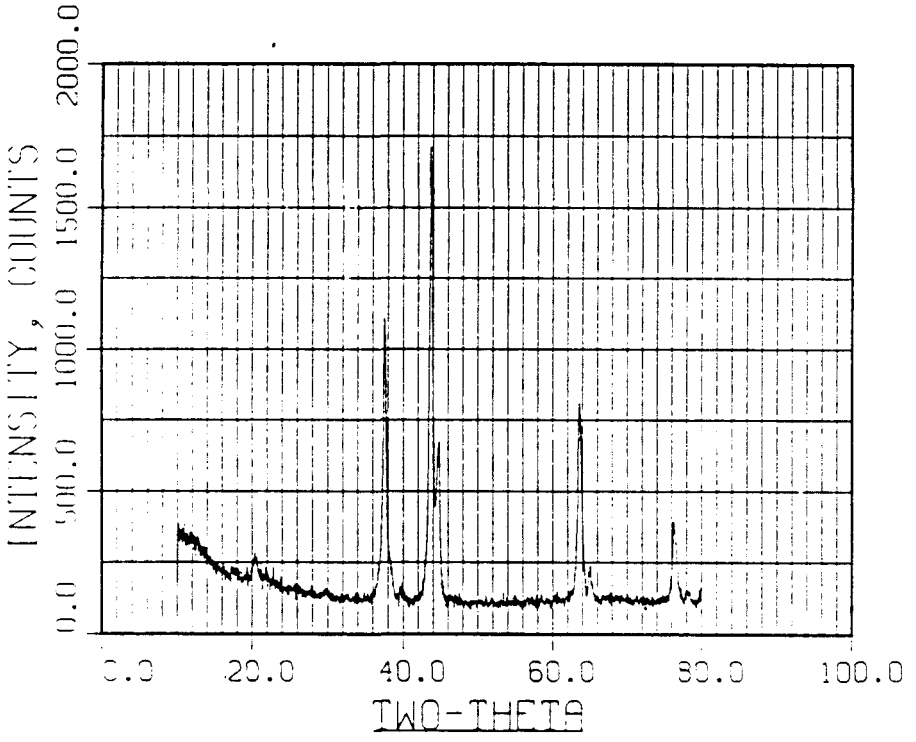

Figure B.22. XRD pattern for product of $H_{3.05}V_2O_5/NH_3$ reaction at 750°C.

* d-spacing, Å	I/I_o	Assignment
2.398	65	1
2.071	100	1
2.023	----	*
1.464	51	1
1.433	----	*
1.248	23	1

1 = VN

* = Aluminum Sample Holder

Table B.22. D-spacings for product of $H_{3.05}V_2O_5/NH_3$ reaction at 750°C.

APPENDIX C: HIGH TEMPERATURE XRD RESULTS

The high temperature XRD results for the reactions of molybdenum trioxide MoO_3, ammonium paramolybdate $(NH_4)_6Mo_7O_{24}\cdot 4H_2O$, and diammonium molybdate $(NH_4)_2MoO_4$ with ammonia are shown in the following figures; the d-spacings and indexing for the XRD patterns are listed in the following tables.

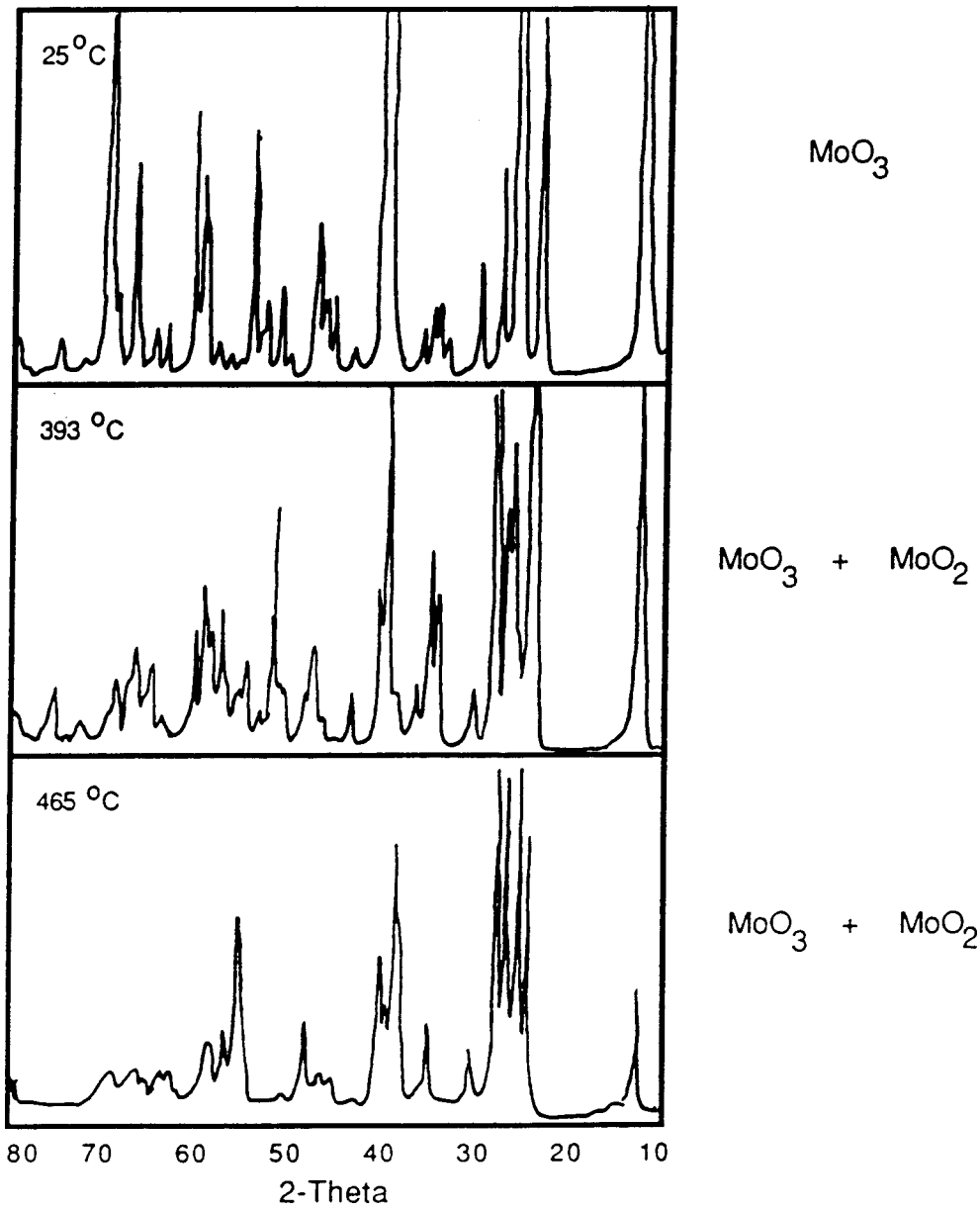

Figure C.1. High temperature XRD patterns for molybdenum trioxide/ammonia reaction at 25°C, 393°C, and 465°C.

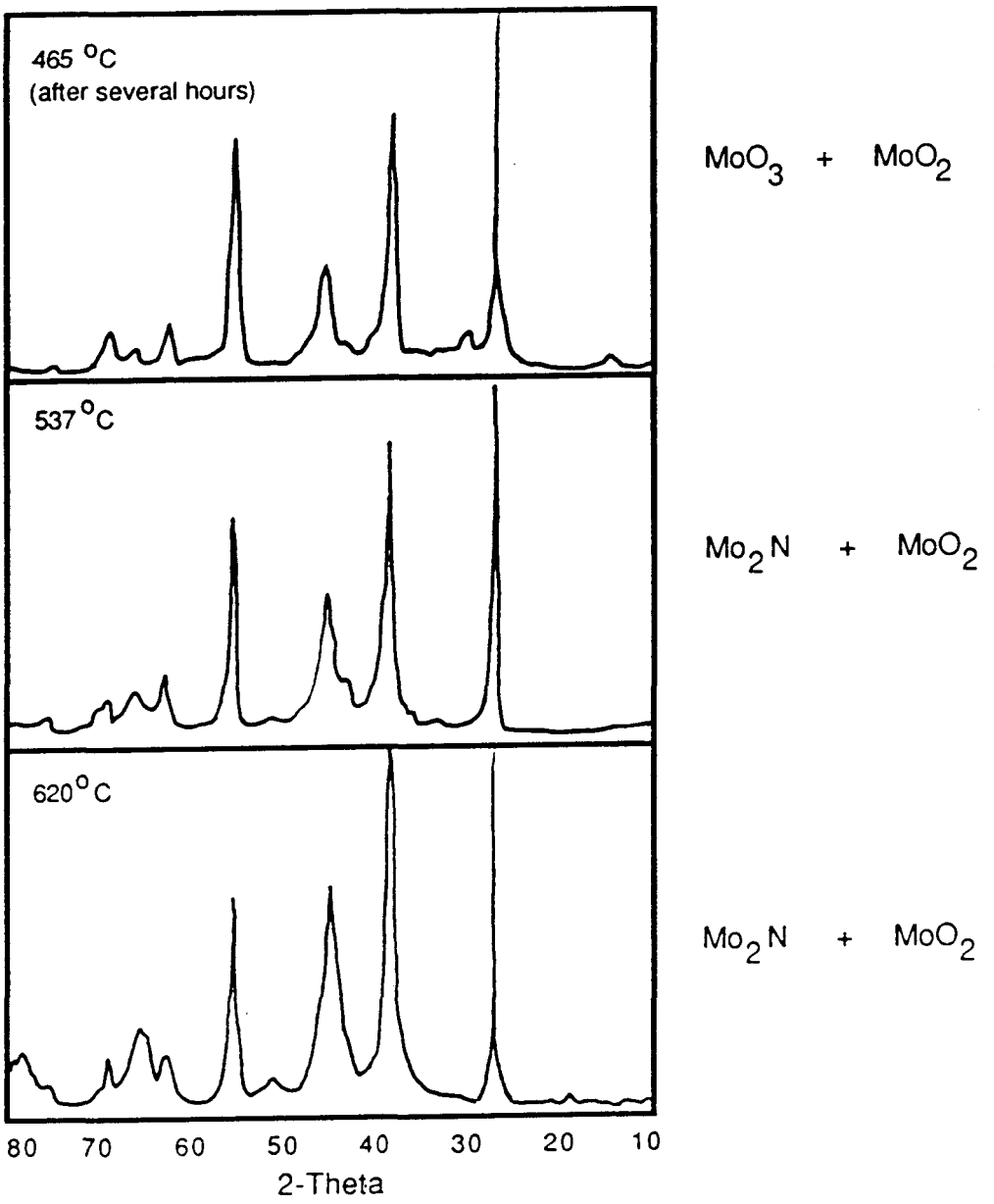

Figure C.2. High temperature XRD patterns for molybdenum trioxide/ammonia reaction at 465°C (after several hours), 537°C, and 620°C.

d-spacing, Å	I/I_o	Assignment	d-spacing, Å	I/I_o	Assignment
6.66	72	1	1.75	7	1
3.75	61	1	1.73	25	1
3.43	100	1	1.71	7	1
3.22	97	1	1.69	9	1
2.98	15	1	1.66	15	1
2.68	15	1	1.62	15	1
2.63	32	1	1.59	33	1
2.59	6	1	1.58	14	1
2.51	11	1	1.56	37	1
2.30	100	1	1.50	11	1
2.26	41	1	1.47	15	1
2.12	10	1	1.45	2	1
2.02	28	1	1.44	11	1
1.99	9	1	1.43	40	1
1.97	15	1	1.43	25	1
1.97	14	1	1.40	18	1
1.95	31	1	1.39	10	1
1.84	26	1	1.38	25	1
1.76	9	1	1.38	17	1

1 = MoO_3 2 = MoO_2 3 = MoO_xN_{1-x} or Mo_2N

* = Aluminum Sample Holder

Table C.1. D-spacings for high temperature XRD pattern of MoO_3/NH_3 reaction at 25°C.

d-spacing, Å	I/I_o	Assignment	d-spacing, Å	I/I_o	Assignment
7.00	100	1	2.00	6	1
3.75	61	1	1.96	10	1
3.68	60		1.92	15	1
3.53	32		1.84	13	1
3.45	46	1	1.83	10	1
3.40	31	2	1.81	5	1
3.25	31	1	1.72	7	1
3.21	95	1	1.70	13	1
2.99	10	1	1.66	20	1
2.67	7	1	1.62	21	1
2.61	42	1	1.61	18	1
2.55	5	1	1.58	11	1
2.51	7	1	1.50	6	1
2.37	20	2	1.46	8	1
2.32	46	1	1.44	15	1
2.28	23	1	1.40	8	1
2.28	23	1	1.34	8	1
2.12	3	1	1.29	4	1
2.03	3	1	1.24	10	1

1 = MoO_3 2 = MoO_2 3 = MoO_xN_{1-x} or Mo_2N

* = Aluminum Sample Holder

Table C.2. D-spacings for high temperature XRD pattern of MoO_3/NH_3 reaction at 393°C.

d-spacing, Å	I/I_o	Assignment	d-spacing, Å	I/I_o	Assignment
6.86	19	1	1.70	48	2
3.67	15	1	1.52	12	2
3.52	21	1	1.45	----	*
3.36	100	2	1.45	----	*
2.40	54	2	1.40	12	2
2.04	----	*			

1 = MoO_3 2 = MoO_2 3 = MoO_xN_{1-x} or Mo_2N

* = Aluminum Sample Holder

Table C.3. D-spacings for high temperature XRD pattern of MoO_3/NH_3 reaction at 465°C.

d-spacing, Å	I/I_o	Assignment	d-spacing, Å	I/I_o	Assignment
6.86	18	1	1.70	47	2
3.67	14	1	1.52	11	2
3.52	20	1	1.45	----	*
3.36	100	2	1.45	----	*
2.40	----	*	1.40	10	2

1 = MoO_3 2 = MoO_2 3 = MoO_xN_{1-x} or Mo_2N
* = Aluminum Sample Holder

Table C.4. D-spacings for high temperature XRD pattern of MoO_3/NH_3 reaction at 465°C after several hours.

d-spacing, Å	I/I_o	Assignment	d-spacing, Å	I/I_o	Assignment
3.34	100	2	1.52	----	*
2.40	61	3	1.52	----	*
2.04	26	3,*	1.45	13	3
1.70	49	2	1.40	11	2

1 = MoO_3 2 = MoO_2 3 = MoO_xN_{1-x} or Mo_2N

* = Aluminum Sample Holder

Table C.5. D-spacings for high temperature XRD pattern of MoO_3/NH_3 reaction at 537°C.

d-spacing, Å	I/I_o	Assignment	d-spacing, Å	I/I_o	Assignment
3.34	100	2	1.70	42	2
2.39	82	3	1.52	----	*
2.04	48	3,*	1.46	17	3
1.70	18	2	1.40	11	2

1 = MoO_3 2 = MoO_2 3 = MoO_xN_{1-x} or Mo_2N

* = Aluminum Sample Holder

Table C.6. D-spacings for high temperature XRD pattern of MoO_3/NH_3 reaction at 620°C.

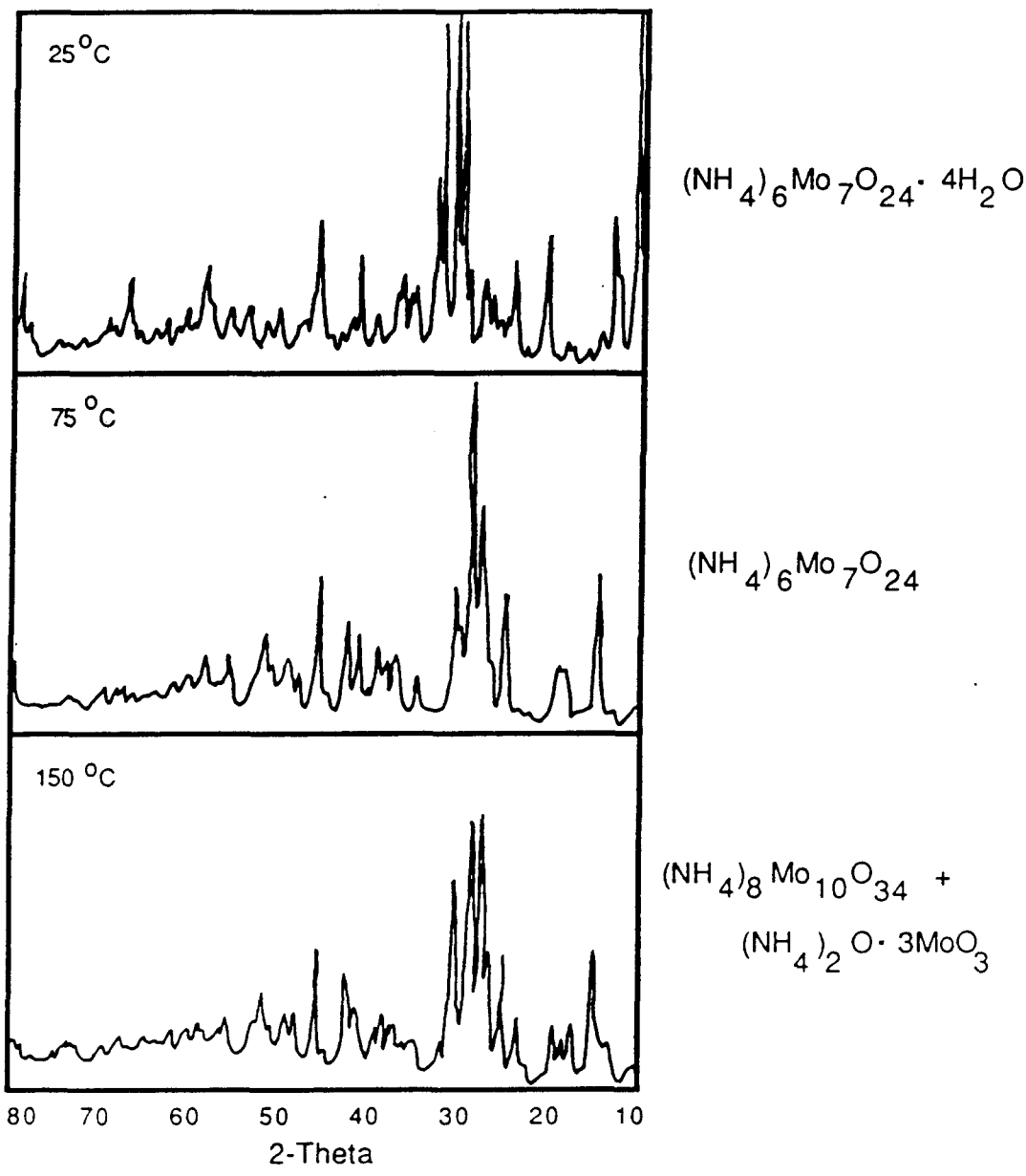

Figure C.3. High temperature XRD patterns for ammonium paramolybdate/ammonia reaction at 25°C, 75°C, and 150°C.

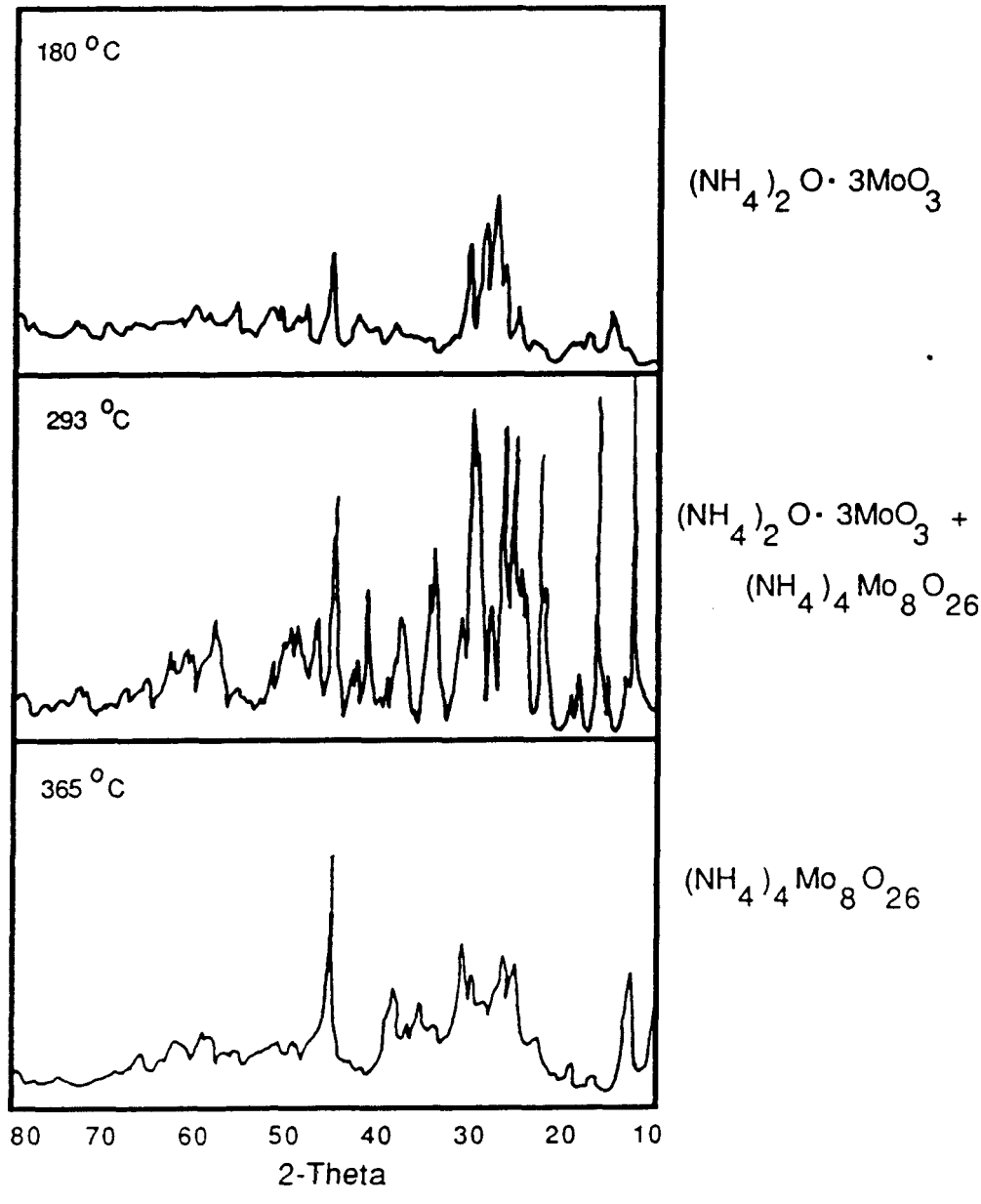

Figure C.4. High temperature XRD patterns for ammonium paramolybdate/ammonia reaction at 180°C, 293°C, and 365°C.

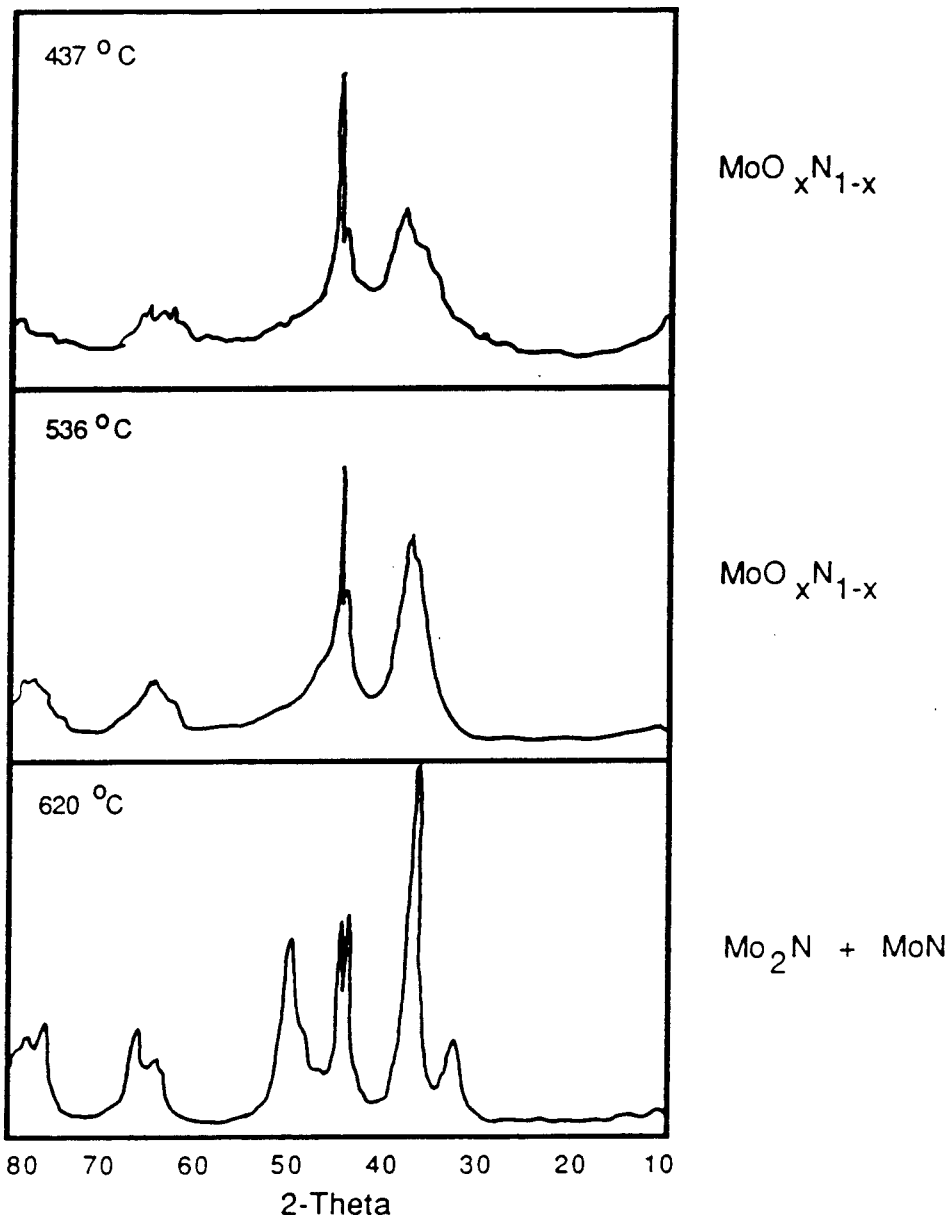

Figure C.5. High temperature XRD patterns for ammonium paramolybdate/ammonia reaction at 437°C, 536°C, and 620°C.

d-spacing, Å	I/I_o	Assignment	d-spacing, Å	I/I_o	Assignment
8.85	100	1	3.51	13	1
8.19	12	1	3.47	12	1
7.41	29	1	3.37	22	1
7.28	31	1	3.27	17	1
7.05	66	1	3.19	32	1
6.35	21	1	3.11	37	1
6.24	8	1	3.08	14	1
5.57	9	1	3.00	21	1
5.37	6	1	2.90	5	1
5.22	5	1	2.79	25	1
4.96	4	1	2.74	17	1
4.73	12	1	2.68	6	1
4.67	10	1	2.64	6	1
4.25	3	1	2.62	5	1
4.11	5	1	2.58	3	1
4.01	10	1	2.54	3	1
3.97	20	1	2.49	14	1
3.85	10	1	2.46	8	1
3.74	10	1	2.43	3	1
3.60	18	1	2.35	15	1

1 = $(NH_4)_6Mo_7O_{24}\cdot 4H_2O$ 2 = $(NH_4)_6Mo_7O_{24}$
3 = $(NH_4)_8Mo_{10}O_{34}$ 4 = $(NH_4)_2O\cdot MoO_3$
5 = $(NH_4)_4Mo_8O_{26}$ 6 = MoO_xN_{1-x} or Mo_2N
7 = MoN *Aluminum Sample Holder

Table C.7. D-spacings for high temperature XRD pattern of $(NH_4)_6Mo_7O_{24}\cdot 4H_2O/NH_3$ reaction at 25°C.

d-spacing, Å	I/I_o	Assignment	d-spacing, Å	I/I_o	Assignment
6.86	6	2	3.15	14	2
5.81	29	2	3.04	45	2
5.57	35	2	2.93	10	2
4.93	74	2	2.81	16	2
3.93	42	2	2.68	8	2
3.82	23	2	2.57	4	2
3.62	25	2	2.47	5	2
3.45	34	2	2.41	7	2
3.24	100	2			

1 = $(NH_4)_6Mo_7O_{24}\cdot 4H_2O$ 2 = $(NH_4)_6Mo_7O_{24}$
3 = $(NH_4)_8Mo_{10}O_{34}$ 4 = $(NH_4)_2O\cdot MoO_3$
5 = $(NH_4)_4Mo_8O_{26}$ 6 = MoO_xN_{1-x} or Mo_2N
7 = MoN

* Aluminum Sample Holder

Table C.8. D-spacings for high temperature XRD pattern of $(NH_4)_6Mo_7O_{24}\cdot 4H_2O/NH_3$ reaction at 75°C.

d-spacing, Å	I/I_0	Assignment	d-spacing, Å	I/I_0	Assignment
7.03	23	4	3.35	82	3,4
6.19	85	3,4	3.33	80	3
5.79	23	4	3.21	97	
5.54	22	3,4	3.19	100	
4.98	30	3	3.14	36	4
4.87	41		3.07	38	3
4.80	30	3	3.00	62	4
3.65	46	3,4	2.88	19	3
3.43	36	3,4			

1 = $(NH_4)_6Mo_7O_{24}\cdot 4H_2O$ 2 = $(NH_4)_6Mo_7O_{24}$
3 = $(NH_4)_8Mo_{10}O_{34}$ 4 = $(NH_4)_2O\cdot MoO_3$
5 = $(NH_4)_4Mo_8O_{26}$ 6 = MoO_xN_{1-x} or Mo_2N
7 = MoN

* Aluminum Sample Holder

Table C.9. D-spacings for high temperature XRD pattern of $(NH_4)_6Mo_7O_{24}\cdot 4H_2O/NH_3$ reaction at 150°C.

d-spacing, Å	I/I_o	Assignment	d-spacing, Å	I/I_o	Assignment
6.86	94	4	2.56	17	
6.22	14		2.40	10	
5.68	14	4	2.34	13	
5.28	100	4	2.29	12	
4.48	10		2.25	13	4
3.92	83	4	2.20	44	4
3.65	40	4	2.13	13	4
3.47	85	4	2.03	21	*
3.33	92	4	2.00	10	4
3.15	27	4	1.95	37	4
3.00	77	4	1.94	23	4
2.97	65	4	1.90	14	4
2.85	31	4	1.87	15	4
2.82	15	4	1.84	28	4
2.61	44	4	1.77	18	4

1 = $(NH_4)_6Mo_7O_{24}\cdot 4H_2O$ 2 = $(NH_4)_6Mo_7O_{24}$
3 = $(NH_4)_8Mo_{10}O_{34}$ 4 = $(NH_4)_2O\cdot MoO_3$
5 = $(NH_4)_4Mo_8O_{26}$ 6 = MoO_xN_{1-x} or Mo_2N
7 = MoN

* Aluminum Sample Holder

Table C.10. D-spacings for high temperature XRD pattern of $(NH_4)_6Mo_7O_{24}\cdot 4H_2O/NH_3$ reaction at 180°C.

d-spacing, Å	I/I_o	Assignment	d-spacing, Å	I/I_o	Assignment
7.00	80	5	2.99	57	4
6.84	100	4	2.94	81	4
6.39	6	4	2.86	26	4
5.64	11	4	2.67	19	4
5.25	94	4	2.61	36	4,5
4.71	19	5	2.56	34	5
4.46	6	5	2.47	11	5
3.99	48	5	2.38	37	5
3.90	72	4	2.24	7	4
3.64	40	4	2.19	35	4
3.60	34	5	2.14	16	4
3.56	56	4	2.10	16	4
3.48	70	4	2.03	----	*
3.41	49	4	2.01	23	4,5
3.31	73	5	1.94	19	4
3.16	33	5	1.90	15	4
3.15	33	4	1.88	26	4

1 = $(NH_4)_6Mo_7O_{24}\cdot 4H_2O$ 2 = $(NH_4)_6Mo_7O_{24}$
3 = $(NH_4)_8Mo_{10}O_{34}$ 4 = $(NH_4)_2O\cdot MoO_3$
5 = $(NH_4)_4Mo_8O_{26}$ 6 = MoO_xN_{1-x} or Mo_2N
7 = MoN

* Aluminum Sample Holder

Table C.11. D-spacings for high temperature XRD pattern of $(NH_4)_6Mo_7O_{24}\cdot 4H_2O/NH_3$ reaction at 293°C.

d-spacing, Å	I/I_0	Assignment
2.35	100	6
2.07	80	6
2.04	----	*
1.46	50	6

1 = $(NH_4)_6Mo_7O_{24}\cdot 4H_2O$ 2 = $(NH_4)_6Mo_7O_{24}$
3 = $(NH_4)_8Mo_{10}O_{34}$ 4 = $(NH_4)_2O\cdot MoO_3$
5 = $(NH_4)_4Mo_8O_{26}$ 6 = MoO_xN_{1-x} or Mo_2N
7 = MoN

* Aluminum Sample Holder

Table C.12. D-spacings for high temperature XRD pattern of $(NH_4)_6Mo_7O_{24}\cdot 4H_2O/NH_3$ reaction at 437°C.

d-spacing, Å	I/I_0	Assignment
2.40	100	6
2.07	81	6
2.04	----	*
1.47	31	6
1.45	33	6

1 = $(NH_4)_6Mo_7O_{24}\cdot 4H_2O$ 2 = $(NH_4)_6Mo_7O_{24}$
3 = $(NH_4)_8Mo_{10}O_{34}$ 4 = $(NH_4)_2O\cdot MoO_3$
5 = $(NH_4)_4Mo_8O_{26}$ 6 = MoO_xN_{1-x} or Mo_2N
7 = MoN

* Aluminum Sample Holder

Table C.13. D-spacings for high temperature XRD pattern of $(NH_4)_6Mo_7O_{24}\cdot 4H_2O/NH_3$ reaction at 536°C.

d-spacing, Å	I/I_o	Assignment
2.78	13	7
2.46	100	7
2.41	33	6
2.08	48	6
2.05	----	*
1.85	39	7
1.46	12	6
1.43	17	7
1.26	20	7

1 = $(NH_4)_6Mo_7O_{24}\cdot 4H_2O$ 2 = $(NH_4)_6Mo_7O_{24}$
3 = $(NH_4)_8Mo_{10}O_{34}$ 4 = $(NH_4)_2O\cdot MoO_3$
5 = $(NH_4)_4Mo_8O_{26}$ 6 = MoO_xN_{1-x} or Mo_2N
7 = MoN

* Aluminum Sample Holder

Table C.14. D-spacings for high temperature XRD pattern of $(NH_4)_6Mo_7O_{24}\cdot 4H_2O/NH_3$ reaction at 620°C.

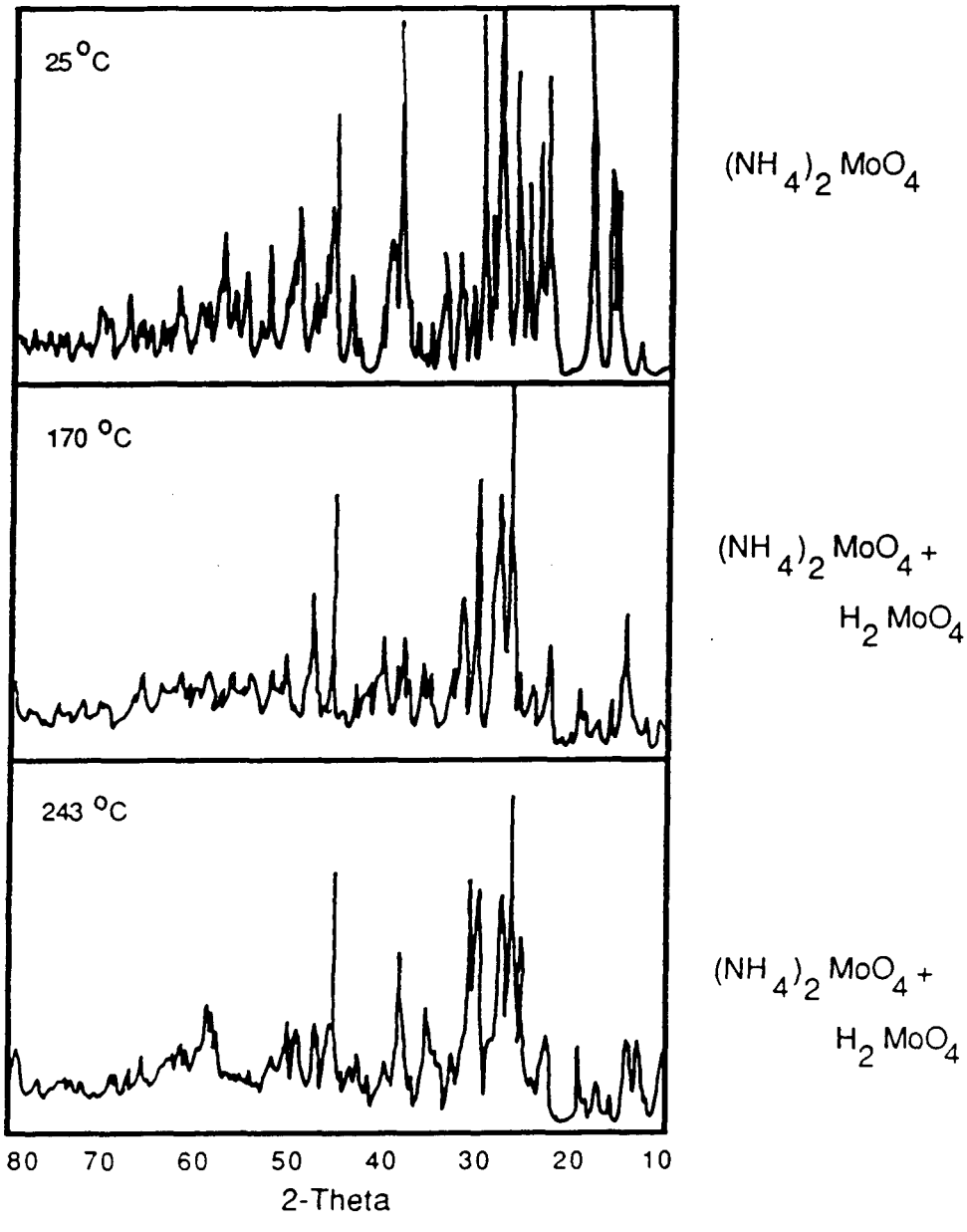

Figure C.6. High temperature XRD patterns for diammonium molybdate/ammonia reaction at 25°C, 170°C, and 243°C.

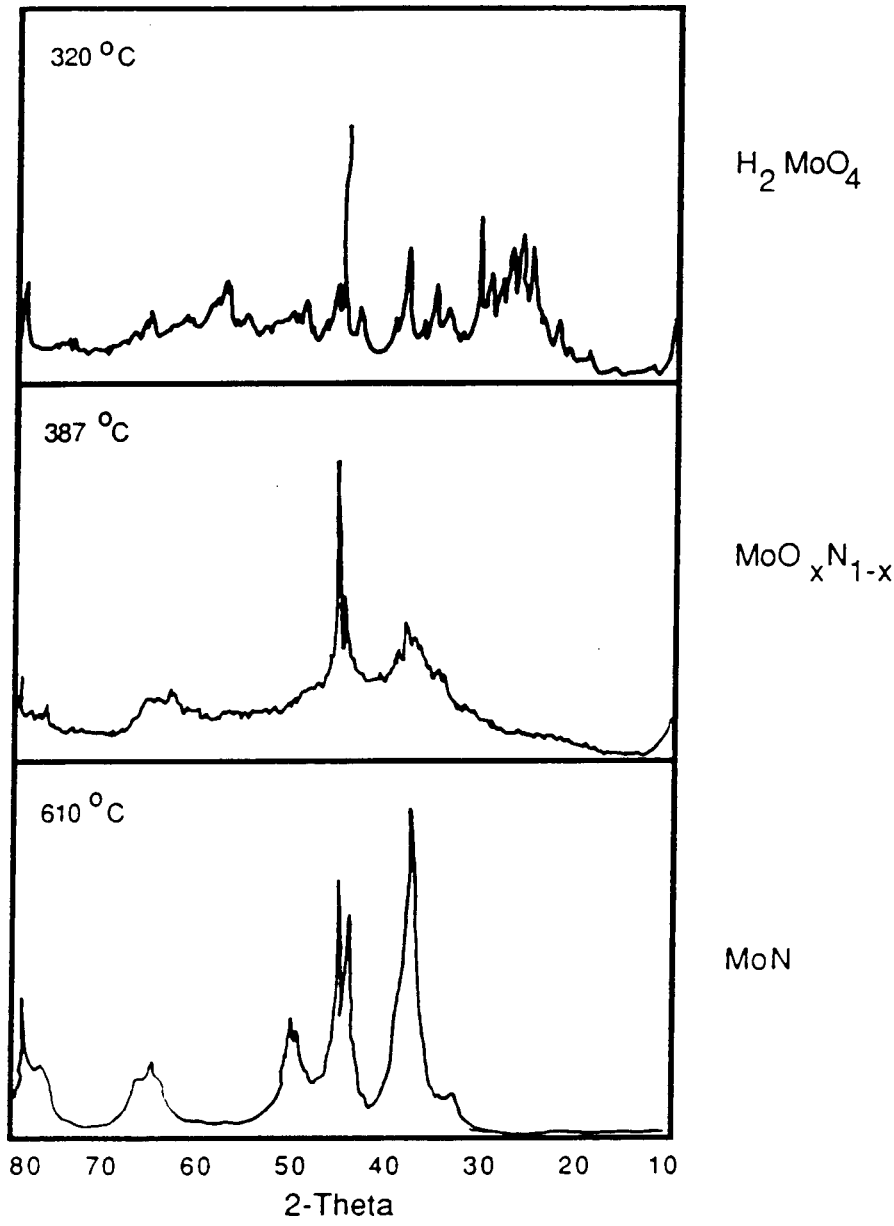

Figure C.7. High temperature XRD patterns for diammonium molybdate/ammonia reaction at 320°C, 387°C, and 610°C.

d-spacing, Å	I/I_o	Assignment	d-spacing, Å	I/I_o	Assignment
6.86	7	1	2.37	38	1
5.81	22	1	2.33	12	1
5.59	35	1	2.30	11	1
5.05	48	1	2.26	3	1
4.96	64	1	2.12	2	1
3.95	37	1	2.09	5	1
3.88	27	1	2.02	25	1
3.66	22	1	2.00	15	1
3.48	35	1	1.99	13	1
3.24	100	1	1.95	5	1
3.15	15	1	1.93	10	1
3.04	42	1	1.87	15	1
2.93	10	1	1.86	12	1
2.84	8	1	1.83	8	1
2.81	13	1	1.82	8	1
2.68	8	1	1.65	7	1
2.57	3	1	1.65	7	1
2.47	4	1	1.62	12	1

1 = $(NH_4)_2MoO_4$ 2 = H_2MoO_4

3 = MoO_xN_{1-x} 4 = MoN

* = Aluminum Sample Holder

Table C.15. D-spacings for high temperature XRD pattern of $(NH_4)_2MoO_4/NH_3$ reaction at 25°C.

d-spacing, Å	I/I_0	Assignment	d-spacing, Å	I/I_0	Assignment
8.27	7	1	2.87	39	1,2
7.28	11	1	2.77	19	1,2
6.66	11	1,2	2.67	12	2
5.64	12	1,2	2.62	14	1,2
5.25	7	2	2.54	21	2
5.05	7	1,2	2.44	19	1,2
4.85	12	1	2.40	21	2
4.67	12	2	2.35	18	1,2
4.00	12	2	2.29	28	1
3.72	19	1	2.25	23	2
3.55	19	1,2	2.13	18	2
3.40	100	1,2	2.02	----	*
3.30	64	2	1.93	37	2
3.01	64	1,2	1.94	27	1,2

1 = $(NH_4)_2MoO_4$ 2 = H_2MoO_4
3 = MoO_xN_{1-x} 4 = MoN
* = Aluminum Sample Holder

Table C.16. D-spacings for high temperature XRD pattern of $(NH_4)_2MoO_4/NH_3$ reaction at 170°C.

d-spacing, Å	I/I_o	Assignment	d-spacing, Å	I/I_o	Assignment
8.27	16	2	2.92	28	1
7.28	11	2	2.87	40	1,2
6.71	14	1	2.79	25	1
6.33	34	2	2.55	30	2
5.63	11	1	2.45	17	1
5.19	15	2	2.39	25	2
4.82	11	1	2.37	25	1
4.70	16	2	2.28	26	1
4.65	16	2	2.19	22	2
3.99	24	2	2.13	20	2
3.86	12	1	2.03	----	*
3.72	17	1	1.94	34	1,2
3.69	15	2	1.88	21	1,2
3.55	26	1	1.84	26	1
3.39	100	1	1.78	21	1,2
3.28	60	2	1.23	----	*
3.01	64	1,2	1.22	----	*

1 = $(NH_4)_2MoO_4$ 2 = H_2MoO_4
3 = MoO_xN_{1-x} 4 = MoN
* = Aluminum Sample Holder

Table C.17. D-spacings for high temperature XRD pattern of $(NH_4)_2MoO_4/NH_3$ reaction at 243°C.

d-spacing, Å	I/I_0	Assignment	d-spacing, Å	I/I_0	Assignment
8.76	33	2	2.62	33	2
6.86	36	2	2.56	39	2
5.22	17	2	2.45	22	2
4.68	33	2	2.37	53	2
3.54	75	2	2.13	25	2
3.39	75	2	2.10	28	2
3.25	61	2	2.03	----	*
3.12	47	2	2.00	36	2
3.01	56	2	1.23	----	*
2.91	100	2	1.23	----	*
2.66	33	2			

1 = $(NH_4)_2MoO_4$ 2 = H_2MoO_4
3 = MoO_xN_{1-x} 4 = MoN
* = Aluminum Sample Holder

Table C.18. D-spacings for high temperature XRD pattern of $(NH_4)_2MoO_4/NH_3$ reaction at 320°C.

d-spacing, Å	I/I_0	Assignment
2.40	79	3
2.07	100	3
2.03	----	*
1.23	----	*
1.23	----	*

1 = $(NH_4)_2MoO_4$ 2 = H_2MoO_4
3 = MoO_xN_{1-x} 4 = MoN
* = Aluminum Sample Holder

Table C.19. D-spacings for high temperature XRD pattern of $(NH_4)_2MoO_4/NH_3$ reaction at 387°C.

d-spacing, Å	I/I_o	Assignment
2.74	20	4
2.46	100	4
2.40	68	3
2.08	66	3
2.04	----	*
1.85	39	4
1.45	24	3
1.43	24	4
1.27	27	3,4
1.24	----	*
1.24	----	*

1 = $(NH_4)_2MoO_4$ 2 = H_2MoO_4
3 = MoO_xN_{1-x} 4 = MoN
* = Aluminum Sample Holder

Table C.20. D-spacings for high temperature XRD pattern of $(NH_4)_2MoO_4/NH_3$ reaction at 610°C.

APPENDIX D: NITROGEN ADSORPTION DATA

This appendix contains the nitrogen adsorption data used to calculate the BET surface areas of the products.

Starting Material: MoO_3

Final Product Temperature: 625°C

BET Surface Area: 57.2 m^2/g

Sample Weight, mg: 97.47

Reduced Pressure, P/P_o	Total Moles of N_2 Adsorbed, $*10^6$
0.041	52.82
0.138	65.31
0.202	72.09
0.284	77.80
0.341	84.94

Table D.1. Adsorption data for MoO_3/NH_3 reaction product.

Starting Material: MoO_2

Final Product Temperature: 750°C

BET Surface Area: 6.31 m^2/g

Sample Weight, mg: 109.93

Reduced Pressure, P/P_o	Total Moles of N_2 Adsorbed, $*10^6$
0.52	6.42
0.139	7.85
0.209	8.57
0.276	9.64
0.350	10.71

Table D.2. Adsorption data for MoO_2/NH_3 reaction product.

Starting Material: $(NH_4)_6Mo_7O_{24}\cdot 4H_2O$

Final Product Temperature: 750°C

BET Surface Area: 56.9 m^2/g

Sample Weight, mg: 79.05

Reduced Pressure, P/P_o	Total Moles of N_2 Adsorbed, $*10^6$
0.062	43.90
0.139	51.04
0.203	56.39
0.272	63.17
0.350	69.95

Table D.3. Adsorption data for $(NH_4)_6Mo_7O_{24}\cdot 4H_2O$ /NH_3 reaction product.

Starting Material: $(NH_4)_6Mo_7O_{24}\cdot 4H_2O$

Final Product Temperature: 625°C

BET Surface Area: 104.2 m^2/g

Sample Weight, mg: 112.58

Reduced Pressure, P/P_o	Total Moles of N_2 Adsorbed, $*10^6$
0.048	102.07
0.125	125.98
0.212	150.25
0.270	165.95
0.345	186.65

Table D.4. Adsorption data for $(NH_4)_6Mo_7O_{24}\cdot 4H_2O/NH_3$ reaction product.

Starting Material: $(NH_4)_2MoO_4$

Final Product Temperature: 625°C

BET Surface Area: 16.5 m^2/g

Sample Weight, mg: 80.64

Reduced Pressure, P/P_o	Total Moles of N_2 Adsorbed, $*10^6$
0.076	9.64
0.140	12.49
0.208	14.99
0.286	17.84
0.351	19.99

Table D.5. Adsorption data for $(NH_4)_2MoO_4/NH_3$ reaction product.

Starting Material: $(NH_4)_6Mo_7O_{24}\cdot 4H_2O$

Reaction Temperature: 345°C

BET Surface Area: 8.94 m^2/g

Sample Weight, mg: 94.59

Reduced Pressure, P/P_o	Total Moles of N_2 Adsorbed, $*10^6$
0.047	8.92
0.120	10.71
0.199	11.06
0.264	11.78
0.349	12.13

Table D.6. Adsorption data for surface area development during $(NH_4)_6Mo_7O_{24}\cdot 4H_2O$ /NH_3 Reaction at 345 °C.

Starting Material: $(NH_4)_6Mo_7O_{24}\cdot 4H_2O$

Reaction Temperature: 379°C

BET Surface Area: 46.5 m^2/g

Sample Weight, mg: 86.86

Reduced Pressure, P/P_o	Total Moles of N_2 Adsorbed, $*10^6$
0.051	41.76
0.126	48.54
0.198	52.82
0.274	56.75
0.351	59.60

Table D.7. Adsorption data for surface area development during $(NH_4)_6Mo_7O_{24}\cdot 4H_2O$ /NH_3 reaction at 379°C.

Starting Material: $(NH_4)_6Mo_7O_{24}\cdot 4H_2O$

Reaction Temperature: 394°C

BET Surface Area: 81.3 m^2/g

Sample Weight, mg: 84.90

Reduced Pressure, P/P_o	Total Moles of N_2 Adsorbed, $*10^6$
0.051	70.31
0.126	81.37
0.206	89.94
0.276	95.29
0.350	99.57

Table D.8. Adsorption data for surface area development during $(NH_4)_6Mo_7O_{24}\cdot 4H_2O$ /NH_3 reaction at 394°C.

Starting Material: $(NH_4)_6Mo_7O_{24}\cdot 4H_2O$

Reaction Temperature: 419°C

BET Surface Area: 96.7 m^2/g

Sample Weight, mg: 83.13

Reduced Pressure, P/P_o	Total Moles of N_2 Adsorbed, $*10^6$
0.050	83.51
0.127	96.72
0.204	105.64
0.276	112.42
0.349	117.77

Table D.9. Adsorption data for surface area Development during $(NH_4)_6Mo_7O_{24}\cdot 4H_2O$ /NH_3 reaction at 419°C.

Starting Material: $(NH_4)_6Mo_7O_{24}\cdot 4H_2O$

Reaction Temperature: 473°C

BET Surface Area: 114.7 m^2/g

Sample Weight, mg: 80.82

Reduced Pressure, P/P_o	Total Moles of N_2 Adsorbed, $*10^6$
0.050	94.22
0.126	109.21
0.201	122.41
0.268	129.55
0.349	138.12

Table D.10. Adsorption data for surface area development during $(NH_4)_6Mo_7O_{24}\cdot 4H_2O$ /NH_3 reaction at 437 °C.

Starting Material: $(NH_4)_6Mo_7O_{24}\cdot 4H_2O$

Reaction Temperature: 536°C

BET Surface Area: 122.4 m^2/g

Sample Weight, mg: 78.71

Reduced Pressure, P/P_o	Total Moles of N_2 Adsorbed, $*10^6$
0.051	93.86
0.126	110.64
0.203	122.77
0.271	133.12
0.342	140.61

Table D.11. Adsorption data for surface area development during $(NH_4)_6Mo_7O_{24}\cdot 4H_2O$ /NH_3 reaction at 536°C.

Starting Material: $(NH_4)_6Mo_7O_{24}\cdot 4H_2O$

Reaction Temperature: 580°C

BET Surface Area: 120.2 m^2/g

Sample Weight, mg: 77.20

Reduced Pressure, P/P_o	Total Moles of N_2 Adsorbed, $*10^6$
0.051	86.01
0.125	101.42
0.201	114.92
0.271	125.27
0.344	135.26

Table D.12. Adsorption data for Surface area development during $(NH_4)_6Mo_7O_{24}\cdot 4H_2O$ /NH_3 reaction at 580°C.

Starting Material: $(NH_4)_6Mo_7O_{24}\cdot 4H_2O$

Reaction Temperature: 629°C

BET Surface Area: 106.1 m^2/g

Sample Weight, mg: 76.12

Reduced Pressure, P/P_o	Total Moles of N_2 Adsorbed, $*10^6$
0.052	74.95
0.126	90.65
0.199	102.43
0.276	113.13
0.346	123.84

Table D.13. Adsorption data for surface area development during $(NH_4)_6Mo_7O_{24}\cdot 4H_2O$ /NH_3 reaction at 629°C.

Starting Material: $(NH_4)_6Mo_7O_{24}\cdot 4H_2O$

Reaction Temperature: 718°C

BET Surface Area: 87.8 m^2/g

Sample Weight, mg: 73.98

Reduced Pressure, P/P_o	Total Moles of N_2 Adsorbed, $*10^6$
0.052	57.10
0.127	68.52
0.203	77.80
0.275	87.08
0.349	97.07

Table D.14. Adsorption data for surface area development during $(NH_4)_6Mo_7O_{24}\cdot 4H_2O$ /NH_3 reaction at 719°C.

Starting Material: MoO_3

Reaction Temperature: 400°C

BET Surface Area: 16.5 m^2/g

Sample Weight, mg: 88.27

Reduced Pressure, P/P_0	Total Moles of N_2 Adsorbed, $*10^6$
0.051	17.49
0.124	18.56
0.197	18.56
0.275	18.56
0.346	18.56

Table D.15. Adsorption data for surface area development during MoO_3/NH_3 reaction at 400°C.

Starting Material: MoO_3

Reaction Temperature: 425°C

BET Surface Area: 58.3 m^2/g

Sample Weight, mg: 82.36

Reduced Pressure, P/P_o	Total Moles of N_2 Adsorbed, $*10^6$
0.051	59.24
0.129	65.31
0.203	67.09
0.273	67.45
0.348	67.81

Table D.16. Adsorption data for surface area development during MoO_3/NH_3 reaction at 425°C.

Starting Material: MoO_3

Reaction Temperature: 450°C

BET Surface Area: 82.4 m^2/g

Sample Weight, mg: 80.97

Reduced Pressure, P/P_o	Total Moles of N_2 Adsorbed, $*10^6$
0.051	81.01
0.127	90.29
0.201	94.58
0.272	96.72
0.347	98.14

Table D.17. Adsorption data for surface area development during MoO_3/NH_3 reaction at 450°C.

Starting Material: MoO_3

Reaction Temperature: 500°C

BET Surface Area: 121.1 m^2/g

Sample Weight, mg: 79.04

Reduced Pressure, P/P_o	Total Moles of N_2 Adsorbed, $*10^6$
0.051	101.71
0.127	119.56
0.198	128.48
0.273	133.83
0.347	136.69

Table D.18. Adsorption data for surface area development during MoO_3/NH_3 reaction at 500°C.

Starting Material: MoO_3

Reaction Temperature: 550°C

BET Surface Area: 141.9 m^2/g

Sample Weight, mg: 77.26

Reduced Pressure, P/P_o	Total Moles of N_2 Adsorbed, $*10^6$
0.051	98.86
0.130	122.06
0.199	138.12
0.271	150.61
0.344	157.39

Table D.19. Adsorption data for surface area development during MoO_3/NH_3 reaction at 550°C.

Starting Material: MoO_3

Reaction Temperature: 600°C

BET Surface Area: 135.0 m^2/g

Sample Weight, mg: 75.89

Reduced Pressure, P/P_o	Total Moles of N_2 Adsorbed, $*10^6$
0.050	86.72
0.128	107.42
0.204	126.34
0.273	141.68
0.349	155.60

Table D.20. Adsorption data for surface area development during MoO_3/NH_3 reaction at 600°C.

Starting Material: MoO_3

Reaction Temperature: 700°C

BET Surface Area: 82.8 m^2/g

Sample Weight, mg: 70.74

Reduced Pressure, P/P_o	Total Moles of N_2 Adsorbed, $*10^6$
0.052	55.32
0.125	64.60
0.199	72.45
0.271	81.37
0.349	91.01

Table D.21. Adsorption data for surface area development during MoO_3/NH_3 reaction at 700°C.

Starting Material: V_2O_5

Final Product Temperature: 750°C

BET Surface Area: 19.4 m^2/g

Sample Weight, mg: 70.71

Reduced Pressure, P/P_o	Total Moles of N_2 Adsorbed, $*10^6$
0.067	13.20
0.145	16.06
0.209	17.49
0.272	18.92
0.346	19.99

Table D.22. Adsorption data for V_2O_5/NH_3 reaction product.

Starting Material: V_2O_5/Pt

Final Product Temperature: 750°C

BET Surface Area: 9.9 m^2/g

Sample Weight, mg: 57.43

Reduced Pressure, P/P_o	Total Moles of N_2 Adsorbed, $*10^6$
0.053	2.50
0.133	5.35
0.204	6.42
0.273	7.49
0.346	8.21

Table D.23. Adsorption data for V_2O_5/Pt/NH_3 reaction product.

Starting Material: VO_2

Final Product Temperature: 750°C

BET Surface Area: 6.8 m^2/g

Sample Weight, mg: 105.00

Reduced Pressure, P/P_o	Total Moles of N_2 Adsorbed, $*10^6$
0.50	7.85
0.131	8.92
0.204	9.28
0.271	9.99
0.348	11.06

Table D.24. Adsorption data for VO_2/NH_3 reaction product.

Starting Material: V_2O_3

Final Product Temperature: 750°C

BET Surface Area: 6.3 m^2/g

Sample Weight, mg: 102.43

Reduced Pressure, P/P_o	Total Moles of N_2 Adsorbed, $*10^6$
0.053	6.99
0.132	7.62
0.197	8.23
0.263	9.00
0.345	10.15

Table D.25. Adsorption data for V_2O_3/NH_3 reaction product.

Starting Material: $H_{0.04}MoO_3$

Final Product Temperature: 750°C

BET Surface Area: 57.5 m^2/g

Sample Weight, mg: 87.07

Reduced Pressure, P/P_o	Total Moles of N_2 Adsorbed, $*10^6$
0.053	37.83
0.132	46.40
0.198	52.82
0.263	59.24
0.331	65.67

Table D.26. Adsorption data for $H_{0.04}MoO_3/NH_3$ reaction product.

Starting Material: $H_{0.13}MoO_3$

Final Product Temperature: 750°C

BET Surface Area: 65.0 m^2/g

Sample Weight, mg: 100.43

Reduced Pressure, P/P_o	Total Moles of N_2 Adsorbed, $*10^6$
0.044	56.03
0.133	68.17
0.197	74.95
0.263	81.73
0.329	88.18

Table D.27. Adsorption data for $H_{0.13}MoO_3/NH_3$ reaction product.

Starting Material: $H_{0.31}MoO_3$

Final Product Temperature: 750°C

BET Surface Area: 65.5 m^2/g

Sample Weight, mg: 91.53

Reduced Pressure, P/P_o	Total Moles of N_2 Adsorbed, $*10^6$
0.040	49.25
0.120	59.60
0.198	66.74
0.265	73.52
0.330	80.30

Table D.28. Adsorption data for $H_{0.31}MoO_3/NH_3$ reaction product.

Starting Material: $H_{0.80}MoO_3$

Final Product Temperature: 750°C

BET Surface Area: 83.8 m^2/g

Sample Weight, mg: 90.87

Reduced Pressure, P/P_o	Total Moles of N_2 Adsorbed, $*10^6$
0.053	82.48
0.132	89.88
0.197	97.47
0.263	105.96
0.329	116.26

Table D.29. Adsorption data for $H_{0.80}MoO_3/NH_3$ reaction product.

APPENDIX E: CHEMICAL ANALYSIS

The chemical analyses of the products are listed in the following tables. Additionally, chemical analyses of the hydrogen molybdenum bronzes are also included. Chemical analysis of the starting materials was not performed, since analyses were provided from the manufacturer.

Starting Material	Final Reaction Temp., ^{o}C	Product Chemical Analysis, Wt% C	H	N	Mo
MoO_3	750	0.24	0.80	9.16	79.8
MoO_2	750	0.41	0.11	10.93	86.9
$(NH_4)_6Mo_7O_{24}\cdot 4H_2O$	625	----	0.57	11.43	----
$(NH_4)_6Mo_7O_{24}\cdot 4H_2O$*	625	0.10	1.42	8.31	----
$(NH_4)_6Mo_7O_{24}\cdot 4H_2O$	750	----	0.15	10.98	----
$(NH_4)_2MoO_4$	625	----	0.47	12.75	----

* After exposure to air for 18 months.

Table E.1. Chemical analysis for products of the reactions at 750^{o}C for ammonia with various molybdenum oxides and ammonium molybdates.

Starting Material	Final Reaction Temp., ^{o}C	Product Chemical Analysis, Wt% C	H	N	V
V_2O_5	750	0.08	0.05	19.26	----
V_2O_5/Pt	750	0.58	0.11	19.44	----
VO_2	750	0.05	0.07	19.48	----
V_2O_3	750	0.06	0.06	19.53	----
NH_4VO_3	750	0.48	0.14	20.28	----

Table E.2. Chemical analysis for products of the reactions at 750^{o}C for ammonia with various vanadium oxides and ammonium vanadates.

Starting Material	Chemical Analysis, Wt% C	H	N	Mo
$H_{0.04}MoO_3$	0.20	0.03	0.00	66.5
$H_{0.13}MoO_3$	0.23	0.09	0.00	65.8
$H_{0.31}MoO_3$	0.30	0.21	0.01	64.4
$H_{0.80}MoO_3$	0.16	0.52	0.01	61.8

Table E.3. Chemical analysis for hydrogen molybdenum bronzes.

Starting Material	Product Chemical Analysis, Wt% C	H	N	Mo
$H_{0.04}MoO_3$	0.35	0.15	10.85	----
$H_{0.13}MoO_3$	0.04	0.36	10.06	----
$H_{0.31}MoO_3$	0.19	0.36	10.56	----
$H_{0.80}MoO_3$	0.09	0.68	10.52	73.6

Table E.4. Chemical analysis for products of the reactions at 750°C for ammonia with hydrogen molybdenum bronzes.